



MINISTÉRIO DA CIÊNCIA, TECNOLOGIA E INOVAÇÃO
INSTITUTO NACIONAL DE PESQUISAS ESPACIAIS

sid.inpe.br/mtc-m21b/2016/01.05.17.40-TDI

MODELING AND SIMULATION OF LAUNCH VEHICLES USING OBJECT-ORIENTED PROGRAMMING

Fábio Antonio da Silva Mota

Doctorate Thesis of the Graduate Course in Space Engineering and Technology/Space Mechanics and Control Division, guided by Drs. Evandro Marconi Rocco, and José Nivaldo Hinckel, approved in dezember 22, 2015.

URL of the original document:

<http://urlib.net/8JMKD3MGP3W34P/3KT98DH>

INPE
São José dos Campos
2015

PUBLISHED BY:

Instituto Nacional de Pesquisas Espaciais - INPE

Gabinete do Diretor (GB)

Serviço de Informação e Documentação (SID)

Caixa Postal 515 - CEP 12.245-970

São José dos Campos - SP - Brasil

Tel.:(012) 3208-6923/6921

Fax: (012) 3208-6919

E-mail: pubtc@sid.inpe.br

**COMMISSION OF BOARD OF PUBLISHING AND PRESERVATION
OF INPE INTELLECTUAL PRODUCTION (DE/DIR-544):****Chairperson:**

Marciana Leite Ribeiro - Serviço de Informação e Documentação (SID)

Members:

Dr. Gerald Jean Francis Banon - Coordenação Observação da Terra (OBT)

Dr. Amauri Silva Montes - Coordenação Engenharia e Tecnologia Espaciais (ETE)

Dr. André de Castro Milone - Coordenação Ciências Espaciais e Atmosféricas
(CEA)

Dr. Joaquim José Barroso de Castro - Centro de Tecnologias Espaciais (CTE)

Dr. Manoel Alonso Gan - Centro de Previsão de Tempo e Estudos Climáticos
(CPT)

Dr^a Maria do Carmo de Andrade Nono - Conselho de Pós-Graduação

Dr. Plínio Carlos Alvalá - Centro de Ciência do Sistema Terrestre (CST)

DIGITAL LIBRARY:

Dr. Gerald Jean Francis Banon - Coordenação de Observação da Terra (OBT)

Clayton Martins Pereira - Serviço de Informação e Documentação (SID)

DOCUMENT REVIEW:

Simone Angélica Del Ducca Barbedo - Serviço de Informação e Documentação
(SID)

Yolanda Ribeiro da Silva Souza - Serviço de Informação e Documentação (SID)

ELECTRONIC EDITING:

Marcelo de Castro Pazos - Serviço de Informação e Documentação (SID)

André Luis Dias Fernandes - Serviço de Informação e Documentação (SID)



MINISTÉRIO DA CIÊNCIA, TECNOLOGIA E INOVAÇÃO
INSTITUTO NACIONAL DE PESQUISAS ESPACIAIS

sid.inpe.br/mtc-m21b/2016/01.05.17.40-TDI

MODELING AND SIMULATION OF LAUNCH VEHICLES USING OBJECT-ORIENTED PROGRAMMING

Fábio Antonio da Silva Mota

Doctorate Thesis of the Graduate Course in Space Engineering and Technology/Space Mechanics and Control Division, guided by Drs. Evandro Marconi Rocco, and José Nivaldo Hinckel, approved in dezember 22, 2015.

URL of the original document:

<http://urlib.net/8JMKD3MGP3W34P/3KT98DH>

INPE
São José dos Campos
2015

Cataloging in Publication Data

Mota, Fábio Antonio da Silva.

M856m Modeling and simulation of launch vehicles using object-oriented programming / Fábio Antonio da Silva Mota. – São José dos Campos : INPE, 2015.

xxviii + 149 p. ; (sid.inpe.br/mtc-m21b/2016/01.05.17.40-TDI)

Thesis (Doctorate in Space Engineering and Technology/Space Mechanics and Control Division) – Instituto Nacional de Pesquisas Espaciais, São José dos Campos, 2015.

Guiding : Drs. Evandro Marconi Rocco, and José Nivaldo Hinckel .

1. Launch vehicles. 2. Propulsion. 3. Liquid rocket engines. 4. Modeling. 5. Simulation. I.Title.

CDU 629.7.085.2



Esta obra foi licenciada sob uma Licença [Creative Commons Atribuição-NãoComercial 3.0 Não Adaptada](https://creativecommons.org/licenses/by-nc/3.0/).

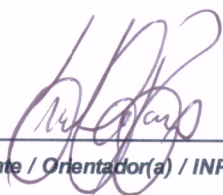
This work is licensed under a [Creative Commons Attribution-NonCommercial 3.0 Unported License](https://creativecommons.org/licenses/by-nc/3.0/).

Aluno (a): **Fábio Antônio da Silva Mota**

Título: "MODELING AND SIMULATION OF LAUNCH VEHICLES USING OBJECT-ORIENTED PROGRAMMING"

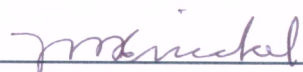
Aprovado (a) pela Banca Examinadora
em cumprimento ao requisito exigido para
obtenção do Título de **Doutor(a)** em
**Engenharia e Tecnologia Espaciais/Mecânica
Espacial e Controle**

Dr. Evandro Marconi Rocco



Presidente / Orientador(a) / INPE / SJC Campos - SP

Dr. José Nivaldo Hinckel



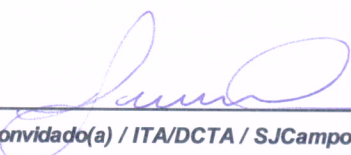
Orientador(a) / INPE / SJC Campos - SP

Dr. Roman Ivanovitch Savonov



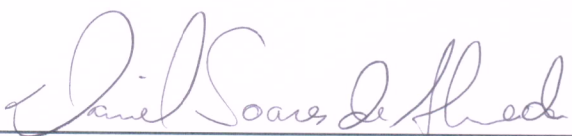
Membro da Banca / INPE / Cachoeira Paulista - SP

Dr. Pedro Teixeira Lacava



Convidado(a) / ITA/DCTA / SJC Campos - SP

Dr. Daniel Soares de Almeida



Convidado(a) / IAE/CTA / SJC Campos - SP

Este trabalho foi aprovado por:

maioria simples

unanimidade

“A vida será mais complicada se você possuir uma curiosidade ativa, além de aumentarem as chances de você entrar em apuros, mas será mais divertida”.

EDWARD SPEYER
em *“Seis Caminhos a Partir de Newton”*, 1994

ACKNOWLEDGEMENTS

I would like to thank my advisers from INPE Dr. José Nivaldo Hinckel and Dr. Evandro Marconi Rocco for their advices and guidances. Special thanks to Dr. Hinckel with whom I shared my room throughout the doctoral project and share with me all your technical knowledge. I also thank Dr. Hanfried Schlingloff who was my adviser in Germany for all the technical advice that makes this work reach another level and also for making easier my stay in Germany and to have provided to me great moments with your lovely family. I would also like to thank my colleagues from the Space Mechanics and Control Division at INPE and my flatmates who have contributed with their relevant comments. I can not fail to mention all friends that I made in Germany for all the unforgettable moments (*es war wahnsinnig super*). I thank my family, of course, for always be there for me. I also express my gratitude to the members of the examiner committee for their valuable comments and suggestions which have improved the quality of this work. Finally but not less important, I thank to the CAPES for their financial support during the doctoral program.

ABSTRACT

Due to the inherent complexity of a launch vehicle, its design is traditionally divided into multiple disciplines, such as trajectory optimization, propulsion, aerodynamics and mass budget. Despite the large number of operational launch vehicles, they usually consist of basic components. In other words, a launch vehicle is an assembly of stages which in turn is divided into propellant system and engine (for a liquid rocket stage), and the engine is an assembly of basic components such as pumps, turbines, combustion chamber, and nozzle. Then, in order to allow future extension and reuse of the codes, it is reasonable that a modular approach would be a suitable choice. In this work, this is accomplished by object-oriented methodology. The UML (Unified Modeling Language) tool was used to model the architecture of the codes. UML diagrams help to visualize the structure of the codes and communication between objects enabling a high degree of abstraction. The purpose of this thesis is the development of a versatile and easily extensible tool capable of analyzing multiple configurations of liquid rocket engines and calculating the performance of satellite launch vehicles. The verification of the codes will be performed by the simulation of power cycle of liquid rocket engines and by the trajectory optimization of the launch vehicles VLS-1 and Ariane 5. In order to verify the applicability of the tool concerning communication between propulsion system and launcher performance, the VLS-Alfa will be simulated for a given mission for different design parameters of the rocket engine upper stage.

MODELAGEM E SIMULAÇÃO DE VEÍCULOS LANÇADORES USANDO PROGRAMAÇÃO ORIENTADA A OBJETO

RESUMO

Devido à inerente complexidade de um veículo lançador, o seu projeto é tradicionalmente dividido em várias disciplinas, como otimização da trajetória, propulsão, aerodinâmica e estimação da massa. Apesar do grande número de veículos lançadores operacionais, eles consistem geralmente de componentes básicos. Em outras palavras, um veículo lançador é um conjunto de estágios que por sua vez é dividido em sistema de propelente e motor (para um estágio a propulsão líquida), e o motor é um conjunto de componentes básicos, tais como bombas, turbinas, câmara de combustão e bocal. Assim, a fim de permitir futura extensão e reutilização dos códigos, é razoável que uma abordagem modular seria uma escolha apropriada. Neste trabalho, isso é realizado por uma metodologia orientada a objeto. A ferramenta UML (Unified Modeling Language) foi usada para modelar a arquitetura dos códigos. Diagramas UML ajudam a visualizar a estrutura dos códigos e comunicação entre objetos proporcionando um elevado grau de abstração. O objetivo desta tese é o desenvolvimento de uma ferramenta versátil e facilmente extensível capaz de analisar várias configurações de motores foguetes a propelente líquido e calcular o desempenho de veículos lançadores de satélites. A verificação dos códigos será realizada pela simulação do ciclo de potência dos motores foguete a propelente líquido e pela otimização da trajetória dos veículos lançadores VLS-1 e Ariane 5. Para verificar a aplicabilidade da ferramenta em relação à comunicação entre o sistema de propulsão e a trajetória ascendente, será simulado o VLS-Alfa para uma determinada missão para diferentes parâmetros de projeto do motor do estágio superior.

LIST OF FIGURES

	<u>Pág.</u>
1.1 Data exchange between disciplines.	1
1.2 Brazilian launch vehicle VLS-Alfa with highlighted L75 rocket engine. . .	3
1.3 Launch Vehicles in the world.	4
1.4 Planet-fixed and local horizon frames.	6
1.5 Flight phases of the European Ariane 5 launch vehicle.	7
1.6 Feed system: (a) Pressure-fed (b) Turbopump-fed.	8
2.1 Redtop: SSME.	13
2.2 EcosimPro Screenshot.	14
3.1 Turbopump configurations.	18
3.2 Gas generator cycle with gases from turbine injected part way down the skirt of the nozzle.	23
3.3 Pressure balance on the thrust chamber walls.	26
3.4 Propellant combination performance.	30
3.5 Dump Cooling.	32
3.6 Theoretical vacuum specific impulse of dumped hydrogen through infinite area ratio nozzle.	33
3.7 Pipe section.	35
3.8 Pressure loss in a tap-off branch related to configuration of the branch. .	36
3.9 (a) Flow guide vanes in sharp elbows of pump inlet lines (b) Flow without and with guide vanes.	36
4.1 Curve fit.	44
4.2 Propellant tank configuration.	47
5.1 Open Cycles. (a) Gas Generator (b) Expander Bleed.	54
5.2 Closed Cycles. (a) Expander Cycle (b) Staged Combustion.	55
5.3 TPA configurations	56
5.4 Comparison of fuel pressure drop levels for GG and SC cycles.	57
5.5 Propulsion model diagram. Possible input/output combinations.	58
5.6 Flow scheme of a gas generator cycle. Seven unknown to be determined are shown.	61
5.7 Flow scheme of an expander bleed cycle. The unknowns required to the simulation are shown.	63

5.8	Flow scheme of staged combustion cycle. The unknowns required to the simulation are shown.	65
5.9	Flow scheme of an expander cycle. The unknowns required to the simulation are shown.	67
6.1	Temperature in atmospheric layers.	71
6.2	Drag coefficients.	72
6.3	Reference Frames	76
6.4	Planet-fixed and local horizon frames for atmospheric flight.	78
6.5	External force resolved in the wind axes.	79
6.6	Schematic of Indirect Shooting Method.	84
6.7	Different Types of Direct Methods.	85
7.1	UML Interface.	93
7.2	Dependency relationship between orbit class and aster class.	93
7.3	UML - Single Shaft TPA.	95
7.4	UML - Dual Shaft TPA.	96
7.5	UML - Thrust Chamber Assembly.	96
7.6	UML diagram of a gas generator cycle.	98
7.7	UML diagram of a staged-combustion liquid rocket engine.	99
7.8	UML - Launch Vehicle Model.	100
8.1	Simplified UML diagram representing the L75 rocket engine.	102
8.2	L75 input/output.	103
8.3	Vulcain input/output.	104
8.4	HM7B input/output.	106
8.5	SSME input/output.	107
8.6	Performance of the L75 rocket engine as function of the chamber pressure.109	
9.1	VLS-1 design parameters.	112
9.2	Velocity profile of the VLS launch vehicle using first formulation of state equations.	113
9.3	Altitude profile of the VLS launch vehicle using first formulation of state equations.	114
9.4	Dynamic pressure profile of the VLS launch vehicle using first formulation of state equations.	114
9.5	Velocity profile of the VLS launch vehicle using second formulation of state equations.	116
9.6	Altitude profile of the VLS launch vehicle using second formulation of state equations.	116

9.7	Dynamic pressure profile of the VLS launch vehicle using second formulation of state equations.	117
9.8	Ground track.	117
9.9	Data: European Launch vehicle.	118
9.10	Altitude profile of the European Ariane 5.	119
9.11	Velocity profile of the European Ariane 5.	119
9.12	Comparison.	120
10.1	Design parameters of the Brazilian launch vehicles (a) VLS-Alfa and (b) VLS-1.	124
10.2	Relative velocity profile of the former and future Brazilian launch vehicle.	125
10.3	Altitude profile of the former and future Brazilian launch vehicle.	125
10.4	Ground track for VLS-Alfa.	126
10.5	Key parameters of the L75 rocket engine.	127
10.6	Influence of the chamber pressure p_c on (a) engine dry mass and (b) stage dry mass.	128
10.7	Influence of the chamber pressure p_c on the payload mass.	128
10.8	Influence of the mixture ratio r_c on (a) engine dry mass and (b) stage dry mass.	129
10.9	Influence of the mixture ratio r_c on the payload mass.	129
A.1	L75 scheme.	145
A.2	Flow schemes Vulcain.	146
A.3	Flow scheme HM7B.	147
A.4	Flow scheme SSME.	148
A.5	RL10-A-3A scheme.	149

LIST OF TABLES

	<u>Pág.</u>
3.1 Typical design parameter values for turbopump of a liquid rocket engine.	22
4.1 Relations for the main engine’s mass of different types of rocket engine cycles.	41
4.2 Mass model validation.	44
4.3 Tank Materials.	48
5.1 LRE with gas generator cycle.	60
5.2 LRE with expander bleed cycle.	62
5.3 LRE with staged combustion cycle.	64
5.4 LRE with expander cycle.	66
6.1 Standard Atmosphere (TEWARI, 2007).	70
7.1 Comparison between object-oriented and function-oriented (procedural) programming.	92
7.2 Overview of the main components functionality of a liquid rocket engine required in order to perform the simulation of the engine cycle.	94
8.1 Verification of the simulated parameters of the L75: Comparison with the literature.	103
8.2 Verification of the simulated parameters of the Vulcain: Comparison with the literature.	105
8.3 Verification of the simulated parameters of the HM7B: Comparison with the literature.	106
8.4 Verification of the simulated parameters of the SSME: Comparison with the literature.	108
8.5 Values of specific impulse and nozzle expansion for different chamber pressures.	109
9.1 Values for state variables at start, inter-stage and end instants.	112
9.2 Optimized control parameters.	113
9.3 Values for state variables at start, inter-stage and end instants.	115
9.4 Optimized control parameters.	115
9.5 Optimized control parameters.	121
10.1 Data: Brazilian launch vehicle VLS	123

10.2 Data: Brazilian launch vehicle VLS-Alfa 123

LIST OF ABBREVIATIONS

ASTOS	–	AeroSpace Trajectory Optimization Software
CEA	–	Chemical Equilibrium with Applications
DLR	–	German Aerospace Center
EC	–	Expander Cycle
EB	–	Expander Bleed Cycle
GA	–	Genetic Algorithm
GEO	–	Geostationary Earth Orbit
GG	–	Gas Generator Cycle
HPOTP	–	High Pressure Oxidizer Turbopump
HPFTP	–	High Pressure Fuel Turbopump
IAE	–	Institute of Aeronautics and Space
LCC	–	Life-Cycle Cost
LEO	–	Low Earth Orbit
LH2	–	Liquid Hydrogen
LOX	–	Liquid Oxygen
LPOTP	–	Low Pressure Oxidizer Turbopump
LPFTP	–	Low Pressure Fuel Turbopump
LRE	–	Liquid Rocket Engine
NASA	–	National Aeronautics and Space Administration
NLP	–	Non Linear Programming Problem
NPSH	–	Net Positive Suction head
OOP	–	Object-Oriented Programming
POST	–	Program to Optimize Simulated Trajectory
PSO	–	Particule Swarm Optimization
REDTOP	–	Rocket Engine Design Tool for Optimal Performance
SC	–	Staged Combustion Cycle
SCORES	–	SpaceCraft Object-oriented Rocket Engine Simulation
SQP	–	Sequential Quadratic Program
SSME	–	Space Shuttle Main Engine
TPA	–	Turbopump Assembly
TCA	–	Thrust Chamber Assmebly
UML	–	Unified Modeling Language
VLS	–	Brazilian Launch Vehicle (Vehículo Lançador de Satélites in Portuguese)

LIST OF SYMBOLS

A	– azimuth [rad]
a	– thermal lapse rate [-]
A_e	– nozzle exit area [m ²]
A_t	– throat area of the nozzle [m ²]
c	– effective exhaust velocity [m/s]
c^*	– characteristic velocity [m/s]
C_D	– drag coefficient [-]
C_L	– lift coefficient [-]
C_f	– thrust coefficient [-]
D	– pipe diameter [m]
	– drag force [N]
F	– thrust force [N]
f	– Darcy friction factor [-]
	– resultant force [N]
G	– gravitational constant [Nm ² /kg ²]
g_0	– standard gravitational acceleration [m/s ²]
h_L	– head loss [m]
H_p	– pump head rise [m]
I_{sp}	– specific impulse [s]
$J_i (i = 1, 2, 3)$	– Jeffery's constants [-]
L	– lift force [N]
l	– length of the pipe [m]
m	– mass [kg]
M	– molar mass [kg/mol]
M_{body}	– Mass of a celestial body [kg]
N_r	– pump's rotational speed [rad/s]
N_s	– stage-specific speed [(m/s) ^{1/3} /m ^{0.75}]
\dot{m}	– mass flow rate [m/s]
P	– power [J/s]
p_a	– ambient pressure [Pa]
p_d	– discharge pressure [Pa]
p_e	– nozzle exit pressure [Pa]
p_i	– inlet pressure [Pa]
$P_i (i = 1, 2, 3)$	– Legendre polynomials
p_v	– vapor pressure [Pa]
p_{Tr}	– turbine pressure ratio [-]
Q	– volume flow rate [m ³ /s]
R_e	– equatorial radius of the Earth [km]
R_p	– polar radius of the Earth [km]
S_{ref}	– reference area of the body [m ²]

t_b	– propellant burn time [s]
T_c	– temperature in combustion chamber [K]
u	– vertical velocity [m/s]
V	– air speed [m/s]
v	– horizontal velocity [m/s]
v_e	– exhaust velocity of gases from combustion [m/s]
z	– variable with no physical meaning

Greek Symbols

α_T	– angle of attack [rad]
β	– thrust angle in flight plane [rad]
Δh	– enthalpy change [J/kg]
γ	– ratio of specific heats [-]
	– flight path angle [rad]
δ	– thrust angle out of flight plane [rad]
η	– efficiency [-]
θ_{cn}	– nozzle cone half angle [degree]
ι	– orbit inclination [degree]
λ	– coestate or adjoint variable
μ	– viscosity of the fluid [Pa.s]
ρ	– density of the fluid [kg/m ³]
ϵ	– measure of the roughness of the pipe wall [-]
ϕ	– latitude [rad]
ξ	– longitude [rad/s]
ζ	– heading angle [rad]
ω_E	– Earth's rotation [rad/s]

Subscripts

a	– ambient
b	– burn
c	– combustion chamber or cylindrical section
$cool$	– cooling system
d	– discharge
dc	– dump cooling
e	– exit
eng	– rocket engine
f	– fuel
gg	– gas generator
i	– inlet
inj	– injector
ne	– nozzle extension
o	– oxidizer

<i>oa</i>	–	overall
<i>pb</i>	–	pre-burner
<i>pl</i>	–	payload
<i>prop</i>	–	propellant
<i>ps</i>	–	propellant system
<i>s</i>	–	sphere
<i>struct</i>	–	structural
<i>t</i>	–	throat
<i>tp</i>	–	turbopump

CONTENTS

	<u>Pág.</u>
1 INTRODUCTION	1
1.1 Motivation	1
1.1.1 Design Phases	2
1.1.2 National Scenario	2
1.2 Objective	3
1.3 Background - Basic Concepts in Space Technology	4
1.3.1 Launch Vehicle	4
1.3.2 Launch of a Satellite into Orbit	5
1.3.2.1 Ascent Trajectory	5
1.3.3 Rocket Propulsion	6
1.4 Work Outline	8
2 LITERATURE REVIEW	11
2.1 Propulsion Performance	11
2.2 Mass Modeling	14
2.2.1 Historical Background	14
2.3 Trajectory Optimization	15
2.3.1 Indirect Method	15
2.3.2 Direct Method	15
2.3.3 Hybrid Method	16
3 COMPONENTS MODELING	17
3.1 Turbopump	17
3.1.1 Pump	17
3.1.2 Turbine	20
3.1.3 Booster Turbopump	24
3.2 Thrust Chamber	24
3.2.1 Rocket-Thrust Equation	25
3.2.2 Specific Impulse and Effective Exhaust Velocity	26
3.2.3 Thrust Coefficient and Characteristic Velocity	27
3.2.4 Real Rocket	28
3.2.5 Approximate Equations for Parameters from Combustion	28
3.2.6 Performance Optimization	29

3.3	Gas Generator or Pre-burner	30
3.4	Injector Head	31
3.5	Heat Exchanger	31
3.6	Pipe System: Feed Lines and Valves	33
3.6.1	Feed Lines	34
3.6.2	Valves	36
4	MASS MODELING	39
4.1	Estimate Engine Mass	39
4.1.1	Simple Relations	39
4.1.2	Detailed Relations	40
4.2	Propellant System Mass	45
4.2.1	Simple Relations	45
4.2.2	Detailed Relations	45
4.2.2.1	Propellant Tanks	46
4.2.2.2	Propellant Mass	50
4.3	Rocket Parameters	51
5	ROCKET ENGINE CYCLES MODELING	53
5.1	Basic Concepts	53
5.1.1	Open Cycles	54
5.1.2	Closed Cycles	55
5.2	Modeling and Simulation	56
5.2.1	Flow and Energy Balance	56
5.2.1.1	Flow Splitter	58
5.2.1.2	Input Parameters Selection	58
5.2.2	Cycle Balance	58
5.2.2.1	Gas Generator Cycle	59
5.2.2.2	Expander Bleed Cycle	62
5.2.2.3	Staged Combustion	63
5.2.2.4	Expander Cycle	66
6	TRAJECTORY MODELING AND OPTIMIZATION	69
6.1	Atmosphere Model	69
6.1.1	Standard Atmosphere	69
6.2	Aerodynamics	70
6.2.1	Aerodynamics Coefficients	71
6.3	Gravitational Model	73

6.4	Equations of the Translational Motion	74
6.4.1	First Formulation	75
6.4.2	Second Formulation	77
6.5	Guidance Programme	80
6.6	Path Constraints	81
6.7	Optimization	82
6.7.1	Background	82
6.7.1.1	Optimal Control Problem	82
6.7.2	Methodology	85
6.7.2.1	First Approach - Direct Method	85
6.7.2.2	Second Approach - Hybrid Method	87
7	PROGRAMME SETUP	91
7.1	Object-oriented Programming (OOP)	91
7.2	Unified Modeling Language (UML)	92
7.3	Overview of the Main Components Functionality	93
7.4	Engine Components Assembly Modeling	95
7.4.1	Turbopump Assembly Modeling	95
7.4.2	Thrust Chamber Assembly Modeling	96
7.5	Engine Cycle Modeling	97
7.6	Launch Vehicle Modeling	99
8	RESULTS 1: SIMULATION OF LIQUID ROCKET ENGINES 101	
8.1	Performance of a Liquid Rocket Engine	101
8.2	Sensitivity Analysis	108
9	RESULTS 2: TRAJECTORY SIMULATION 111	
9.1	Direct Method	111
9.1.1	VLS launch Vehicle	111
9.1.2	Ariane 5 Launch Vehicle	118
9.2	Hybrid Method	120
10	MISSION ANALYSIS 123	
10.1	Flight Simulation	123
10.2	Influence of Engine Parameters on the Launcher Performance	126
11	CONCLUSION AND SUGGESTIONS 131	
11.1	Conclusion	131
11.1.1	Contribution of This Work	132

11.2 Suggestions	133
REFERENCES	135
ANEXO A - Flow Schemes of Liquid Rocket Engines	145
A.1 L75	145
A.2 Vulcain	145
A.3 HM7B	146
A.4 SSME	147
A.5 RL10-A-3A	148

1 INTRODUCTION

1.1 Motivation

Although it has been almost six decades since the Soviet Union put the first artificial satellite into orbit, launch vehicles are still based on the fundamental technologies developed at the dawn of the space era.

Space launch systems are composed of a large number of components grouped into a hierarchy of subsystems. The performance of the vehicle depends on the individual performance of each of the subsystems which in turn depend on material properties and design parameters. Changes in design parameters are propagated throughout the cluster hierarchy of subsystems and components, flight trajectory and payload capability (HINCKEL, 1995).

The design of launch vehicles is inherently a task of great complexity. Thus, in order to manage such complexity its design is usually divided into multiple disciplines, such as trajectory, propulsion, mass and geometry (see Figure 1.1). Since the slightest mistake may induce economical, material and human disastrous consequences we can consider equally important the disciplines cost and reliability. Traditionally, design tools and computer codes have been developed to treat these disciplines separately. Unfortunately, the disciplines are not isolated from each other, instead they are all interconnected in a unit system.

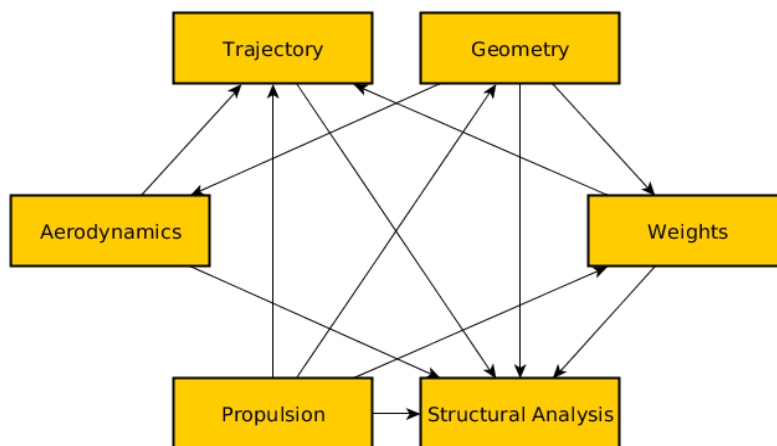


Figure 1.1 - Data exchange between disciplines.
SOURCE: Wiegand et al. (2010)

1.1.1 Design Phases

The design phases for most systems including launch vehicles can be divided into three project phases: conceptual, preliminary and detailed. Specifically, it has been shown that 80 % a vehicle's life-cycle cost (LCC) is determined by the conceptual design while efforts for optimization in further steps only result in less significant improvement (HAMMOND, 2001). This could be translated in the statement: "engineering can never right a poor concept selection" (Hammond (2001) in turn taken from Pugh (1991)).

1.1.2 National Scenario

In an attempt to get autonomous access to space, starting from 1964 Brazil has developed a series of sounding (research) rockets, named Sonda I, II, III, and IV in which were the basis for building the Brazilian Satellite Launch Vehicle VLS-1 (Veículo Lançador de Satélite - in Portuguese). To date, three prototypes have been built and two launches attempted. Unfortunately due to failures, the vehicle however could not be qualified up to now. The tragedy occurred in the launch pad in 2003 affected drastically the launcher program and more than one decade later there was no attempt to a new launching. Brazil has a strategically located launch site in the proximity of the equator called Alcântara Launch Center. Due to its prime location, fuel consumption for launching satellites into equatorial orbit (e.g., communication satellites in GEO orbit) is lower when compared to launch sites located at higher latitudes.

The Brazilian space program has been aimed at vehicles using solid propellants with launch capability limited to a few hundred kilograms into Low Earth Orbit (LEO). To enlarge the launch envelope and payload mass to get higher orbits and also to improve the launch injection accuracy, rocket engines driven by liquid propulsion are not an option, but a must. The propellant choice, cycles, design parameters and structural materials involves countless simulations and trade-off studies. During the simulations and trade-off studies phase, the availability of a versatile tool for this purpose is very useful. The development of the tool itself can also be used as a learning tool and improvement of researchers, students and engineers who will be further engaged in the program.

A program for the development of a liquid rocket engine is currently being carried out at Aeronautics and Space Institute (IAE) to be used in the upper stage of the Brazilian launch vehicle. The idea is to replace the last two solid stages of the VLS-

1 launch vehicle by a single liquid rocket stage (see Figure 1.2). The LRE named L75 will be capable of reaching a thrust range of (75 ± 5) kN using the propellants combination LOX/Ethanol.

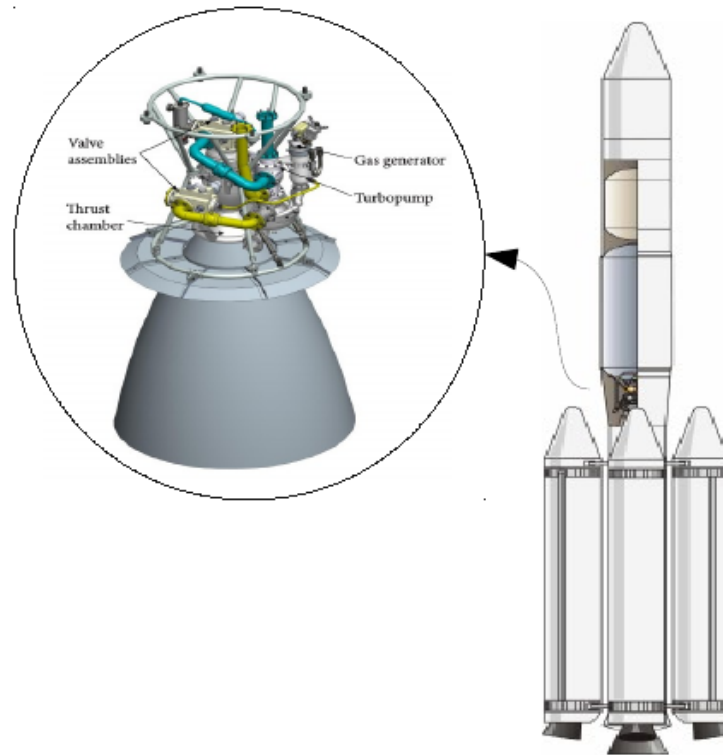


Figure 1.2 - Brazilian launch vehicle VLS-Alfa with highlighted L75 rocket engine.
SOURCE: The circled rocket engine was taken from Almeida and Pagliuco (2014) and the launch vehicle from Moraes Junior et al. (2011)

1.2 Objective

The purpose of this work is to develop a tool which can be easily reused and extended to model and simulate a launch vehicle. In the framework of this thesis the focus will be on propulsion system and trajectory. Thus, the tool is intended to be capable of modeling and simulating different configurations of liquid rocket engines, modeling and optimizing flight trajectory until orbit injection, and analyzing the influence of engines parameters on the trajectory. Despite the large number of operational launch vehicles, they usually consist of basic components and subsystems. In other words a launch vehicle is an assembly of stages which in turn is divided into propellant system and engine (for a liquid rocket engine), and the engine is an assembly of basic components such as pumps, turbines, and combustion chamber. Then in order

to permit a better extensibility and reusability of the codes, a modular approach is chosen. Mathematical models for determination of the mass and performance of liquid rocket engine cycle as well as the complete launch vehicle will be described and discussed. With the engine design parameters and the mass models of the vehicle along with models for atmosphere and gravitational field, the flight trajectory can be determined. The launch vehicle performance will be measured by payload mass for a given mission.

1.3 Background - Basic Concepts in Space Technology

1.3.1 Launch Vehicle

A launch vehicle is a space rocket used to carry a payload from the Earth's surface to outer space. The launch vehicles can be classified as reusable, when it is used in more than one mission, and expendable when they are used for a single mission (the stages are being discarded in certain phases of the ascent trajectory). The most famous reusable launch vehicle is the American Space Shuttle. Although, in fact it is partially reusable since the external tank storing liquid hydrogen and liquid oxygen is expendable. In Figure 1.3 some launch vehicles of the world are shown.

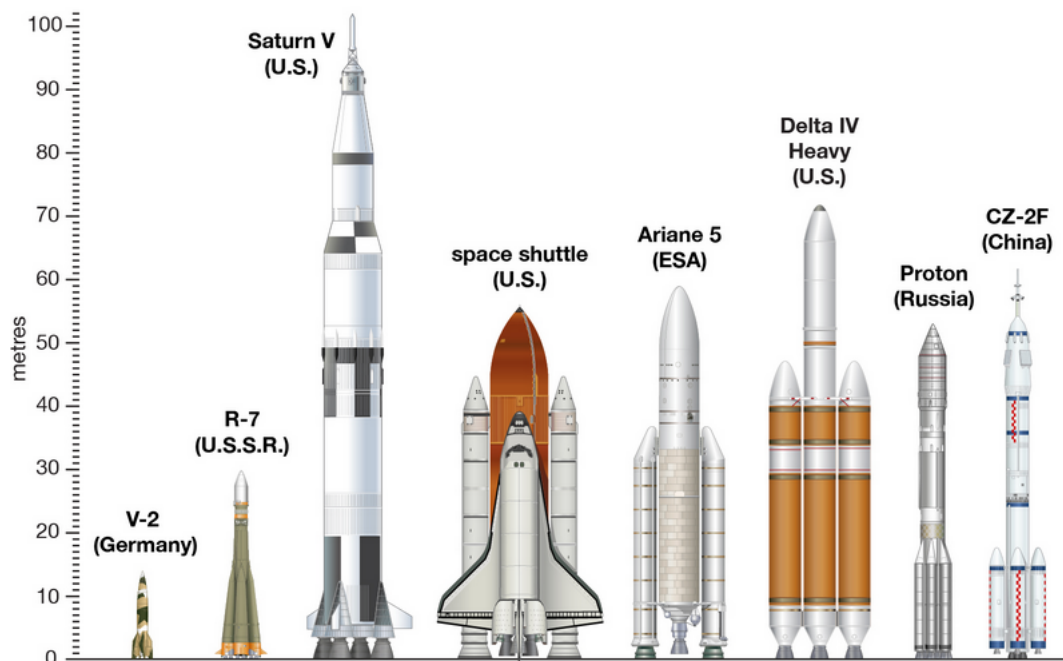


Figure 1.3 - Launch Vehicles in the world.

SOURCE: *Encyclopaedia Britannica* (2015)

In order to make use of atmospheric oxygen during the ascent flight to replace the heavy oxidizer propellant (LOX) of a liquid rocket engine (LRE), and accordingly, reducing the gross lift-off mass (GLOW), air-breathing launch vehicles have been recently studied (MUSIELAK, 2012; SEGAL, 2004). However, the technology to develop such a propulsion system which condenses the air in a split second and extracts LOX still represents a task of great challenge in current engineering, thus so far, all the operational launch vehicles store their propellant combination inside tanks before the flight.

1.3.2 Launch of a Satellite into Orbit

The injection of a satellite into orbit is normally done by a multistage rocket. There are basically two types of launching, by direct ascent and through a parking orbit. The parking orbit is a temporary LEO (Low Earth Orbit), which has an altitude of approximately 200 km, staying just above the denser layers of the atmosphere (CORNELISSE et al., 1979). There are several reasons to make use of a parking orbit, among them we can mention the increased launch window and missions to geostationary orbit. The inclination of the desired orbit ι depends on the latitude of the launch site ϕ , and azimuth A (TEWARI, 2007):

$$\cos \iota = \cos \phi \sin A \quad (1.1)$$

Eq. 1.1 can be deduced from spherical trigonometry to the triangle formed by arcs MO , ON and NM , as shown in Figure 1.4.

From Eq. 1.1 is evident that the smallest possible inclination of the orbit is achieved when the rocket is launched eastward, i.e., when $A = 90^\circ$. Thus, the orbit inclination will never be less than the launch latitude.

1.3.2.1 Ascent Trajectory

During the ascent trajectory, the vehicle performs five distinct phases in its way from the launch pad to orbit (Figure 1.5):

- **Vertical ascent:** It needs to gain altitude quickly to minimize the gravitational losses. Roll maneuver aligns launch azimuth with the correct orbital plane.
- **Pitch over:** Begin to gain velocity downrange (horizontally).

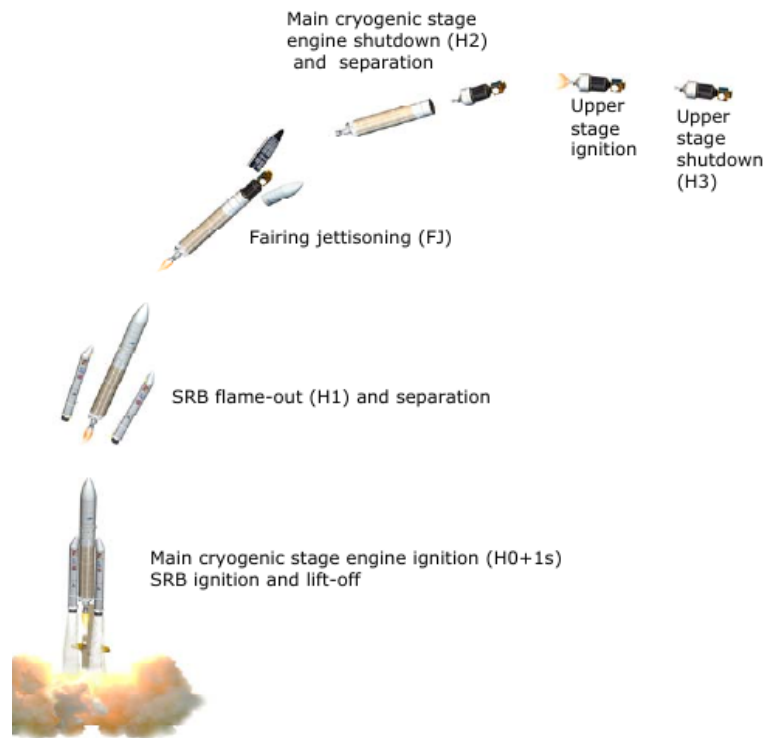


Figure 1.5 - Flight phases of the European Ariane 5 launch vehicle.
 SOURCE: [Arianespace \(2011\)](#)

The thrust chamber assembly consists of injector head, combustion chamber, nozzle, igniter and cooling system. In the thrust chamber the propellants which come from the feed system are injected, mixed, burned, and converted into hot gases at high speeds. By the principle of conservation of energy, we can understand that in the thrust chamber takes place a conversion of random motion of molecules at high speeds (heat) in an ordered flow of gases at high speed (kinetic energy).

The feed system of a liquid rocket engine can be classified in two categories, i.e., pressure-fed and turbopumps-fed (Figure 1.6). In pressure-fed are used pressure accumulators so that one can proceed the pressurization of the propellant tanks. Because the entire tank is subjected to pressurization throughout the operation, their application is restricted to engines which employ relatively low chamber pressure, and lower thrust accordingly. This is due to the strong increase in the weight of the tanks caused by required structural loads. (Figure 1.6a). For a turbopump system, the pump, either axial or radial, is always coupled to one turbine, which in turn is driven by working fluid from a gas generator. This allows to make use of lighter tanks, since they are not under high internal pressures. Consequently, this engine can

operate at higher chamber pressures, which results in increased thrust (Figure 1.6b).

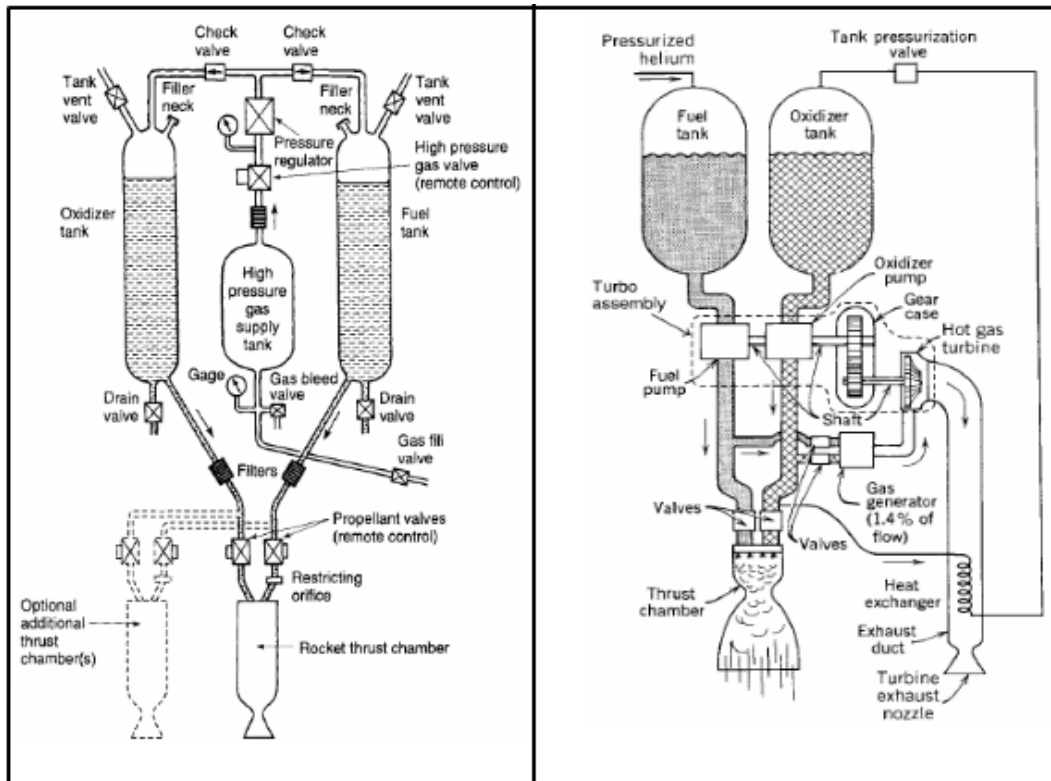


Figure 1.6 - Feed system: (a) Pressure-fed (b) Turbopump-fed.
SOURCE: Sutton and Biblarz (2010)

1.4 Work Outline

To give an overview of what comes next in this work, the following chapters can be divided in:

- Literature Review (Chapter 2). The focus of this chapter is to present the main tools used in the literature and by the industry to model space systems.
- Mathematical Modeling (Chapters 3-6). These Chapters are intended to expose all the equations and technical recommendations which are necessary to model a launch system.
- Programme Architecture (Chapter 7). This topic is responsible for gathering all information contained in Chapters 3-6 and to explicit the commu-

nication between systems, subsystems and components.

- Results (Chapters 8-10). These chapters are designed to show the applicability and limitations of the developed codes.
- Conclusion (Chapter 11). The conclusions about the main results and suggestions for future works are given in the last chapter of this work.

2 LITERATURE REVIEW

In the second chapter of this Thesis will be discussed the historical background of design for the disciplines trajectory, mass and performance for launch vehicles along with the main tools developed during the last decades.

2.1 Propulsion Performance

This section begins with a short description of the well-known tool to calculate engine performance CEA and then it follows with historical background of the most notable works and tools developed from them, namely:

- SEQ
- EcoSimPRO
- REDTOP
- SCORES/SCORES-II

CEA

CEA, which stands for Chemical Equilibrium with Applications is a recognized standard program for chemical equilibrium calculation. The tool calculates complex chemical equilibrium product concentrations from any set of reactants and determines thermodynamics and transport properties for the product mixture. The program open source is freely distributed on the website [NASA Glenn Research Center \(2010\)](#), where you can find a well documented report describing the theoretical principles (GORDON; MCBRIDE, 1994) and the user's manual (GORDON; MCBRIDE, 1996). Applications include:

- theoretical rocket performance (which is, of course, the one of interest in this work),
- assigned thermodynamic states,
- Chapman-Jouguet detonations, and
- shock-tube parameters for incident and reflected shocks.

SEQ and LRP2

One of the most important and robust tools for vehicle/propulsion analysis was developed when DLR and NASA combined computer codes to provide a capability to optimize rocket engines cycles and its parameters as well as launch vehicles considering the coupling between them. In many publications you can find applications of this tool (amongst them we can cite [Manski and Martin \(1990\)](#), [Manski and Martin \(1991\)](#), [Goertz \(1995\)](#), [Manski et al. \(1998\)](#), [Burkhardt et al. \(2002\)](#), [Sippel et al. \(2003\)](#), [Burkhardt et al. \(2004\)](#), [Sippel et al. \(2012\)](#)).

SCORES and SCORES-II

SCORES, which stands for SpaceCraft Object-oriented Rocket Engine Simulation, is a web-based tool suitable to use for use in conceptual level spacecraft and launch vehicle design. The tool is written in C++. Performance parameters provided by SCORES are thrust, specific impulse and thrust to weight ratio. Initially, the tool was created to support only LOX/LH2 propellants combination, but this was later expanded to include a number of hydrocarbon fuels. SCORES does not model the powerhead, instead works similar to CEA regarding its equilibrium analysis and capabilities ([WAY; OLDS, 1998](#); [WAY; OLDS, 1999](#)). Later this design tool would become commercial with its capabilities greatly expanded and now with the name SCORES-II ([BRADFORD, 2002](#)).

REDTOP

Rocket Engine Design Tool for Optimal Performance (REDTOP) is a commercial design tool for use in conceptual and preliminary design of space transportation systems (STS) using liquid rocket engines ([BRADFORD et al., 2004](#)) . Currently there are two distinct versions called REDTOP-Lite and REDTOP-Pro. The latter version supports over 20 different flowpaths and variations of staged-combustion, gas-generator, expander, split-expander, tap-off, and pressure-fed designs for rocket engines ([SPACEWORKS SOFTWARE, 2015](#)). A engine scheme flow for the Space Shuttle Main Engine (SSME) is shown in [Figure 2.1](#).

EcosimPro

EcosimPro is an object-oriented visual simulation tool capable of modeling zero dimensional or one dimensional multidisciplinary continuous-discrete systems in both steady state a transient studies (see [Figure 2.2](#)). It was originally developed for space applications, namely to assist in the modeling of the Environmental and Con-

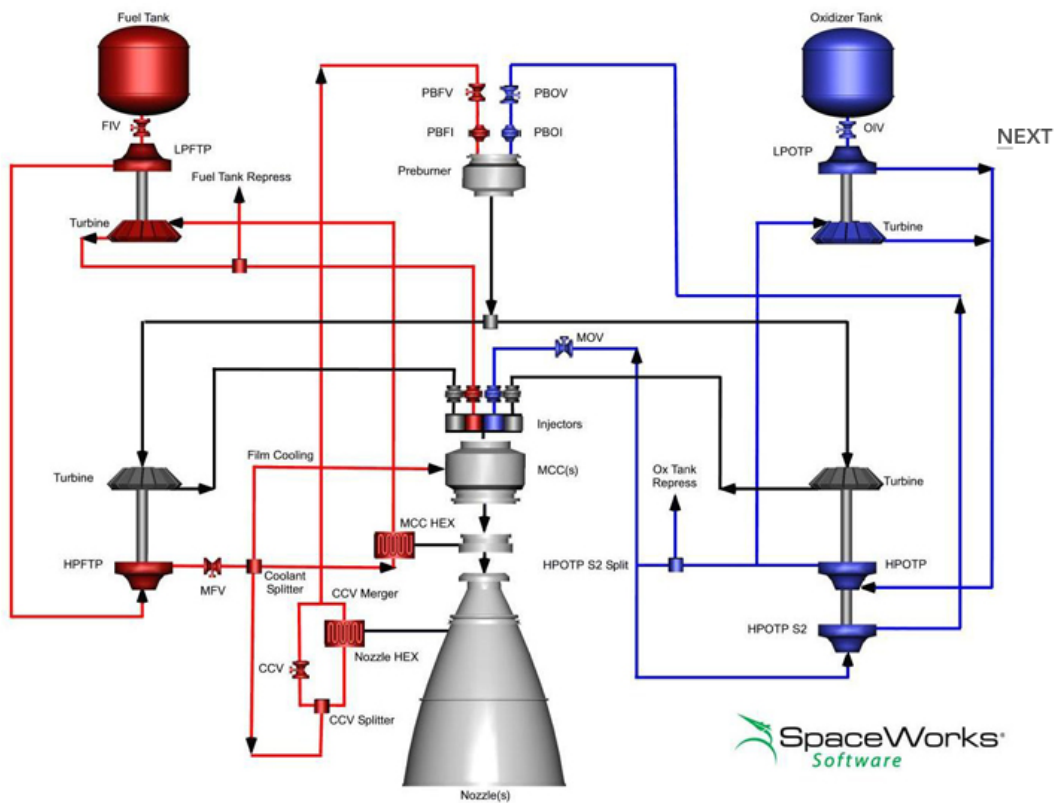


Figure 2.1 - Redtop: SSME.

SOURCE: Spaceworks Software (2015)

ontrol Life Support Systems (ECLSS) for European Space Agency (ESA)'s HERMES and COLUMBUS projects, however today one can find applications in a wide range of fields. The first version of the tool was released in 1993. The tool employs a set of multidisciplinary libraries in which allow components to be created that mix disciplines such as mechanical, electrical, fluids, control, etc (ECOSIMPRO, 2015).

LiRa

Recently, in his Master Thesis, Ernst (2014) developed a tool to simulate liquid rocket engines at steady conditions called LiRa (Liquid Rocket Engine Analysis). The cycle balance differs from the traditional approach in the sense of instead of creating a system of nonlinear equations based on power, flow and pressure balance, his modeling starts from the thrust chamber.

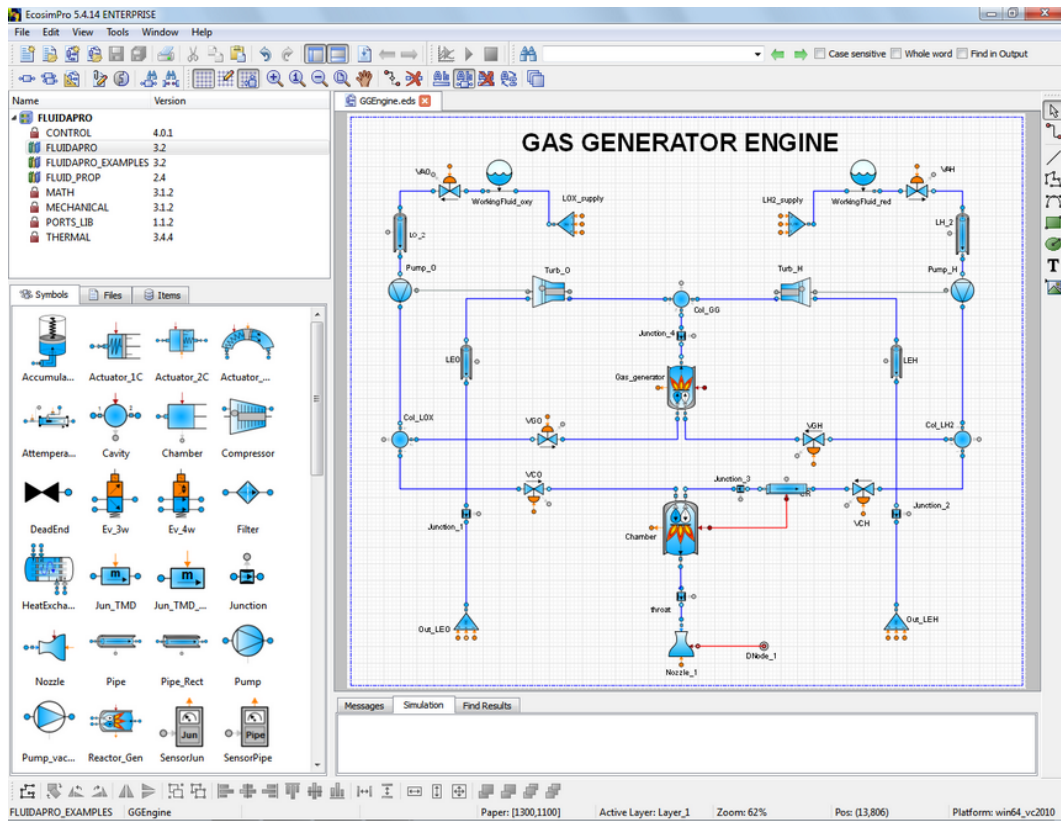


Figure 2.2 - EcosimPro Screenshot.
SOURCE: Ecosimpro (2015)

2.2 Mass Modeling

Most of the modeling approaches rely on historical data for comparison to the analytic equations, so that correction factors can be estimated. Because of this statistical dependency, usually these models are relatively inaccurate.

2.2.1 Historical Background

To identify the coupling of nominal rocket design parameters on the trajectory Verderaiame (1964) developed a parametric method to derive approximate equations for large liquid rocket engine mass and envelope. The engine mass was calculated by the sum of three subsystems; turbopump, rocket chamber and accessories. To allow mixture ratio shifts and propellant mass throttling performance equations which are well known in the literature were modified.

Felber (1979) presents an empirical/analytical method to determine the mass of the main components of a liquid rocket engines along with historical data to esti-

mate the engine mass. Firstly detailed expressions for the components were derived: turbopump, injector, combustion chamber, nozzle and valves; and then taking the propellants combination LOX/LH2 simplified relations were achieved. Finally the engine mass is calculated summing all the main components multiplied by a correction factor to take into account the remaining elements. To determine the correction factor it was considered the engines HM7, H20, RL-10, SSME, J-2 and ASE.

Using a data base with 51 LRE, linear, quadratic, power law and logarithmic curves were analyzed in [Castellini \(2012\)](#). The best resulting regression in terms of quadratic fit error for each technology were implemented within the propulsion models.

Using historical data from 43 rocket engines and taking into account the type of propellant, chamber pressure, the nozzle area expansion ratio, and the number of thrust chamber, [Zandbergen \(2015\)](#) presented simple relations to compute engine mass making distinction with one use pressure-fed, turbopump fed, and if the propellants are storable, cryogenic or semi-cryogenic.

2.3 Trajectory Optimization

In order to get the best performance of a given launch vehicle, and consequently, to make the access to space less costly, trajectory optimization techniques has been for decades a subject of intense research. Trajectory optimization can be categorized basically into direct and indirect methods. In [Betts \(1999\)](#) and [Rao \(2009a\)](#) was made a comprehensive discussion about both of two methods.

2.3.1 Indirect Method

The reason for this method to be called “indirect” comes from the strategy to convert the original optimal control problem into a boundary-value problem. The most common indirect methods found in the literature are the shooting method, the multiple-shooting method, and collocation methods as one can see in former reports ([BROWN et al., 1969](#); [TEREN](#); [SPURLOCK, 1966](#)), recent works as in the paper of [Miele \(2003\)](#) and in the Master thesis of [Zerlotti \(1990\)](#) which uses the algorithm BNDSCO ([OBERLE](#); [GRIMM, 1990](#)).

2.3.2 Direct Method

Presumably because of the possibility of solving complex problems with a minimum effort of mathematical analysis, this method is the one chosen for most of the researchers ([BUENO NETO, 1986](#); [HARGRAVES](#); [PARIS, 1987](#); [HERMAN](#); [CONWAY, 1996](#);

SEYWALD, 1994; SILVA, 1995; BALESIDENT, 2011). One of the most popular software used extensively in many publications is called POST (Program to Optimize Simulated Trajectories) (BRAUER et al., 1977).

In the framework of this method, the problem is characterized by a set of parameters which define the control law. This problem is a typical Non Linear Programming Problem (NLP) and can be solved using classical Gradient-based methods (deterministic methods) such as Sequential Quadratic Program (SQP) or by heuristic methods. According to Betts (1999), heuristic optimization algorithms are not computationally competitive with gradient methods. Even though presumably due to ease of implementation without a detailed understanding of the system, in the last two decades a lot of papers using Particle Swarm Optimization (PSO), genetic algorithms (GA) among others were applied to solve trajectory optimization problems. As for indirect methods, the direct methods can be categorized in direct (multiple shooting or collocation. In the case where only the control variables are adjusted by a function, the method is called a shooting method. When both the state and control are parameterized, the method is called a collocation method. A well-known software developed by the University of Stuttgart which addresses the direct collocation method is *the AeroSpace Trajectory Optimization Software* (ASTOS). For either direct or indirect approaches, perhaps the most important benefit gained from a multiple shooting formulation compared to its precursor (single shooting) is enhanced robustness.

2.3.3 Hybrid Method

To take advantage of both methods previously described, a hybrid method can also be considered (STRYK; BULIRSCH, 1992; PONTANI; TEOFILATTO, 2014; GATH; CALISE, 2001; GATH, 2002). The idea behind this approach is to divide the flight trajectory into two distinct phases, namely atmospheric and exo-atmospheric phase, applying the direct method in the first phase and indirect method in the second one. Here, exo-atmospheric phase means that the vehicle is virtually in vacuum space, i.e., the aerodynamic effects can be ignored.

Pontani and Teofilatto (2014) proposed a simple method to evaluate the performance of multistage launch vehicles for given structural data, aerodynamic and propulsive parameters.

3 COMPONENTS MODELING

The common components for all liquid rocket engine turbopump-fed are pumps, turbine(s), valves, pipes and thrust chamber. Depending on the configuration a gas generator (for gas generator cycle), a pre-burner(s) (for staged combustion cycle) and booster-pumps can be found as well. This chapter presents the modeling of the main components of a liquid rocket engine which will be essential to model and simulate the LRE cycles. Thus the design equations, the design parameters, limitations and restrictions of each component will be presented and discussed.

3.1 Turbopump

The turbopump assembly (TPA) is required when it is desired a higher pressure in the combustion chamber, i.e, when it is dealing with launch vehicles. Usually if the density of the propellants are relatively close, an arrangement with single shaft TPA can be applied. However, when it is dealing with propellants with strongly different densities as the case of the combination LOX/LH2, a dual shaft TPA is required. A TPA with two turbines (dual shaft) is still distinguished between configurations working in series and working in parallel. There is still a configuration using gear case, but this configuration implies in a more complicated design and then a single shaft TPA is commonly preferred. Schematics of typical turbopump arrangements are presented in Figure 3.1.

3.1.1 Pump

For space application weight is a key parameter, so centrifugal pumps are preferred because they can handle a large amount of mass flow rate. Nevertheless axial and mixed pumps are used. The required pump mass flow is parameterized by the engine design parameters; thrust, effective exhaust velocity and mixture ratio, and propellant densities. Assuming steady flow, the pump basically increases the Bernoulli head between the pump inlet and outlet (WHITE, 1998):

$$H_p = \left(\frac{p}{\rho g_0} + \frac{v^2}{2g_0} + z \right)_{discharge} - \left(\frac{p}{\rho g_0} + \frac{v^2}{2g_0} + z \right)_{inlet} \quad (3.1)$$

For a liquid rocket engine the terms in the right side related to kinetic $[v^2/2g_0]$ and potential energy $[z]$ can be neglected, so the net pump head is essentially equal to the change in pressure head:

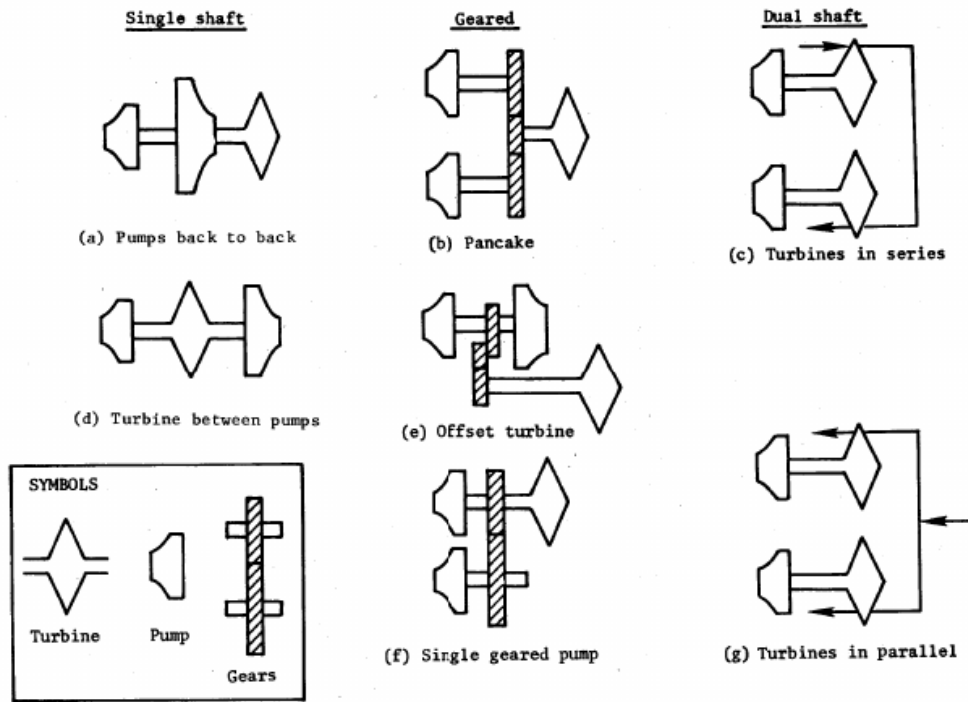


Figure 3.1 - Turbopump configurations.
SOURCE: SP-8107 (1974)

$$H_p = \frac{p_d - p_i}{g_0 \rho} \quad (3.2)$$

where

H_p = pump head rise [m]

p_i = inlet pressure [Pa]

p_d = discharge pressure [Pa]

g_0 = standard gravitational acceleration [= 9.81 m/s²]

ρ = density of the working fluid [kg/m³]

The required pump power is given by (HUMBLE et al., 1995):

$$P_P = \frac{g_0 \dot{m} H_p}{\eta_P} \quad (3.3)$$

where

P_p = pump power [J/s]

η_P = pump efficiency [-]

\dot{m} = propellant mass flow rate [kg/s]

The required pump power is a key parameter to balance cycle. For preliminary analysis, [Humble et al. \(1995\)](#) gives an efficiency of 0.75 for LH2 and 0.80 for all other types of propellants. Since Eq. 3.3 is for incompressible flow, substantial deviations from the predictable value can be found when extremely high pressure is applied for a low density propellant as will be seen for the LH2 in Chapter 8. For those cases, the pump power can be calculated in terms of enthalpy change Δh as presented in the following equation:

$$P_P = \frac{\dot{m}\Delta h}{\eta_P} \quad (3.4)$$

To keep the liquid from cavitation or boiling, the head required at the pump inlet or the so-called net positive-suction head (NPSH) is defined:

$$NPSH = \frac{p_i - p_v}{g_0\rho} \quad (3.5)$$

Where p_v is the vapor pressure of the propellant. If the NPSH is given, it must be ensured that the right-hand side is equal or greater to suppress pump cavitation. A similarity parameter that characterizes pumps and influence the pump's hydraulic efficiency η_P is the stage-specific speed N_s ([HUMBLE et al., 1995](#)):

$$N_s = \frac{N_r\sqrt{Q}}{(H_p/n)^{0.75}} \quad (3.6)$$

The stage-specific speed is function of the rotational speed of the pump N_r , volume flow rate Q , head rise H_p and number of pump stages n . In this work the efficiency of the pump η_P is a parameter given by the user, however this parameter could be easily estimated using the N_s as presented in [Humble et al. \(1995\)](#).

3.1.2 Turbine

The turbine is a device that extracts energy from a flowing working fluid which can be hot gases from a gas generator in a gas-generator cycle, by warm gases leaving the cooling jacket in an expander cycle, or by hot gases from a pre-burner in a staged-combustion cycle. For an auxiliary turbopump arrangement, hydraulic turbines which derives its energy from liquid propellant coming from the main pump can also be found. Ideally there are two types of turbines of axial-flow of interest to rocket pump drives: impulse turbines and reaction turbines. The power of the turbine can be determined by:

$$P_T = \eta_T \dot{m} \Delta h \quad (3.7)$$

where

η_T = turbine efficiency [-]

\dot{m}_T = mass flow rate [kg/s]

The turbine pressure ratio is defined as:

$$p_{Tr} = \frac{p_{Ti}}{p_{Td}} \quad (3.8)$$

where p_{Tr} is the turbine pressure ratio and the indexes Ti , Td refer to turbine inlet and turbine discharge respectively. Thus if the specific heat c_p , the inlet temperature T_i and the ratio of specific heats γ is defined, then the power of the turbine can be given as:

$$P_T = \eta_T \dot{m}_T c_p T_i \left[1 - \left(\frac{1}{p_{Tr}} \right)^{(\gamma-1)/\gamma} \right] \quad (3.9)$$

In this work, the parameters Δh , c_p and γ from Eqs. 3.7 and 3.9 are calculated using the well known program CEA (see the reports of Gordon and McBride (1994) and Gordon and McBride (1996)). However, CEA can be used only for gas turbines driven by gases from combustion. For example, in the expander cycle the turbine are driven by hot gases from the heat exchanger and booster pumps can be driven

by hydraulic turbines, thus in these cases only Eq. 3.7 can be used and the enthalpy change will be a parameter given by the user.

For staged-combustion or expander cycles, as the turbine is in series with the thrust chamber, turbines design should aim for the lowest pressure ratio in order to minimize pressure drop and then obtaining the best engine and vehicle performance (SP-8110, 1974). According to Humble et al. (1995) for a preliminary estimate the following values can be used:

$$p_{Tr} = \begin{cases} 1.5, & \text{if staged-combustion or expander cycles,} \\ 20, & \text{if gas generator cycle.} \end{cases}$$

To model a thermodynamic rocket cycle, a power balances must be performed. So assuming that a single shaft turbopump (a turbine drives each pump) is used and the the mechanical loss ($\eta_m = 1.0$) is negligible, the power of the turbine must be equal the power used by the pump:

$$\eta_m P_T = P_P \quad (3.10)$$

or

$$P_{req} = \frac{g_0 \dot{m} H_p}{\eta_p} = \eta_T \dot{m}_T c_p T_i \left[1 - \left(\frac{1}{p_{Tr}} \right)^{(\gamma-1)/\gamma} \right] \quad (3.11)$$

For a geared turbopump at design operating point Walsh and Fletcher (2008) state a typical mechanical efficiency between 97.5 and 99%.

The design goal of a given cycle is function of the arrangement between turbine and thrust chamber, i.e., if the cycle is open (turbine and thrust chamber are in parallel) or if the cycle is closed (turbine and thrust chamber are in series). For a gas-generator cycle, the turbine is in parallel with the thrust chamber, and the drive gases are either dumped overboard or injected in the divergent section of the nozzle, then the secondary flow gives a loss in efficiency (it means reduction of 1-2.5% of the overall I_{sp}). Thus the design goal for this cycle is to minimize turbine flow rate. For closed cycles (e.g., staged-combustion and expander cycles), as the turbine is in series with the thrust chamber, the negative impact of turbine mass

flow rate on engine efficiency no longer exists. However, a pressure drop increment through the turbine takes place and, hence, the design goal of an open cycle is to minimize turbine pressure ratio. To estimate the design parameters of a turbopump, the engine cycle and type of propellant must be taken into account. Recommended design parameters are summarized in Table 3.1.

Table 3.1 - Typical design parameter values for turbopump of a liquid rocket engine.

parameter	Gas generator cycle	Staged combustion cycle	Expander cycle
η_P [-]	0.80 (0.75 for hydrogen)	0.80 (0.75 for hydrogen)	-
η_T [-]	0.70	0.80	-
p_{Tr} [-]	20*	1.5-2.0	1.5-2.0
T_i [K]	1100	1100	250-650

*Overall ratio for turbines in series. For LH2/LOX turbines, the individual ratios are around 2.5 and 8.0, respectively and for RP-1/LOX are about 4.0 and 5.0.

SOURCE: [Humble et al. \(1995\)](#)

Just like the pump has a parameter (stage-specific speed) that can be used to estimate its efficiency, the turbine has the theoretical gas spouting velocity C_0 . In [Humble et al. \(1995\)](#) is presented a method to estimate the efficiency of the turbine based on C_0 . The spouting velocity derived from enthalpy drop is defined as that velocity which will be obtained during an isentropic expansion of the gas from the turbine inlet conditions to the turbine exit static pressure at the rotor blade inlet ([HUMBLE et al., 1995](#); [HUZEL](#); [HUANG, 1992](#)):

$$C_0 = \sqrt{2c_p T_i \left[1 - \left(\frac{1}{p_{Tr}} \right)^{(\gamma-1)/\gamma} \right]} \quad (3.12)$$

Thrust of the Nozzle Turbine

For an open cycle a relatively small amount of thrust can be delivered by a nozzle coupled with the turbine outlet. To determine the thrust of the turbine nozzle, one can make use of the thrust coefficient $C_{f,T}$ and characteristic velocity c^* (see Section 3.2.3). In [Schmucker \(1973\)](#) the following equations are presented:

$$C_{fT} = \sqrt{\frac{2\gamma^2}{\gamma-1} \left(\frac{2}{\gamma+1}\right)^{(\gamma+1)/(\gamma-1)} \left[1 - \left(\frac{p_e}{p_{T_e}}\right)^{(\gamma-1)/\gamma}\right]} + \left(\frac{p_e - p_a}{p_{T_e}}\right) \frac{A_e}{A_t} \quad (3.13)$$

where A_t is the throat area, A_e is the nozzle exit area, p_e is the nozzle exit pressure and p_a is the ambient pressure. The turbine pressure ratio can be given as (see Figure 3.2):

$$\frac{p_e}{p_{T_e}} = \left(\frac{p_g}{p_{T_e}}\right) \left(\frac{p_c}{p_g}\right) \left(\frac{p_e}{p_c}\right) \quad (3.14)$$

The pressure ratio p_e/p_c can be formulated as (SCHMUCKER, 1973):

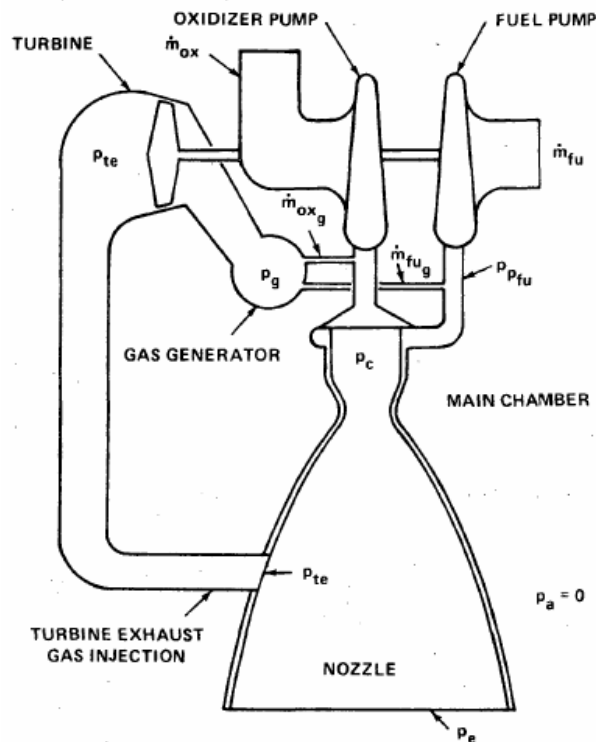


Figure 3.2 - Gas generator cycle with gases from turbine injected part way down the skirt of the nozzle.

SOURCE: Schmucker (1973)

$$\frac{p_e}{p_c} = - \exp \left[(1.38 - 5.68 \times 10^{-4} r_c) \ln \left(\frac{A_e}{A_t} \right) + 1.58 - 0.1(r_c - 3) \left(\frac{p_c}{70 \times 10^4} \right)^{-0.555} \right] \quad (3.15)$$

The nozzle expansion ratio can be given by:

$$\epsilon_T = \frac{A_e}{A_t} = \left(\frac{2}{\gamma + 1} \right)^{1/\gamma+1} \left(\frac{p_{Te}}{p_e} \right)^{1/\gamma} \left\{ \frac{\gamma + 1}{\gamma - 1} \left[1 - \frac{1}{p_{Te}/p_e} \right]^{\gamma-1/\gamma} \right\}^{-1/2} \quad (3.16)$$

3.1.3 Booster Turbopump

In a few applications, in order to prevent cavitation in the main pump an increase in pump inlet pressure can be carried out. To this end, one of the following approaches can be chosen:

- Increase the propellant tanks pressure
- Add an auxiliary turbopump

The first option implies an extra structural mass of the tanks. So to minimize the structure mass, the second approach is usually chosen. According to [Sutton and Biblarz \(2010\)](#), a typical booster-turbopump can provide about 10% of the required pump pressure rise and then the main pump would be responsible for the remaining 90%. Important applications of booster-turbopumps can be seen in the American Space Shuttle Main Engine (SSME) and the Russian RD-170.

3.2 Thrust Chamber

The thrust chamber assembly consists of combustion chamber, nozzle and igniter. In the thrust chamber the propellants that come from the feed system, are injected, atomized, mixed and burned to turn into hot gases that are ejected at high speeds. By the principle of conservation of energy, it can be understood that in the thrust chamber occurs a conversion of random motion of the molecules at high speeds (heat) into an ordered stream of gas at high speed (kinetic energy). As it is not possible to model the real behavior of the fluid flow inside the thrust chamber, to derive the theory the following assumptions must hold:

- Chemical equilibrium within the combustion chamber and frozen flow through the nozzle.
- Steady-state flow.
- Unidimensional flow.
- The fluid obeys the ideal gas law.
- Isentropic flow, i.e. the flow is reversible and adiabatic. From adiabatic it is meant that there is no heat loss to the surroundings. For large rockets the heat lost to the walls is usually less than 1% (SUTTON; BIBLARZ, 2010). The second assumption says that irreversible phenomena can be neglected, i.e. the friction and fluid viscosity are not considered and does not occur shock waves as well.

3.2.1 Rocket-Thrust Equation

The thrust equation can be derived from the Newton's second law which states, in an inertial reference frame, that the net force is equal to rate of change of momentum (product of the velocity and mass). In a rocket the flow of gases from combustion causes a reaction force (thrust) on the structure, thus:

$$F = -\frac{d(mv_e)}{dt} \quad (3.17)$$

where v_e is the exhaust velocity of the gases assuming optimum expansion $p_e = p_a$ (see Figure 3.3). As the steady state condition was assumed in the beginning of this chapter:

$$F = -\frac{d(m)}{dt}v_e = \dot{m}v_e \quad (3.18)$$

In the next two sections, rocket performance parameters will be presented in which the thrust F can be deduced, namely:

- Specific impulse
- Effective exhaust velocity
- Characteristic velocity

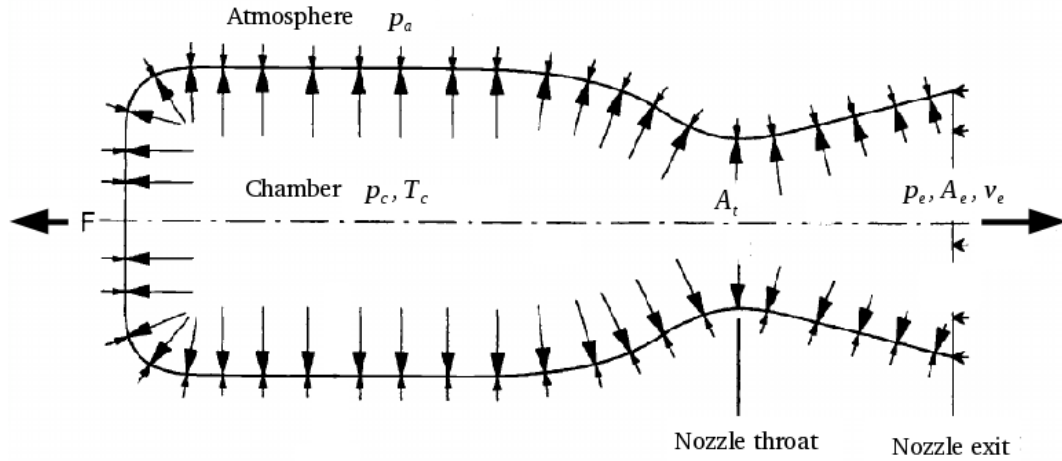


Figure 3.3 - Pressure balance on the thrust chamber walls.
SOURCE: Huzel and Huang (1992)

- Thrust coefficient

3.2.2 Specific Impulse and Effective Exhaust Velocity

One of the key parameters to estimate the performance of a rocket engine is the specific impulse I_{sp} , which is defined as the total impulse per unit weight of the propellant

$$I_{sp} = \frac{\int_0^{t_b} F dt}{g_0 \int_0^{t_b} \dot{m} dt} \quad (3.19)$$

where F is the thrust force integrated over propellant burn time t_b , and \dot{m} is the mass flow rate of burned propellant. However, as aforementioned, steady flow was assumed, so the parameters are not time-dependent, thus:

$$I_{sp} = \frac{F}{g_0 \dot{m}} \quad (3.20)$$

$$F = \dot{m} I_{sp} g_0 \quad (3.21)$$

A better way to visualize this important parameter is by the following relation

$$I_{sp} = \frac{c}{g_0} \quad (3.22)$$

where c is the effective exhaust velocity of the flow [m/s]. So the I_{sp} is can be seen as measure of the exhaust velocity. In Russian literature c is usually used instead of I_{sp} . Replacing I_{sp} from Eq. 3.4 into Eq. 3.21 the thrust force turns

$$F = \dot{m}c \quad (3.23)$$

3.2.3 Thrust Coefficient and Characteristic Velocity

The thrust coefficient C_f is defined as thrust divided by the chamber pressure p_c . This parameter has values ranging from 0.8 to 1.9 (SUTTON; BIBLARZ, 2010). Another way to represent C_f is given by the following equation:

$$C_f = \sqrt{\frac{2\gamma^2}{\gamma-1} \left(\frac{2}{\gamma+1}\right)^{(\gamma+1)/(\gamma-1)} \left[1 - \left(\frac{p_e}{p_c}\right)^{(\gamma-1)/\gamma}\right]} + \left(\frac{p_e - p_a}{p_c}\right) \frac{A_e}{A_t} \quad (3.24)$$

As stated before, the thrust can also be obtained from C_f by:

$$F = C_f A_t p_c \quad (3.25)$$

The characteristic velocity c^* is basically a function of the propellant characteristics and combustion chamber design; it is independent of nozzle characteristics. Thus, it can be used as a figure of merit in comparing propellant combinations and combustion chamber designs.

$$c^* = \frac{p_c A_t}{\dot{m}} = \frac{\eta_c^* \sqrt{\gamma R T_c}}{\left(\frac{2\gamma}{\gamma+1}\right)^{(\gamma+1)/(2\gamma-2)}} \quad (3.26)$$

The first version of this equation is general and allows the determination of c^* from experimental data of \dot{m} , p_1 , and A_t . The last version gives the maximum value of c^* as a function of gas properties, namely γ , the chamber temperature T_c , and the

molecular mass M (SUTTON; BIBLARZ, 2010).

The properties of combustion gases, namely molar mass M , nozzle exit pressure p_e and combustion temperature T_c are calculated using the software CEA.

Finally, from both rocket parameters:

$$F = \dot{m}C_f c^* \quad (3.27)$$

3.2.4 Real Rocket

To take into account deviations from the ideal behavior, correction factor must be included. When one makes use of the CEA program, the output results are theoretical and must be corrected. In the framework of this thesis, the interest is on the rocket performance parameters related to combustion chamber and nozzle extension which are c^* and C_f , respectively. Losses associated with the combustion process η_{comb} can be modeled establishing a suitable efficiency factor to the characteristic velocity term. Based on literature the value of 0.98 was conveniently chosen (SUTTON; BIBLARZ, 2010), (CASTELLINI, 2012). To correct the remaining parameter C_f , two contributions were implemented. Losses due to nozzle geometry can be correct introducing the nozzle efficiency:

$$\eta_{nozzle} = \begin{cases} 0.992, & \text{if bell-shaped,} \\ (1 + \cos \theta_{cn})/2, & \text{if conical.} \end{cases}$$

where $\cos \theta_{cn}$ is the nozzle cone half angle which typically ranges from 12 to 18 degree (HUMBLE et al., 1995). Finally, to deal with losses due to viscous effects, an efficiency of 0.986 was defined (CASTELLINI, 2012) which in turn took from (O'LEARY; J.E., 1992). Thus, the real specific impulse can be given by:

$$I_{sp} = \frac{\eta_{comb}\eta_{nozzle}\eta_{viscous}c^*C_f}{g_0} \quad (3.28)$$

3.2.5 Approximate Equations for Parameters from Combustion

The CEA program is the standard tool to compute properties of gas from combustion. The ideal case would be to completely integrate this tool in the modeling equations. Another approach commonly used in the literature is to work with data

generated from CEA simulations. For LOX/LH2, Schmucker (1973) derived closed forms for the thermodynamics properties:

$$c^* = \frac{3660 - 160r_c \left(\frac{p_c}{70 \times 10^4}\right)^{-0.022}}{1 + 1/r_c} \quad (3.29)$$

$$\gamma = \exp \left[0.00534 \ln \frac{A_e}{A_t} + 0.234 - 0.0311(r_c - 3) \left(\frac{p_c}{70 \times 10^4}\right)^{-0.0555} \right] \quad (3.30)$$

$$\frac{p_e}{p_c} = - \exp \left[(1.38 - 5.68 \times 10^{-4}r_c) \ln \left(\frac{A_e}{A_t}\right) + 1.58 - 0.1(r_c - 3) \left(\frac{p_c}{70 \times 10^4}\right)^{-0.555} \right] \quad (3.31)$$

The Equation 3.29 is valid for a mixture ratio ranging from 4 to 7 and $50 \leq p_c \leq 300$ bar. In addition to these limits, Equations 3.30 and 3.31 are applicable for nozzle expansion ratio within the ranges of 50 to 500.

Although this approach is less accurate, for preliminary design it is a good option for simplifying calculations.

3.2.6 Performance Optimization

Normally a liquid rocket engine does not operate with the proportion of propellants in the stoichiometric mixture ratio. For example, the stoichiometric mixture ratio of the propellants LOX/LH2 is 8.0, however, its operational mixture ratio for high-performance typically ranges between 4.5 and 6.0 (SCHLINGLOFF, 2005). The fact of the operational engines operate in this range (fuel-rich) is due to two conflicting considerations:

- Size of molecules from combustion. Fuel-rich allows lightweight molecules such as hydrogen to remain unreacted; this reduces the average molecular mass of the reaction products, which in turn increases the specific impulse.
- Density of the propellants. Fuel-rich promotes also the drawback of increasing fuel tank mass and size, resulting in a lower vehicle velocity increment and a higher vehicle drag (less net thrust).

In Figure 3.4 the influence of mixture ratio r_c on the rocket performance c is shown.

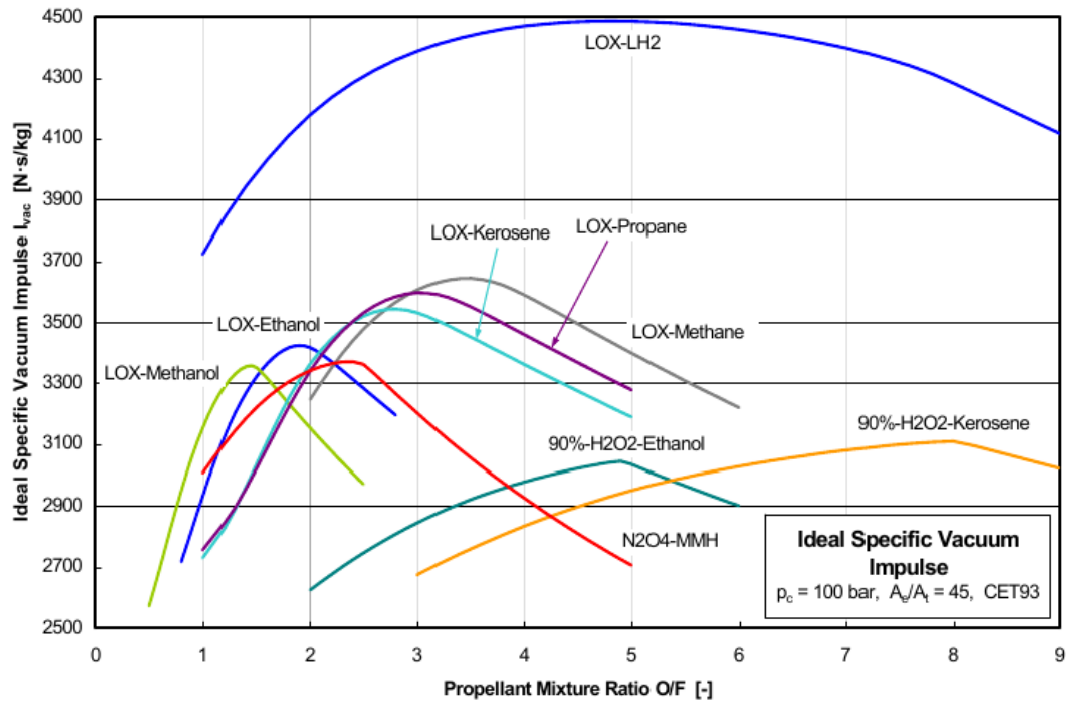


Figure 3.4 - Propellant combination performance.
SOURCE: Haidn (2008)

From the Figure 3.4 it can be seen that, concerning the performance, the cryogenic propellants LOX/LH2 prevails over the remaining propellant combinations. Although LOX-Ethanol combination which will be used in the rocket engine L75 shows an intermediate performance, it is important to highlight the handling advantage of being a semi-cryogenic combination.

3.3 Gas Generator or Pre-burner

The gas generator or the pre-burner operate exactly the same way, they are responsible to burn an amount of propellant in order to drive the turbine(s) by means of gases from combustion. The difference between them is that the gas generator is applied for open cycle engines and the pre-burner performs a first stage of combustion, i.e., this mixture is not dumped off, it is completely burned in the combustion chamber instead.

To obtain the properties of the gases from combustion, as for the combustion chamber, the software CEA can be used. However, it is important to point out that CEA does not work properly with long organic molecules when used in fuel rich application. This problem was also verified by Kauffmann et al. (2001) and a method was

presented to circumvent the anomaly.

For the gas generator, as mentioned before, about 2-5% of the propellant bypasses the thrust chamber to feed the turbine, this implies an reduction of 1-2.5% of the overall I_{sp} , thus the design goal for this cycle is to minimize turbine flow rate. Instead, for a pre-burner, as the turbine works in series with the thrust chamber, there is no flow rate constraint.

3.4 Injector Head

The injector is responsible to accelerate the propellants through small holes in order to atomize them inside the combustion chamber. As a rule thumb, the pressure drop across injector head Δp_{inj} is some percentage of the chamber pressure (HUMBLE et al., 1995):

$$\Delta p_{inj} = \begin{cases} 0.20p_c, & \text{if unthroattled,} \\ 0.30p_c, & \text{if throattled,} \\ \text{as low as } 0.05p_c, & \text{if pintle-type.} \end{cases}$$

Some amount of pressure drop is desirable to isolate chamber-pressure oscillations from the feed system, reducing coupling between the combustion chamber and the feed system. An alternative relation can be given as (KESAEV; ALMEIDA, 2005):

$$\Delta p_{inj} = \begin{cases} 0.8 \times 10^2 \sqrt{10p_c}, & \text{if liquid propellant,} \\ 0.4 \times 10^2 \sqrt{10p_c}, & \text{if gas propellant.} \end{cases}$$

where p_c is given in [Pa]. A detailed modeling of the injector is not within the scope of this work. Only the pressure drop which can be a user defined or given by the correlations above (rough estimation) are of interest in this work.

3.5 Heat Exchanger

The heat exchanger (or cooling system) is responsible to absorb heat from the walls of the thrust chamber in order to prevent the wall material from change phase, i.e., the material can be melted or even evaporated. The most used and efficient for a LRE is the regenerative cooling system where the working fluid (usually the fuel) exchanges heat from the thrust chamber and then the fluid is burned in the combustion chamber. With this cooling system all heat absorbed can be used for purposes

of propulsion, hence the name “regenerative”. Another common cooling system is the so-called dump cooling, which drop off at supersonic speeds the propellant overboard. Because such a high speed, normally a small portion of thrust is generated as illustrated in Figure 3.5). Although the propellant remains unburned, the heated propellant can give very reasonable values of specific impulse therefore the negative impact on the overall specific impulse is little if any (PAVLI; CURLEY, 1966). The performance of the dumped coolant as shown in Figure 3.6 increases with increasing temperature.

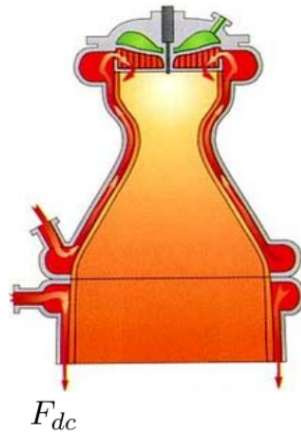


Figure 3.5 - Dump Cooling.
SOURCE: Boeing Engineering (2015)

According to Humble et al. (1995), pressure drops in the cooling jacket Δp_{cool} can vary between 10% and 20% of the chamber pressure p_c and then, for preliminary analysis the author suggests:

$$\Delta p_{cool} = 0.15 p_c \quad (3.32)$$

In Kesaev and Almeida (2005) the following range can be found:

$$\Delta p_{cool} = \begin{cases} (0.25 - 0.30) p_c, & \text{if } p_c < 80 \text{ MPa,} \\ (0.30 - 0.35) p_c, & \text{if } p_c > 80 \text{ MPa.} \end{cases}$$

In this work Δp_{cool} will be an input given by the user, but if no input are given, it will be used a simple relation function of the chamber pressure as the ones previously

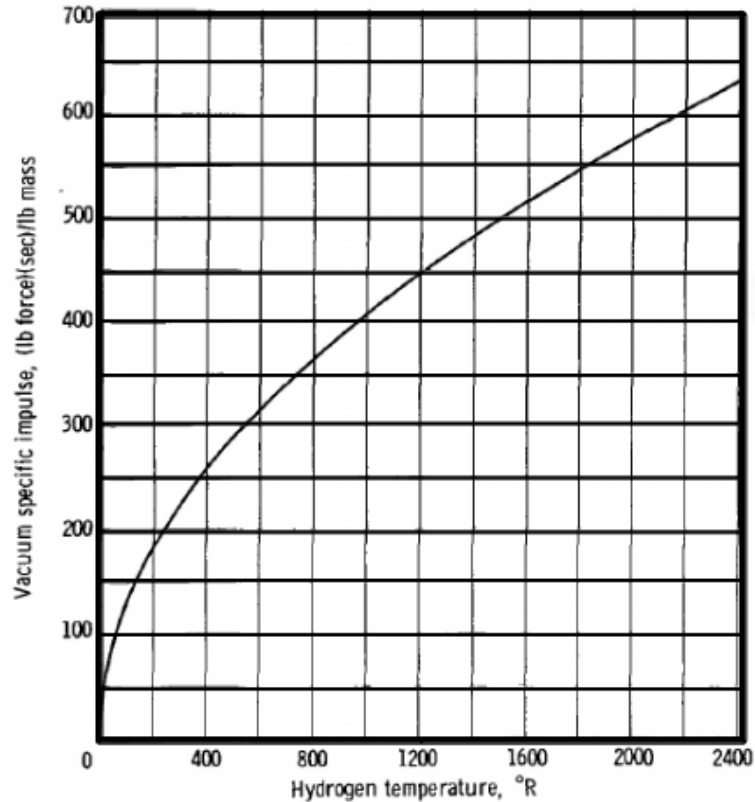


Figure 3.6 - Theoretical vacuum specific impulse of dumped hydrogen through infinite area ratio nozzle.

SOURCE: Pavli and Curley (1966)

presented.

3.6 Pipe System: Feed Lines and Valves

The feed system is responsible to conduct the propellants to the thrust chamber providing enough pressure energy to overcome all the pressure losses in the lines and components and reaching the established combustion chamber pressure (p_c). The required pump discharge pressure is determined from the chamber pressure and the hydraulic losses in valves, lines, cooling jacket (for the fuel), and injector head. To obtain the rated flow at the rated pressure, an additional adjustable pressure drop for a flow orifice is usually included which permits a calibration adjustment or change in the required feed pressure (SUTTON; BIBLARZ, 2010). For a gas generator cycle, the stagnation pressure drop of the propellants between the pump discharge and the combustion chamber is the sum of pressure drop in pipes, valves, elbows, cooling system (for the fuel) and injectors.

$$p_{pump,f} - p_c = \Delta p_{f,lines} + \Delta p_{f,valves} + \Delta p_{f,cool} + \Delta p_{f,inj} \quad (3.33)$$

$$p_{pump,o} - p_c = \Delta p_{o,lines} + \Delta p_{o,valves} + \Delta p_{o,inj} \quad (3.34)$$

The pressure drops in the right side of the equations can be estimated by relations that are function of chamber pressure.

3.6.1 Feed Lines

In [Kesaev and Almeida \(2005\)](#) is given the following relation for the pressure drop through the hydraulic lines:

$$\Delta p_{lines} = (0.05 - 0.1)p_c \quad (3.35)$$

and for duct gas (section between turbine and thrust chamber for a closed engine cycle) the equations are:

$$\Delta p_{duct}^{gas} = \begin{cases} 0.025p_c, & \\ 0.15p_c, & \text{if distribution grid are used..} \end{cases}$$

[Humble et al. \(1995\)](#) recommends in his book the following values

$$\Delta p_{lines} = \begin{cases} 30 \text{ kPa,} & \text{If desired to be aggressive, or if the lines are relative short,} \\ 50 \text{ kPa,} & \text{If desired to be conservative, or the lines are relative long.} \end{cases}$$

In this thesis all the pressure drop in the feed system are user input, but if no value is given, the simple relations previously presented are assumed. Because of the lack of data about dimensions of the feed system, such as length of pipes, number of elbows, and so on, a detailed modeling of the feed system is out of the scope of this work. Nevertheless, a brief about the theory involved is discussed below. Assuming steady incompressible fully developed flow, from the energy equation applied between two

sections (see Figure 3.7) or between two components of a LRE (MUNSON et al., 2009):

$$\left(\frac{p}{\rho g_0} + \frac{v^2}{2g_0} + z \right)_1 = \left(\frac{p}{\rho g_0} + \frac{v^2}{2g_0} + z \right)_2 + h_L \quad (3.36)$$

where h_L is the head loss between sections (1) and (2). In rocket system, normally the cross sectional area is constant, so that the flow velocity does not change and then the term of kinetic energy can be discarded. The elevation change is also small in comparison with the pressure drop, thus:

$$\Delta p = p_1 - p_2 = \rho g_0 h_L \quad (3.37)$$

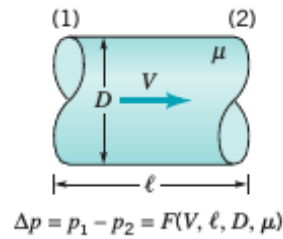


Figure 3.7 - Pipe section.
SOURCE: Munson et al. (2009)

As presented in Figure 3.7, the pressure drop between the sections (1) and (2) can be written in functional form as (MUNSON et al., 2009):

$$\Delta p = F(v, D, l, \epsilon, \mu, \rho) \quad (3.38)$$

From dimensional analysis:

$$\Delta p = f \frac{l}{D} \frac{\rho v^2}{2} \quad (3.39)$$

where

f = Darcy friction factor [-]

l = length of the pipe [m]

D = pipe diameter [m]

ϵ = measure of the roughness of the pipe wall [-]

μ = viscosity of the fluid [Pa.s]

Pressure drops can also be associated with split flow (see Figure 3.8) and elbows (Figure 3.9). In order to minimize the pressure drop in an elbow, vanes can be used.

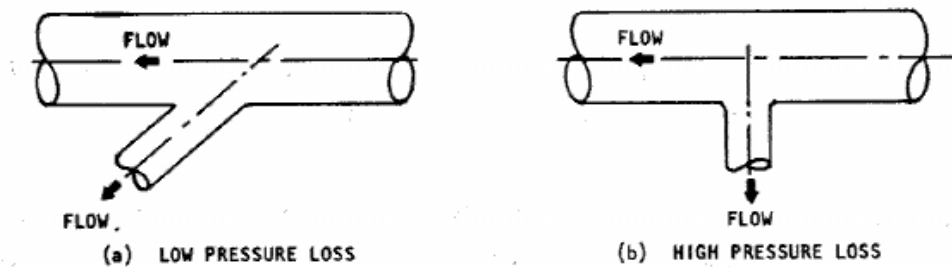


Figure 3.8 - Pressure loss in a tap-off branch related to configuration of the branch.
SOURCE: SP-8123 (1977)

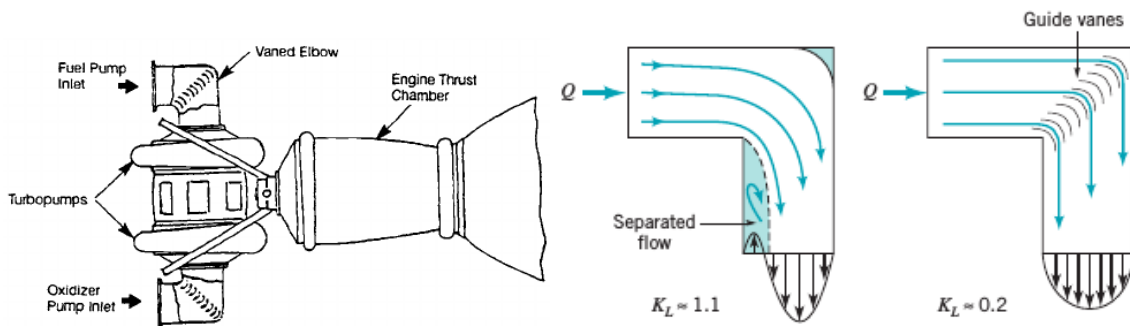


Figure 3.9 - (a) Flow guide vanes in sharp elbows of pump inlet lines (b) Flow without and with guide vanes.
SOURCE: (a) SP-8123 (1977)(b) Munson et al. (2009)

3.6.2 Valves

The valves are devices to control the fluid flow. The main valves used in rocket application are (SP-8097, 1973):

- Poppet (including cavitating venturi)
- Butterfly
- Ball
- Blade (rotary or linear)
- Sleeve (linear travel or rotary travel)
- Spool, cylindrical slide or piston (sequence valves)
- Plug (explosive-actuated normally open valve)
- Blade (rotary or linear)

In this work no distinction among the types of valves used will be made. Concerning the valves, only the pressure drop which in turn will be a parameter given by the user are of interest in this work.

4 MASS MODELING

There are numerous relations for estimating engine and stage mass in the literature, but most of them have a common approach - they are based on historical and empirical data. This chapter is divided into three sections, the first two of them are devoted to estimate engine and stage dry mass and the last section describes the mass distribution of a launch vehicle. To estimate the engine and stage dry mass two methodologies will be considered.

4.1 Estimate Engine Mass

For engine we understand the feed system and the thrust chamber assembly. The tanks of propellants and inert gas are not taken into account.

4.1.1 Simple Relations

Although the mass and envelope of a liquid rocket engine depends on many parameters (e.g., cycle, propellant combination, material, technology), for a quick estimation the thrust magnitude is sufficient for a conceptual design. In other words, the mass and dimensions of existing and historical liquid rocket systems can be given as simple functions of the thrust magnitude (HUMBLE et al., 1995). It must be pointed out that real mass can deviate drastically from this rough estimation. Making use of least square fit of engines data, Humble et al. (1995) presents the following equations for launch-vehicle, space bi-propellant and mono-propellant engines:

I. Launch-vehicle engines

$$m_{eng} = \frac{F}{g_0(25.2 \log F - 80.7)} \quad (4.1)$$

II. Space bipropellant engines

$$m_{eng} = \frac{F}{g_0(0.0006098F + 13.44)} \quad (4.2)$$

III. Monopropellant engines

$$m_{eng} = \frac{F}{g_0[-3.7405 \times 10^{-10}F^4 + 7.1685 \times 10^{-7}F^3 - 5.2221 \times 10^{-4}F^2 + 0.18761F - 0.039763]} \quad (4.3)$$

Taken into account the type of propellant, chamber pressure p_c [bar], the nozzle area expansion ratio A_e/A_t , and the number of thrust chamber N , in [Ernst \(2014\)](#) in turn taken from [Zandbergen \(2013\)](#) is presented the following relations:

- Pressure fed

$$m_{eng} = \begin{cases} 0.1005F^{0.6325}, & \text{if storable propellant,} \\ \text{no relation given,} & \text{if other.} \end{cases}$$

- Turbo-pump fed

$$m_{eng} = \begin{cases} 0.006F^{0.858}p_c^{0.117}(A_e/A_t)^{0.034}, & \text{if cryogenic,} \\ (0.001F + 49.441)N^{0.030}(A_e/A_t)^{0.004}, & \text{if storable or semi-cryogenic.} \end{cases}$$

Using a data base with 51 LRE, linear, quadratic, power law and logarithmic curves were analyzed in [Castellini \(2012\)](#). The best resulting regression in terms of quadratic fit error for each technology were implemented within the propulsion models [see [Table 4.1](#)].

4.1.2 Detailed Relations

Another way to estimate the engine mass is calculating the mass of the basic components of the engine and then summing them. However, unfortunately the total engine mass is not simply given by the sum of the basic components. Some major components such as the electrical system, the hydraulic control system and the flight instrumentation system and minor components such as igniter and starter are not taken into account. Thus, this can cause large dispersion to the actual value. The

Table 4.1 - Relations for the main engine's mass of different types of rocket engine cycles.

Prop	Feed	T_{vac} [kN]	Components	N_{LRE}	WER equations (M_{WER} in [kg], T_{vac} in [N])
Cryogenic	SC	[500; 5000]	Pre-combustor(s) & turbopump(s) Valves and piping Injector and igniter Thrust chamber	5	$M_{WER} = a \cdot (T_{vac})^b + c$ $\begin{cases} a = -1.17899e+008 \\ b = -7.380845e-001 \\ c = +6.09805e+003 \end{cases}$
Cryogenic	EC	[50; 300]	Turbopump(s) Valves and piping Injector and igniter Thrust chamber	5	$M_{WER} = a \cdot (T_{vac})^b + c$ $\begin{cases} a = -9.76421e+004 \\ b = -4.27622e-001 \\ c = +8.97980e+002 \end{cases}$
Cryogenic	GG	[0; 8000]	Gas-generator(s) & turbopump(s) Valves and piping Injector and igniter Thrust chamber	6	$M_{WER} = a \cdot (T_{vac})^b + c$ $\begin{cases} a = 7.54354e-003 \\ b = 8.85635e-001 \\ c = 2.02881e+001 \end{cases}$
Cryo-Storable	SC	[0; 10000]	Pre-combustor(s) Turbopump(s) Valves and piping Injector and igniter Thrust chamber	8	$M_{WER} = a \cdot (T_{vac})^b + c$ (a_1, b_1, c_1) for $T_{vac} < 2050$ kN $\begin{cases} a_1 = 8.51852e-003 & a_2 = +1.65368e+000 \\ b_1 = 8.52826e-001 & b_2 = +5.69842e-001 \\ c_1 = 1.06632e+002 & c_2 = -4.37849e+003 \end{cases}$
Cryo-Storable	GG	[200; 2000]	Gas-generator(s) & turbopump(s) Valves and piping Injector and igniter Thrust chamber	5	$M_{WER} = a \cdot (T_{vac})^b + c$ $\begin{cases} a = +3.75407e+003 \\ b = +7.05627e-002 \\ c = -8.84790e+003 \end{cases}$
Cryo-Storable	PF	[0; 400]	Valves and piping Injector and igniter Thrust chamber	5	$M_{WER} = a \cdot (T_{vac})^2 + b \cdot T_{vac} + c$ $\begin{cases} a = -2.13325e-009 \\ b = +1.70870e-003 \\ c = +6.38629e+000 \end{cases}$
Storable	SC	[0; 5000]	Pre-combustor(s) & turbopump(s) Valves and piping Injector and igniter Thrust chamber	5	$M_{WER} = a \cdot (T_{vac})^b + c$ $\begin{cases} a = +4.74445e-001 \\ b = +5.35755e-001 \\ c = -7.73681e+000 \end{cases}$
Storable	GG	[0; 3000]	Gas-generator(s) & turbopump(s) Valves and piping Injector and igniter Thrust chamber	6	$M_{WER} = a \cdot (T_{vac})^b + c$ $\begin{cases} a = +6.37913e+000 \\ b = +3.53665e-001 \\ c = -1.48832e+002 \end{cases}$
Storable	PF	[0; 150]	Valves and piping Injector and igniter Thrust chamber	6	$M_{WER} = a \cdot (T_{vac})^2 + b \cdot T_{vac} + c$ $\begin{cases} a = -3.36532e-008 \\ b = +4.74402e-003 \\ c = -1.93920e+001 \end{cases}$

SOURCE: Castellini (2012)

usual approach makes use of regression techniques to fit a curve to data obtained from historical rocket engines. Using SSME, J-2, HM-60, HM7, H20, RL-10 and ASE, [Felber \(1979\)](#) developed the following equation valid to thrust varying between 60 and 2091 kN . The following equation represents a so-called analytical/statistical model, which means it considers not only statistical data but also physical relationships. If m_{tp} = turbo-pump mass, m_{valve} = mass of all valves, m_{inj} = injector mass, m_{cc} = combustion chamber plus gas generator mass and m_{ne} = nozzle extension mass, we have:

$$m_{eng} = 1.34(m_{tp} + m_{valve} + m_{inj} + m_{cc} + m_{ne}) \quad (4.4)$$

where

$$m_{tp} = 0.18VF^{0.73}p_c^{0.69}$$

$$m_{cc} = 1.6(0.125P_1 + 0.147P_2F/p_c)(0.166p_c + 10 + 0.3\sqrt{Fp_c})$$

$$m_{ne} = \epsilon(F/p_c)(0.15 + K_{c1}0.025p_c^{K_{c2}})$$

$$m_{inj} = 1.1F/\sqrt{p_c}$$

$$m_{valve} = 0.07F^{0.7}p_c^{0.5}$$

$$V = \begin{cases} 1, & \text{if with boost-pumps,} \\ 0.5, & \text{if no boost-pumps.} \end{cases}$$

$$P_1 = \begin{cases} 1, & \text{if with pre-burner,} \\ 0.80, & \text{if no pre-burner.} \end{cases}$$

$$P_2 = \begin{cases} 1, & \text{if with pre-burner,} \\ 0.94, & \text{if no pre-burner.} \end{cases}$$

$$K_{c1} = \begin{cases} 1, & \text{if with regenerative cooling,} \\ 33, & \text{if with dump cooling.} \end{cases}$$

$$K_{c2} = \begin{cases} 1, & \text{if with regenerative cooling,} \\ 0, & \text{if with dump cooling.} \end{cases}$$

This model is sufficiently detailed when the influence of the engine parameters on the engine mass or payload mass are aim of study. Considering propellant type, feeding cycle, chamber pressure, and nozzle expansion ratio ϵ , [Schlingloff \(2005\)](#) proposed a similar model:

$$m_{eng} = 1.34(m_{tp} + m_{valve} + m_{inj} + m_{cc} + m_{ne}) \quad (4.5)$$

with

$$m_{tp} = C_{propellant} \cdot C_{tp}(F \cdot p_c)^{0.71}$$

$$m_{valve} = 0.02(F \cdot p_c)^{0.71}$$

$$m_{inj} = 0.25F^{0.85}$$

$$m_{cc} = 0.75F^{0.85}$$

$$m_{ne} = \epsilon F(0.00225C_{nozzle} + (0.225 - 0.075C_{nozzle})/p_c)$$

$$C_{propellant} = \begin{cases} 0.19, & \text{for high energetic propellant,} \\ 0.11, & \text{for low energetic propellant.} \end{cases}$$

$$C_{tp} = \begin{cases} 0.5, & \text{for with prepumps,} \\ 1.0, & \text{for no prepumps.} \end{cases}$$

$$C_{nozzle} = \begin{cases} 1.0, & \text{for regenerative cooling,} \\ 0.0, & \text{for dump cooling.} \end{cases}$$

Where the mass has dimensions of kilograms, the vacuum thrust F of the engine is specified in kN and the chamber pressure p_c in bar.

In both of the models the mixture ratio r_c has no influence. Thus, in order to take into account this parameter, we can replace the turbopump equation in [Schlingloff \(2005\)](#)'s model by a more generic equation which was taken from [Felber \(1979\)](#):

$$m_{tp} = \frac{0.178}{k_{TB}} \rho^{0.148} P_T^{0.73} \quad (4.6)$$

where

$$k_{TB} = \begin{cases} 1, & \text{if no boost-pumps,} \\ 2, & \text{if with boost-pumps.} \end{cases}$$

This equation is valid for power varying between 300 to 6×10^4 kW. As the turbopump mass equation was altered, the correction factor in Eq. 4.5 is no longer valid. To determine a new correction factor, the rocket engines HM7B, HM60, Le-5, J-2, H-1, and RS-27 were considered (see Table 4.2). The correction factor was determined by means of a curve fit to the actual versus calculated data (Figure 4.1), thus we finally have:

$$m_{eng} = 1.59921(m_{tp} + m_{valve} + m_{inj} + m_{cc} + m_{ne}) \quad (4.7)$$

Table 4.2 - Mass model validation.

LRE	propellant	actual [kg] (HUGH, 1995)	calculated [kg]	error %
HM7B	LOX/LH2	158.0	167.2	5.8
HM60	LOX/LH2	1719.0	1809.2	5.2
LE-5	LOX/LH2	255.0	324.2	27.1
J-2	LOX/LH2	1542.0	1440.4	6.6
H-1	LOX/RP-1	878.2	932.2	6.2
RS-27	LOX/RP-1	1146.6	1060.7	7.5

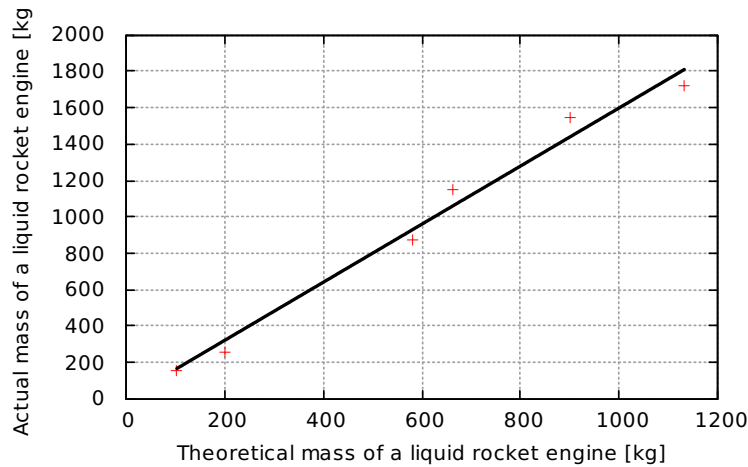


Figure 4.1 - Curve fit.

4.2 Propellant System Mass

To estimate the stage mass, two contributions are considered:

- Propellant mass
- Structural mass

In the book of [Humble et al. \(1995\)](#), the author states that for preliminary analysis, the mass of all the structural mounts and associated hardware can be assumed to be 10% of the inert mass (stage mass minus propellant and pressurant).

4.2.1 Simple Relations

In [Schlingloff \(2005\)](#) the dry mass of the stage can be calculated by the sum of engine mass m_{eng} , and structural mass of the propellant system m_{ps} , which is function of the propellant mass

$$m_{ps} = C \left(\frac{m_{prop}}{\rho} \right)^{0.666} \quad (4.8)$$

with

$$C = \begin{cases} 225, & \text{for } \rho \approx 280 \text{ kg/m}^3, \\ 350, & \text{for } \rho \approx 1220 \text{ kg/m}^3 \end{cases}$$

Existing hardware was used to find the constants in the model above: the constant C assumes approximately the value 225 for high energetic propellant and 350 for low energetic propellant.

4.2.2 Detailed Relations

As in the case of the engine, we can not estimate the stage dry mass simply adding the mass of the main components. Again the statistics plays an important role and historical data from rocket stages are a requisite. Thus, we can approach the problem by means of the following formulations:

- Estimate propellants tank mass and then with historical data use a regression to fit into a curve

- Estimate propellants and inert gas tank mass and then with historical data use a regression to fit into a curve

Thus, being cf a correction factor, the formulations can assume the forms, respectively

$$m_{ps} = cf(m_{tank,o} + m_{tank,f}) \quad (4.9)$$

$$m_{ps} = cf(m_{tank,o} + m_{tank,f} + m_{tank,gas}) \quad (4.10)$$

4.2.2.1 Propellant Tanks

For most applications, the walls of the tanks are outer-walls of the vehicle. They must provide the necessary strength to bending moments on the vehicle and they have to transfer the thrust. Depending on the feed system, the tank will be submitted to high or moderate internal pressures. For pressure-fed engines, where the tank has to overcome the chamber pressure and the pressure loss in feed lines, turbine (for closed cycles) and injector, the tank pressure may be as high as 60 bar. For pumped systems usually pressures up to 5 bar are sufficient. These tank pressures are necessary to suppress cavitation in the pumps inlet, but also to provide the vehicle a certain stiffness to withstand the flight loads (CORNELISSE et al., 1979). Basically in rocket applications we can find either tanks in cylindrical shape, in spherical shape or even toroidal shape, being the latter used exclusively for upper stages. It is known that the spherical shape provides the minimum mass per volume value, however due to diameter constraints, cylindrical tanks are preferred for first phases of the flight. Depending on the mission requirements a different arrangement of the propellants and inert gas tanks can be established as shown in Figure 4.2. Figure 4.2 (a) presents tandem arrangement which is the standard configuration. The lowest amount of mass is found with the arrangement of Figure 4.2 (b) but the expense of gain in complexity in design. Arrangements shown in Figures 4.2 (c) and (d) make easier the design but provide an extra amount of mass in order of 18 % and 62% respectively.

To calculate the tank mass we need to select a tank material (see Table 4.3), establish safety coefficients and to know propellant mass m_{prop} , mixture ratio r_c and stage diameter. The propellant volume can be calculated as:

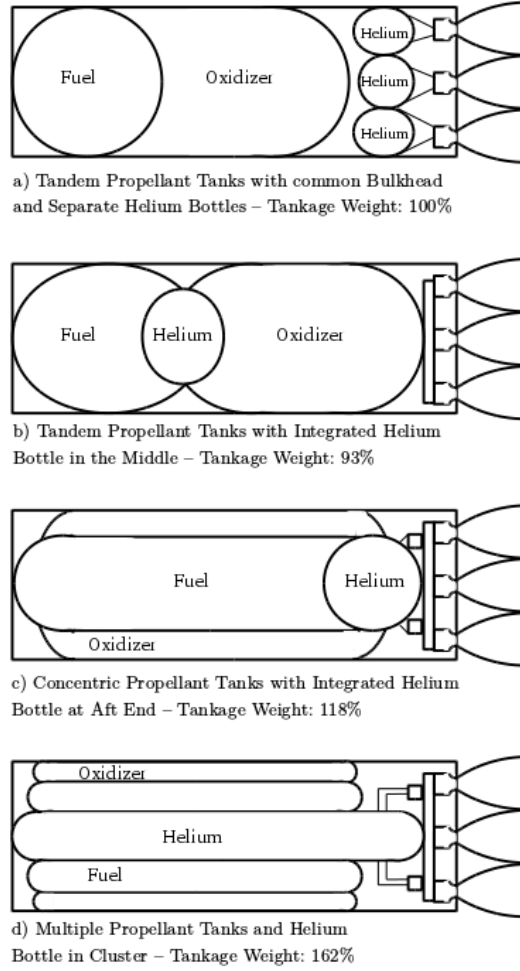


Figure 4.2 - Propellant tank configuration.

SOURCE: Adapted from Huzel and Huang (1992).

$$V_{ox} = \frac{1}{\rho_{ox}} \frac{m_{prop} r_c}{r_c + 1} \quad (4.11)$$

$$V_{fuel} = \frac{1}{\rho_{fuel}} \frac{m_{prop}}{r_c + 1} \quad (4.12)$$

Below equations to model spherical and cylindrical tanks in which are based on Humble et al. (1995) and Huzel and Huang (1992) are presented.

I. Spherical Tanks

The equations for a spherical tank are given as follows:

Table 4.3 - Tank Materials.

Material	ρ [kg/m ³]	F_{tu} [GPa]	$F_{tu}/\rho g_0$ [km]
2219-Aluminum	2800	0.413, 0.214 welded	15.04
Titanium	4460	1.23	28.81
4130 Steel	7830	0.862	11.23
Graphite	1550	0.895	58.88

SOURCE: Humble et al. (1995)

$$m_s = A_s t_s \rho_{mat} \quad (4.13)$$

$$V_s = \frac{4}{3} \pi r_s^3 \quad (4.14)$$

$$A_s = 4\pi r_s^2 \quad (4.15)$$

$$t_s = \frac{p_b r_s}{2F_{all}} \quad (4.16)$$

where

r_s - radius of the sphere [m]

A_s - surface area of the sphere [m²]

V_s - volume of the sphere [m³]

t_s - wall thickness of the sphere [m]

p_b - design burst pressure [Pa]

F_{all} - allowable material strength [Pa]

m_s - mass of a sphere tank [kg]

ρ_{mat} - density of the tank structure material [kg/m³]

II. Cylindrical Tanks

Here, the formulation is not so simple as the one previously presented, instead we must consider the length of the tanks and if the end shapes are spherical or elliptical. For the cylindrical section, the main equations are:

$$m_c = A_c t_c \rho_{mat} \quad (4.17)$$

$$V_c = \pi r_c^2 l_c \quad (4.18)$$

$$A_c = 2\pi r_c l_c \quad (4.19)$$

$$t_c = \frac{p_b r_c}{F_{all}} \quad (4.20)$$

where

r_c - radius of the cylindrical section [m]

l_c - length of the cylindrical section [m]

A_c - surface area of the cylindrical section [m²]

V_c - volume of the cylindrical section [m³]

t_c - thickness of the cylindrical wall [m]

p_b - design burst pressure [Pa]

F_{all} - allowable material strength [Pa]

m_c - mass of the cylindrical tank section [kg]

ρ_{mat} - density of the tank structure material [kg/m³]

To calculate the mass of end caps of the tank if we consider spherical ends, then the mass of both half simply given as the mass of a sphere, hence the formulation presented in the previous section can be used. A method to model elliptical shape

can be found in [Huzel and Huang \(1992\)](#), however this is out of scope of this work, thus only equations for spherical ends are implemented.

4.2.2.2 Propellant Mass

The design of a propellant tank is mainly influenced by physical and chemical characteristics of the propellants. The storage temperature or boiling point of a propellant gives the operating temperature range of the tank assembly. Cryogenic propellants bring greater complexity in tank design due to thermal gradients, need for insulation, and need for construction materials capable of remaining ductile at very low temperatures. For a given propellant, the density can be a limiting factor of engine performance, e.g., a certain mixture ratio r_c which gives the best performance I_{sp} directly affects the volume of the tanks which in turn can affect the launcher performance. The selection of tank materials must take into account non-desirable propellant properties of being highly corrosive or reactive ([HUZEL; HUANG, 1992](#)).

We can estimate the total propellant mass required from the ideal rocket equation ([HUMBLE et al., 1995](#)):

$$m_{prop} = \frac{m_{pl}[e^{\frac{\Delta V}{I_{spg0}}} - 1](1 - f_{inert})}{1 - f_{inert}e^{\frac{\Delta V}{I_{spg0}}}} \quad (4.21)$$

where

m_{prop} - total mass of propellant [kg]

m_{pl} - payload mass [kg]

ΔV - effective velocity change required [m/s]

f_{inert} - inert mass fraction, i.e., the inert mass of the stage divided by the total mass of the stage

The following equations give us the fuel and oxidizer mass

$$m_{fuel} = \frac{m_{prop}}{1 + r_c} \quad (4.22)$$

$$m_{ox} = m_{prop} \frac{r_c}{1 + r_c} \quad (4.23)$$

If we already know the mass flow rate of the propellants and the burn time, the mass of fuel and oxidizer can be simply calculated by:

$$m_{fuel} = \dot{m}_{fuel} \cdot t_b \quad (4.24)$$

$$m_{ox} = \dot{m}_{ox} \cdot t_b \quad (4.25)$$

4.3 Rocket Parameters

To correlate the mass distribution of the rocket with its performance some dimensionless parameters are defined. The initial mass of the rocket m_0 , can be divided into 3 parts: the payload mass m_{pl} the structural mass m_{struct} and the useful mass of propellant m_{prop} .

$$m_0 = m_{pl} + m_{struct} + m_{prop} \quad (4.26)$$

The structural mass m_{struct} is the mass of the vehicle structure, the mass of auxiliary structures such as pipes, thermal insulation, weight of installed equipment such as engine, guidance and control systems, pressurization systems and electrical and hydraulic power supply, and unconsumed mass of propellant, thus m_{prop} is not the total mass of propellants, but the useful mass of propellants. Now some dimensionless parameters related to these contribution mass can be defined:

Mass ratio:

$$\Lambda = \frac{m_0}{m_{pl} + m_{struct}} \quad (4.27)$$

Payload ratio:

$$\lambda = \frac{m_{pl}}{m_0} \quad (4.28)$$

Structural efficiency:

$$\epsilon = \frac{m_{struct}}{m_{struct} + m_{prop}} \quad (4.29)$$

Propellant ratio:

$$\phi = \frac{m_{prop}}{m_0} \quad (4.30)$$

5 ROCKET ENGINE CYCLES MODELING

This chapter describes a methodology to model and simulate liquid rocket engine cycles operating under steady-state condition. Although many methods and tools (both commercial and in-house) to model and simulate a powerhead of LRE do exist, there are not so many available works in the open literature. This fact is presumably due to sensitive technology characteristic. The basic ideas which this chapter is organized were taken from Silva (1995), Kesaev and Almeida (2005), Germain (2003), Goertz (1995), Bradford et al. (2004) and Matteo (2011) and the basic concepts were taken mainly from Sutton and Biblarz (2010), Humble et al. (1995) and Huzel and Huang (1992).

The modeling of a given cycle depends on the turbopump(s) arrangement (single or dual-shaft), if there is or not booster-turbopumps and split flows or bypass. In this work the cycles considered are:

- Gas Generator Cycle (GG)
- Expander Bleed Cycle (EB)
- Staged Combustion Cycle (SC)
- Expander Cycle (EC)

5.1 Basic Concepts

A liquid rocket engine can be divided into feed system and thrust chamber assembly. The feed system is responsible to lead the propellants to the thrust chamber providing enough pressure energy to overcome all the pressure losses in the lines and components and reaching the established combustion chamber pressure p_c . To provide such pressure energy, pressure-fed and turbopump fed system are the options available for launch vehicles technology.

To take a launch vehicle from the ground a sufficiently high amount of energy must be supplied. The heavy initial gross lift-off mass (GLOW) must be accelerated against a gravitational field and a dense atmospheric layer. This task is accomplished by first stages (e.g., booster stage or core stage) of launch vehicles which are equipped with turbopump fed engine cycle (solid engines are also used, mainly as booster stages). However, for upper stages of launch vehicles, moderate chamber pressure (or thrust) are usually sufficient, hence pressure-fed can also be used for this application.

The turbopump assembly (TPA) is designated to delivery the required energy to the propellants. Many configurations of turbopump fed cycle can be found in the literature, nevertheless most of them are derived from the traditional gas generator cycle (GG), staged combustion (SC), and expander cycle (EC). Another way to categorize the engine cycles is based on the turbine and thrust chamber arrangement. Within this framework, the cycles can be classified as open and closed.

5.1.1 Open Cycles

With this cycle the turbine is in parallel with the thrust chamber, and the drive gases are either dumped overboard or injected in the divergent section of the nozzle. A typical gas-generator cycle and an expander bleed cycle which is derived from the traditional expander cycle is schematically shown in Figure 5.1. Control valves are designated as MFV (main fuel valve), MOV (main oxidizer valve), GGFV (gas generator fuel valve), GGOV (gas generator oxidizer valve), CCV (cooland control valve) and OTBV (oxidizer turbine bypass valve).

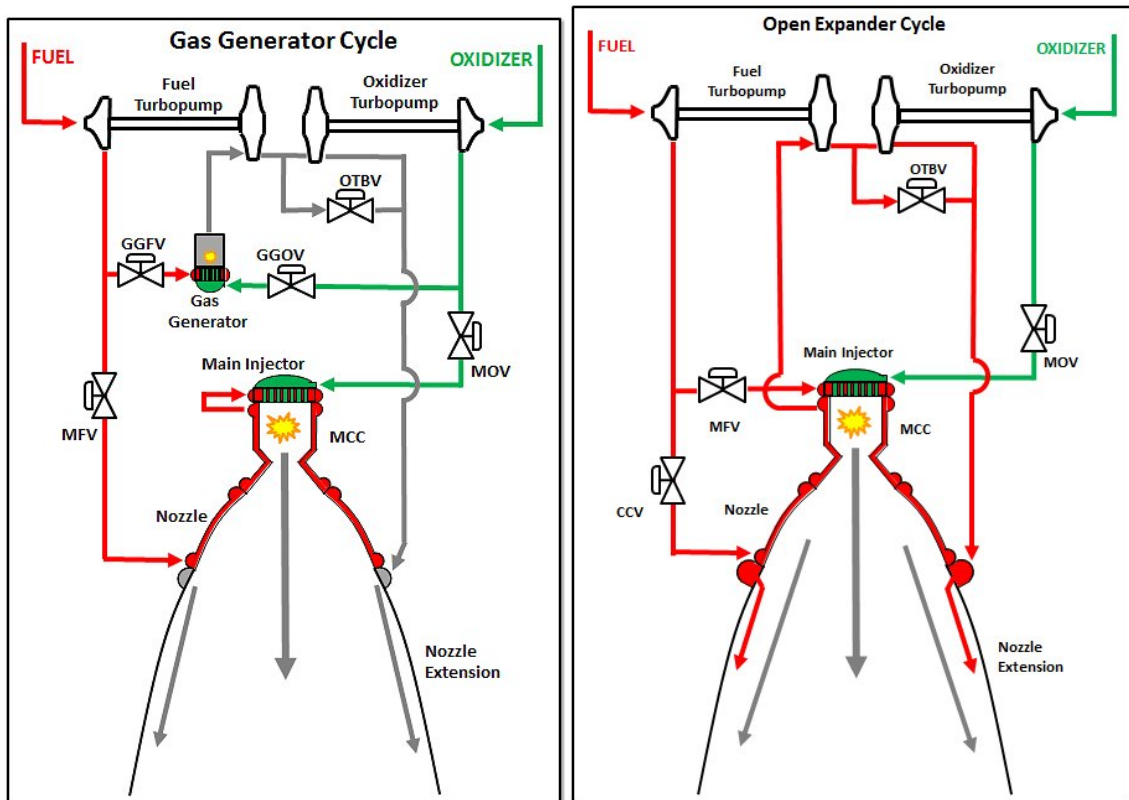


Figure 5.1 - Open Cycles. (a) Gas Generator (b) Expander Bleed.
SOURCE: (a)NASA (2015a) (b)NASA (2015b)

Usually the specific impulse generated by secondary flow of gases from turbine is the order of just one-half of the one generated in the main nozzle. This implies an overall reduction of 1-2.5% in specific impulse (HUMBLE et al., 1995). Thus, for this type of cycle is desired to minimize the turbine flow rate. The fact that the turbine is in parallel with the thrust chamber has also a bright side. Such arrangement brings simplification in design. As the turbine and thrust chamber are decoupled they can be tested separately.

5.1.2 Closed Cycles

With this arrangement the turbine is in series with the thrust chamber, thus the negative impact of turbine flow rate on engine efficiency no longer applies. The traditional expander and staged combustion cycles are the most used arrangement within this category (see Figure 5.2).

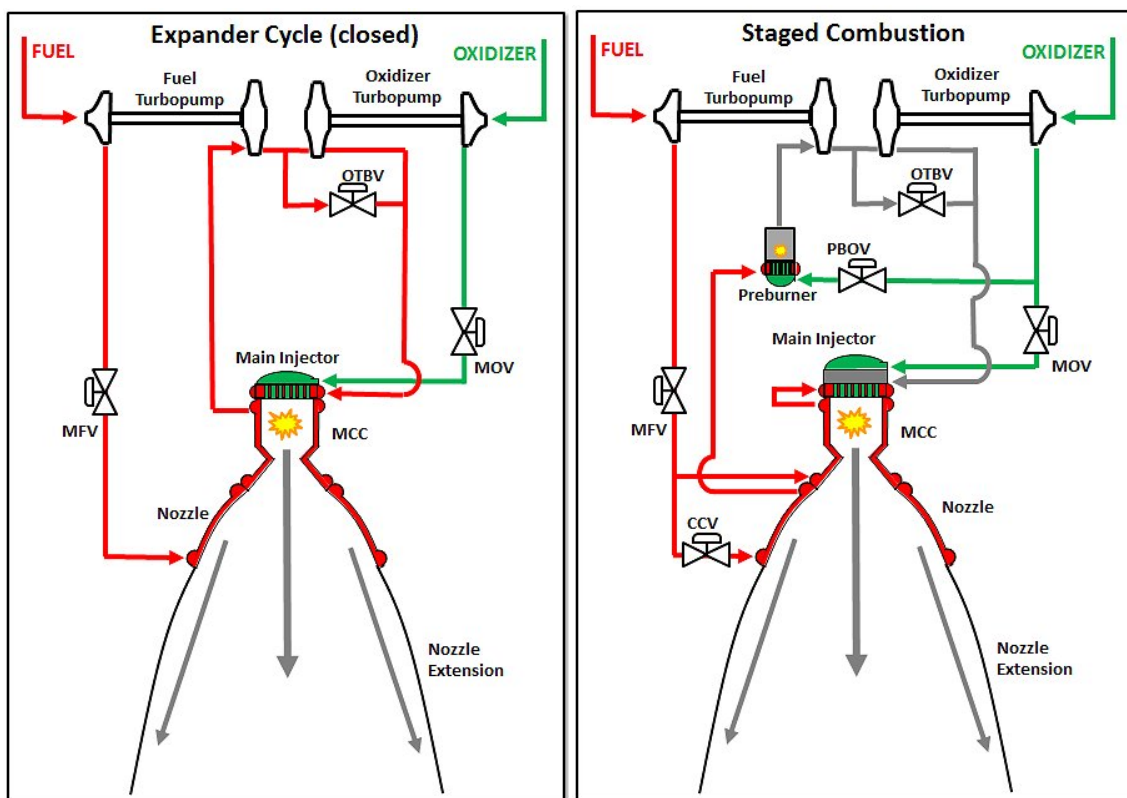


Figure 5.2 - Closed Cycles. (a) Expander Cycle (b) Staged Combustion.
SOURCE: NASA (2015a)

As the turbine is in series with the thrust chamber, a rising pressure ratio through

the turbine greatly rises the required pump discharge pressure. Therefore, with these cycles the design goal is to minimize turbine pressure ratio.

5.2 Modeling and Simulation

To simulate a LRE cycle is necessary to make use of mass and energy conservation laws. Components and global mass balance, turbomachinery power balance, pressure balance and a thrust force balance can define a set of nonlinear algebraic equations. For each type of cycle, turbopump arrangement, and split flows or bypass a different set of equations can be stated. To perform the simulation the following considerations will be take into account:

- The propellants flow under steady state condition
- The liquid propellants behave as incompressible fluid
- There is no heat loss to the environment
- There is no change variation of the temperature in the pipes

5.2.1 Flow and Energy Balance

Depending on the turbopump arrangement a different power balance can be established. In this work, it will be distinguished among four types of turbopumps, namely single shaft, geared, dual shaft with turbines in series and with turbines in parallel as illustrated in Figure 5.3.

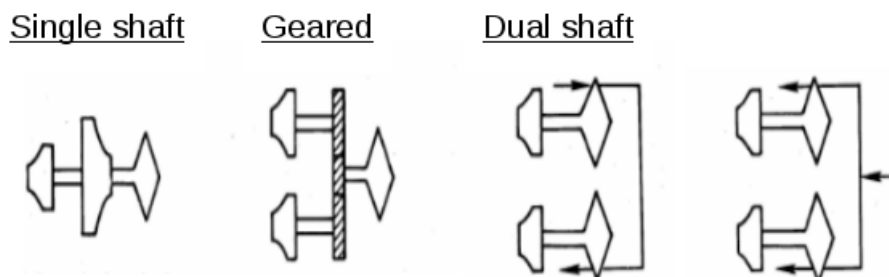


Figure 5.3 - TPA configurations
 SOURCE: SP-8107 (1974)

The required pump discharge pressure p_d is determined by the chamber pressure and the hydraulic losses through the feed system. In order to obtain the rated flow at the

rated pressure, usually a flow orifice is conveniently added. It adjusts the pressure drop which permits a calibration adjustment or change in the required feed system pressure. For a gas generator cycle, the stagnation pressure drop of the propellants between the pump discharge and the combustion chamber is the sum of pressure drop in feed lines, valves, cooling system (for the fuel) and injectors as expressed in following equations:

$$p_{d,f} - p_c = \Delta p_{f,lines} + \Delta p_{f,valves} + \Delta p_{f,cool} + \Delta p_{f,inj} \quad (5.1)$$

$$p_{d,o} - p_c = \Delta p_{o,lines} + \Delta p_{o,valves} + \Delta p_{o,inj} \quad (5.2)$$

For closed cycles in which the turbine(s) is in series with the thrust chamber, exists an extra pressure drop associated with the turbine and, specially for the staged combustion cycle, in the injector head of the pre-burner as illustrated in Figure 5.4.

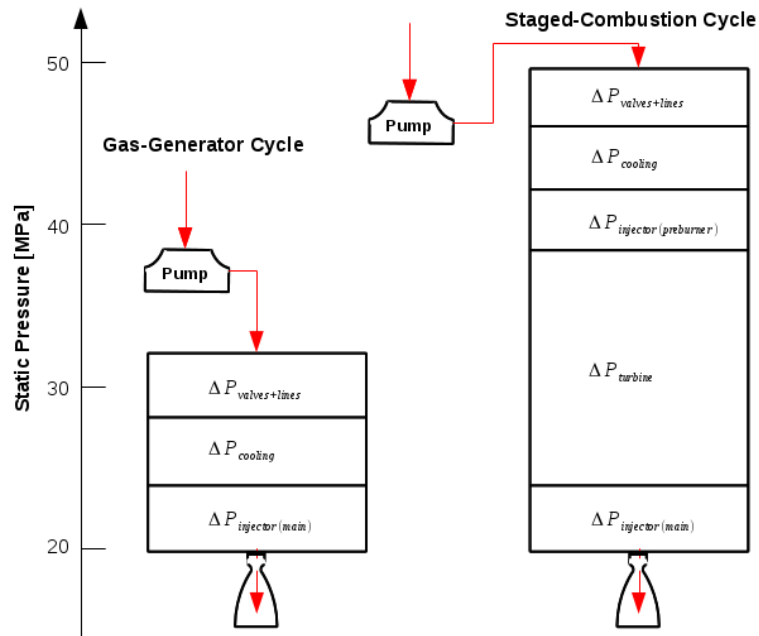


Figure 5.4 - Comparison of fuel pressure drop levels for GG and SC cycles.
SOURCE: Adapted from Humble et al. (1995) in turn taken from Bissel (1985).

5.2.1.1 Flow Splitter

A flow splitter is used to divide a given flow stream in two branches. The reason to split a flow arises from applications from cooling system to thrust control. For example, an expander cycle makes use of a bypass around the turbine to control the thrust.

5.2.1.2 Input Parameters Selection

The formulation of the set of equations can also be modified depending on the input and output parameters. For example, in order to close the balance of the thermodynamic cycle, in this work the thrust force of the engine cycle or the overall mass flow rate can be selected by the user as input parameters (Figure 5.5).

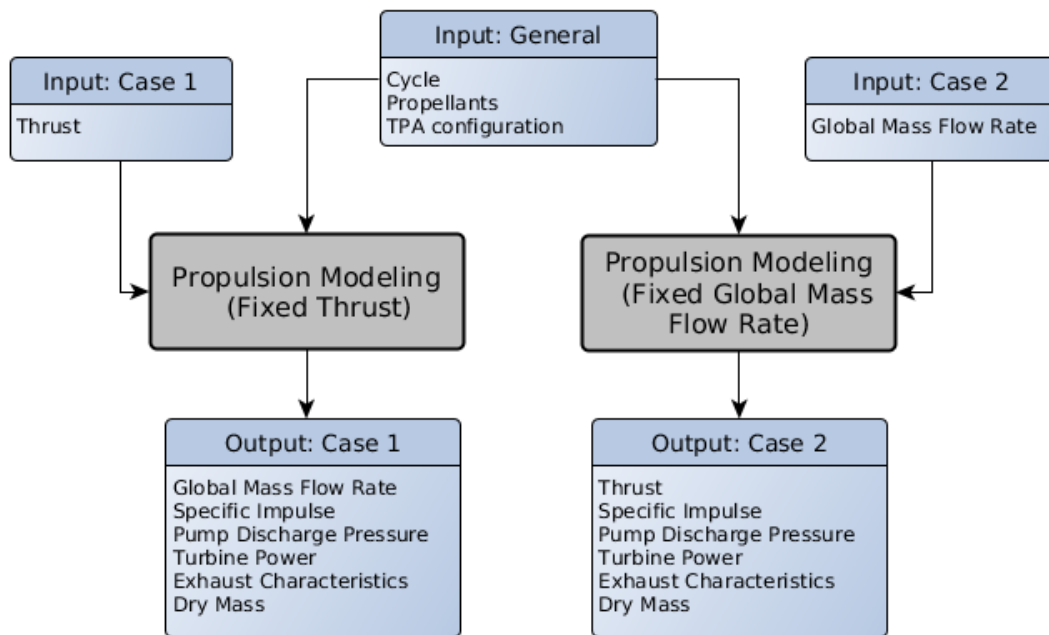


Figure 5.5 - Propulsion model diagram. Possible input/output combinations.

5.2.2 Cycle Balance

As already stated before the cycles considered are:

- Gas Generator Cycle (GG),
- Expander Bleed Cycle (EB),
- Staged Combustion Cycle (SC), and

- Expander Cycle (EC)

in which depending on

- main TPA arrangement,
- existence of booster-turbopumps, and
- bypass

new configurations can be obtained.

5.2.2.1 Gas Generator Cycle

Among the many applications of this traditional open cycle, the European Vulcain 2 (used as the main engine in Ariane 5), the retired F-1 (used as the main engine in Saturno-V), and engines under development, e.g. the Brazilian L75 (it will be used to power the upper stage of the future VLS-Alfa), and the European Aestus II (also known as RS-72 - it is a turbopump version of the Aestus) may be noted. Liquid rocket engines powered by gas generator cycle are described in Table 5.1 with their propellants combination and turbopump arrangement which is important to define the modeling equations.

To define a possible set of equations of this power cycle the Brazilian L75 was conveniently chosen. Since this engine uses the propellant combination LOX/Ethanol, a single shaft turpompump is allowed. Thus, if the vector of variables are considered (see Figure 5.6):

$$\mathbf{X} = \begin{bmatrix} p_{d,o} \\ p_{d,f} \\ \dot{m}_{o,g} \\ \dot{m}_{f,g} \\ \dot{m}_T \\ \dot{m}_{o,c} \\ \dot{m}_{f,c} \end{bmatrix} = \begin{bmatrix} \text{discharge pressure of the oxidizer pump} \\ \text{discharge pressure of the fuel pump} \\ \text{oxidizer mass flow rate in gas generator} \\ \text{fuel mass flow rate in gas generator} \\ \text{turbine mass flow rate} \\ \text{oxidizer mass flow rate in combustion chamber} \\ \text{fuel mass flow rate in combustion chamber} \end{bmatrix}$$

a nonlinear system of equations can be defined as follows:

$$\eta_m P_T(\dot{m}_T) = P_{P,o}(p_{d,o}, \dot{m}_{o,g}, \dot{m}_{o,c}) + P_{P,f}(p_{d,f}, \dot{m}_{f,g}, \dot{m}_{f,c}) \quad (5.3)$$

Table 5.1 - LRE with gas generator cycle.

GG	propellant	Booster-pump	main TPA	Application
L75	LOX-Ethanol	no	Single Shaft	VLS-Alfa/Upper stage
HM7B	LOX-LH2	no	Geared	Ariane-5/Upper stage
Vulcain 2	LOX-LH2	no	Dual Shaft/ in parallel	Ariane-5/Main stage
HM60	LOX-LH2	no	Dual Shaft/ in parallel	Ariane-5/Main stage
Aestus II	LOX-LH2	no	Dual Shaft/ in parallel	Ariane-5/Upper stage
RS-68	LOX-LH2	no	Dual Shaft/ in parallel	Delta-IV/First stage
LE-5	LOX-LH2	no	Dual Shaft/in series	H I-II/Upper stage
RD-0109	LOX-RP-1	no	Single Shaft	Vostok/Upper stage
RD-107	LOX-RP-1	no	Single Shaft	Soyuz/Booster stage
RD-0110	LOX-RG-1	no	Single Shaft	Soyuz/Upper stage
F-1	LOX-RP-1	no	Single Shaft	Saturno-V/Main stage
Merlin	LOX-RP-1	no	Single Shaft	Falcon/Main & Upper stage
RS-27A	LOX-RP-1	no	Single Shaft	Delta II-III/Booster stage

$$\dot{m}_T = \dot{m}_{f,g} + \dot{m}_{o,g} \quad (5.4)$$

$$r_c = \frac{\dot{m}_{o,c}}{\dot{m}_{f,c}} \quad (5.5)$$

$$r_g = \frac{\dot{m}_{o,g}}{\dot{m}_{f,g}} \quad (5.6)$$

$$p_{d,f} - p_c = \Delta p_{lines}^{fuel} + \Delta p_{valves}^{fuel} + \Delta p_{cool}^{fuel} + \Delta p_{inj}^{fuel} \quad (5.7)$$

$$p_{d,o} - p_c = \Delta p_{lines}^{ox} + \Delta p_{valves}^{ox} + \Delta p_{inj}^{ox} \quad (5.8)$$

$$F = F_c + F_T + F_{dc} \quad (5.9)$$

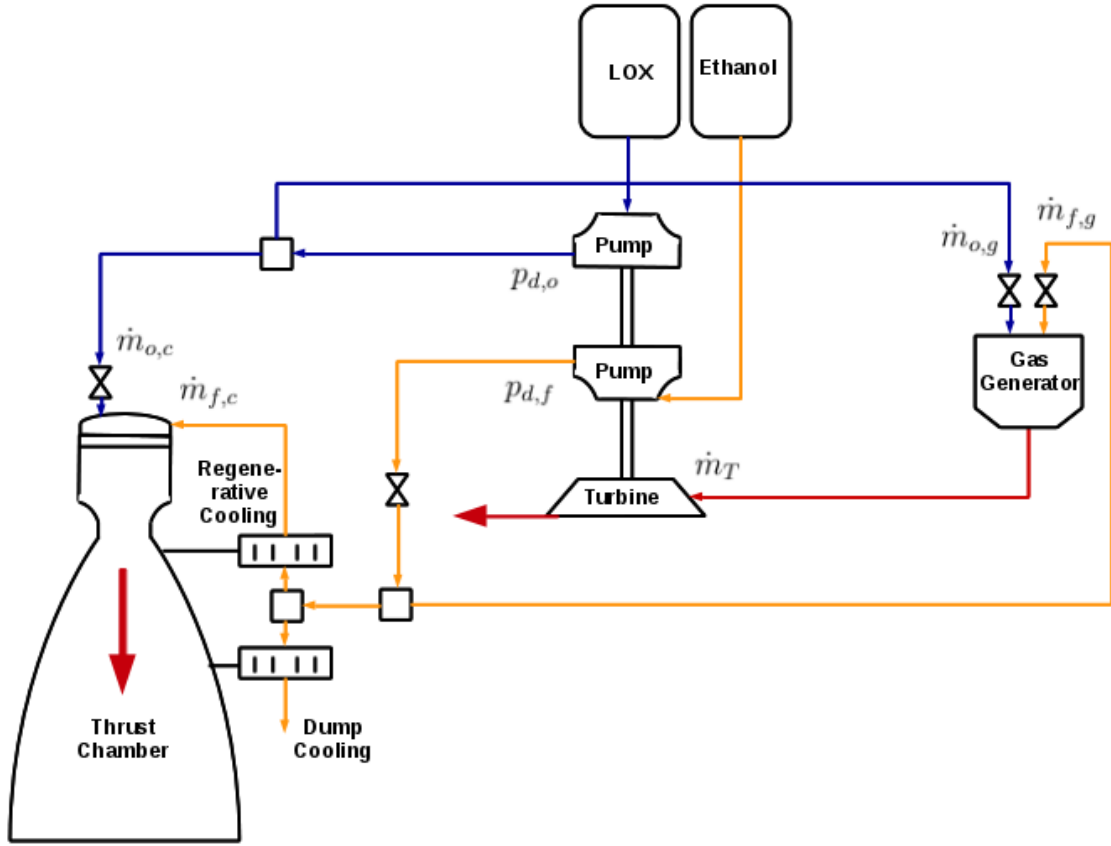


Figure 5.6 - Flow scheme of a gas generator cycle. Seven unknown to be determined are shown.

$$\mathbf{F}(\mathbf{X}) = \begin{bmatrix} f_1 \\ f_2 \\ f_3 \\ f_4 \\ f_5 \\ f_6 \\ f_7 \end{bmatrix} = \begin{bmatrix} P_T - P_{P,o} - P_{P,f} \\ \dot{m}_T - \dot{m}_{f,g} - \dot{m}_{o,g} \\ r_c \dot{m}_{f,c} - \dot{m}_{o,c} \\ r_g \dot{m}_{f,g} - \dot{m}_{o,g} \\ p_{d,f} - p_c - \Delta p_{lines}^{fuel} - \Delta p_{valves}^{fuel} - \Delta p_{cool}^{fuel} - \Delta p_{inj}^{fuel} \\ p_{d,o} - p_c - \Delta p_{lines}^{ox} - \Delta p_{valves}^{ox} - \Delta p_{inj}^{ox} \\ F - F_c - F_T - F_{dc} \end{bmatrix} = \begin{bmatrix} 0 \\ 0 \\ 0 \\ 0 \\ 0 \\ 0 \\ 0 \end{bmatrix}$$

As the number of unknowns is equal to the number of equations this problem can be solved by numerical methods. In these equations p_c , F , r_c and r_g are given. In the above set of equations the overall thrust remains constant, however if the overall mass flow through the engine is set to be constant, then Eq. 5.9 can be replaced by:

$$\dot{m}_{stage} = \dot{m}_g + \dot{m}_c + \dot{m}_{dc} \quad (5.10)$$

5.2.2.2 Expander Bleed Cycle

The expander bleed cycle is an open cycle version of the traditional expander cycle. In Table 5.2 the engines used in the Japanese H-II launch vehicle are shown.

Table 5.2 - LRE with expander bleed cycle.

EB	propellant	Booster-pump	main TPA	Application
LE-5A	LOX-LH2	no	Dual Shaft/in series	H-II/Second stages
LE-5B	LOX-LH2	no	Dual Shaft/in series	H-II/Second stages

A flow scheme of this type of cycle is presented in Figure 5.7 along with the variables of the problem which can be set in a vector form as:

$$\mathbf{X} = \begin{bmatrix} p_{d,o} \\ p_{d,f} \\ \dot{m}_{T,o} \\ \dot{m}_{T,f} \\ \dot{m}_{o,c} \\ \dot{m}_{f,c} \end{bmatrix} = \begin{bmatrix} \text{discharge pressure of the oxidant pump} \\ \text{discharge pressure of the fuel pump} \\ \text{mass flow rate in the oxidant turbine} \\ \text{mass flow rate in the fuel turbine} \\ \text{oxidant mass flow rate in combustion chamber} \\ \text{fuel mass flow rate in combustion chamber} \end{bmatrix}$$

Thus, the resulting nonlinear system of equations can be given as:

$$\eta_m P_{T,o}(x_5) = P_{P,o}(p_{d,o}, \dot{m}_{o,c}) \quad (5.11)$$

$$\eta_m P_{T,f}(x_6) = P_{P,f}(p_{d,f}, \dot{m}_{f,c}) \quad (5.12)$$

$$r_c = \frac{\dot{m}_{o,c}}{\dot{m}_{f,c}} \quad (5.13)$$

$$p_{d,f} - p_c = \Delta p_{lines}^{fuel} + \Delta p_{valves}^{fuel} + \Delta p_{inj}^{fuel} \quad (5.14)$$

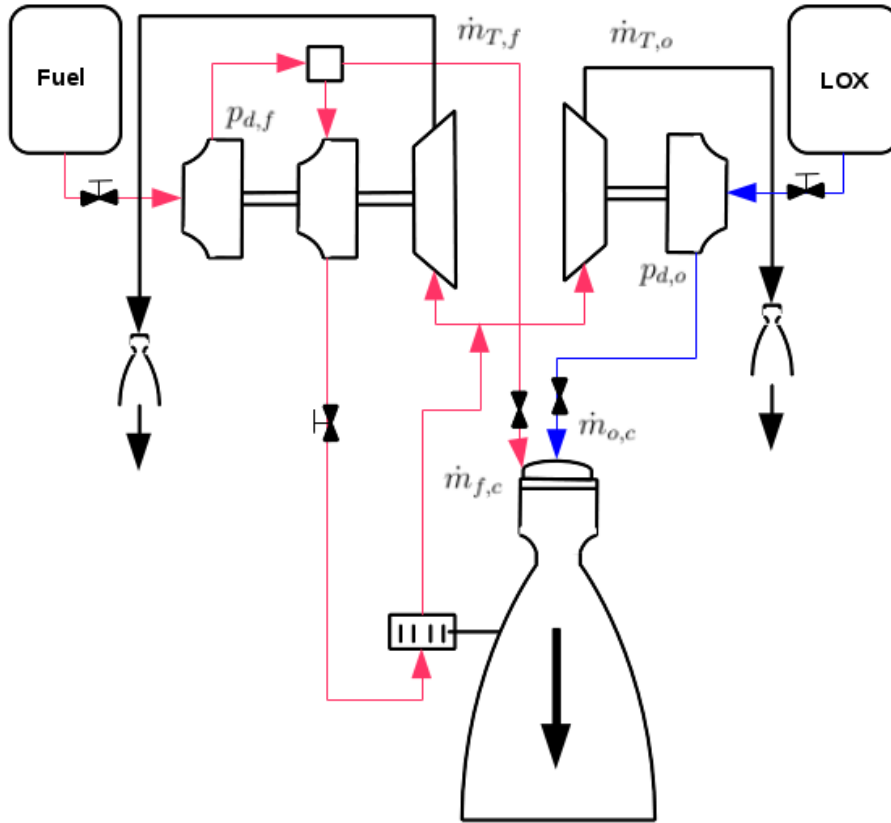


Figure 5.7 - Flow scheme of an expander bleed cycle. The unknowns required to the simulation are shown.

$$p_{d,o} - p_c = \Delta p_{lines}^{ox} + \Delta p_{valves}^{ox} + \Delta p_{inj}^{ox} \quad (5.15)$$

$$F = F_c + F_{T,o} + F_{T,f} \quad (5.16)$$

5.2.2.3 Staged Combustion

The modeling of this power cycle was derived taking the Space Shuttle Main Engine (SSME) as the reference engine (see Figure 5.8). SSME was responsible to power the core stage of the Space Shuttle. This rocket engine has two main turbopumps (HPOTP and HPFTP) driven by a fuel-rich pre-burner and two booster-turbopumps (LPOTP and LPFTP) responsible to increase the inlet pressure of both of the main pumps.

From Figure 5.8 a vector of variables can be stated as:

Table 5.3 - LRE with staged combustion cycle.

SC	propellant	Booster-pump	main TPA	Application
SSME	LOX-LH2	yes	2-Single Shaft	Space Shuttle/Main stage
LE-7/7A	LOX-LH2	yes	2-Single Shaft	H-II/Booster stage
RD-170	LOX-RP-1	yes	Dual Shaft	Energia/Main stage
RD-253	N2O4/UDMH	yes	Dual Shaft	Proton/First stages
RD-270	N2O4/UDMH	yes	Dual Shaft	Never flown
RD-120	LOX/RG-1	yes	Dual Shaft	Zenit/Upper stage
Raptor5	LOX/methane	yes	Dual Shaft	SpaceX

$$\mathbf{X} = \begin{bmatrix} p_{d,os1} \\ p_{d,os2} \\ p_{d,f} \\ \dot{m}_{o,pb1} \\ \dot{m}_{f,pb1} \\ \dot{m}_{o,pb2} \\ \dot{m}_{f,pb2} \\ \dot{m}_{T,LPOTP} \\ \dot{m}_{T,LPFTP} \\ \dot{m}_{o,c} \\ \dot{m}_{f,c} \end{bmatrix} = \begin{bmatrix} \text{discharge pressure of the oxidant pump stage 1} \\ \text{discharge pressure of the oxidant pump stage 2} \\ \text{discharge pressure of the fuel pump} \\ \text{oxidizer mass flow rate in the pre-burner 1} \\ \text{fuel mass flow rate in the pre-burner 1} \\ \text{oxidant mass flow rate in the pre-burner 2} \\ \text{fuel mass flow rate in the pre-burner 2} \\ \text{oxidizer mass flow rate through the hydraulic turbine} \\ \text{fuel mass flow rate in LPFTP} \\ \text{oxidizer mass flow rate in combustion chamber} \\ \text{fuel mass flow rate in combustion chamber} \end{bmatrix}$$

so the nonlinear system of equations can be defined as follows:

$$\eta_m P_{T,HPOTP}(\dot{m}_{T,o}) = P_{Ps1,HPOTP}(p_{d,os1}, \dot{m}_{o,c}, \dot{m}_{T,LPOTP}) + P_{Ps2,HPOTP}(p_{d,os2}, \dot{m}_{o,pb1}, \dot{m}_{o,pb2}) \quad (5.17)$$

$$\eta_m P_{T,HPFTP}(\dot{m}_{T,f}) = P_{P,HPFTP}(p_{d,f}, \dot{m}_{f,c}) \quad (5.18)$$

$$\eta_m P_{T,LPOTP}(\dot{m}_{T,LPOTP}) = P_{P,LPOTP}(\dot{m}_{o,c}) \quad (5.19)$$

$$\eta_m P_{T,LPFTP}(\dot{m}_{T,LPFTP}) = P_{P,LPFTP}(\dot{m}_{f,c}) \quad (5.20)$$

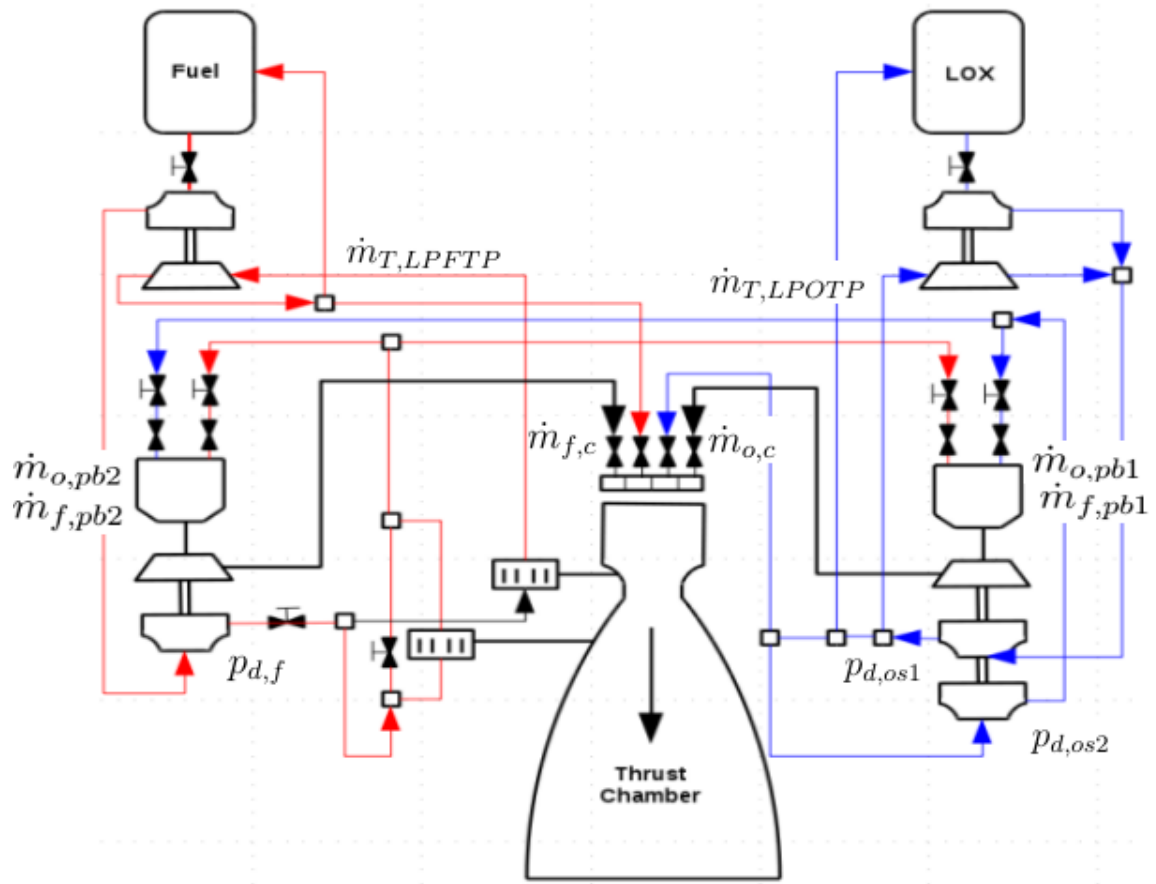


Figure 5.8 - Flow scheme of staged combustion cycle. The unknowns required to the simulation are shown.

$$r_c = \frac{\dot{m}_{o,c}}{\dot{m}_{f,c}} \quad (5.21)$$

$$r_{pb1} = \frac{\dot{m}_{o,pb1}}{\dot{m}_{f,pb1}} \quad (5.22)$$

$$r_{pb2} = \frac{\dot{m}_{o,pb2}}{\dot{m}_{f,pb2}} \quad (5.23)$$

$$p_{d,f} - p_c = \Delta p_{lines}^{fuel} + \Delta p_{valve,Thrust}^{fuel} + \Delta p_{inj,gg}^{fuel} + \Delta p_{turbine}^{gas} + \Delta P_{duct}^{gas} + \Delta p_{inj,c} \quad (5.24)$$

$$p_{d,o} - p_c = \Delta p_{lines}^{ox} + \Delta p_{inj,pb1}^{ox} + \Delta p_{turbine}^{gas} + \Delta p_{duct}^{gas} + \Delta p_{inj,c} \quad (5.25)$$

$$p_{d,o} - p_c = \Delta p_{lines}^{ox} + \Delta p_{inj,c} \quad (5.26)$$

$$F = F_c \quad (5.27)$$

5.2.2.4 Expander Cycle

In this cycle the energy to drive the turbomachinery does not come from combustion, instead it is derived from change phase. The fuel propellant extract heat from the cooling jacket, changes phase, and the resulting hot gas powers the turbine. To control the thrust, usually an amount between 5%-15% of gas fuel bypasses the turbine. In Table 5.4 is presented the American RL10-A-3A and the European Vinci (under development). Vinci is fed with LH2 and LOX and will replace the HM7B (which powers Ariane 5 upper stage). Its biggest improvement from its predecessor, the HM7B, is the capability of restarting up to five times.

Table 5.4 - LRE with expander cycle.

EC	propellant	Booster-pump	main TPA	Application
Vinci	LOX-LH2	no	Dual Shaft/in series	Ariane-5/Upper stage
RL10-A-3A	LOX-LH2	no	Geared	Atlas, Titan, DeltaIV/Upper stage

To model this cycle, it is used the reference engine flow scheme shown from Figure 5.9.

$$\mathbf{X} = \begin{bmatrix} p_{d,o} \\ p_{d,f} \\ \dot{m}_T \\ \dot{m}_{bypass} \\ \dot{m}_{o,c} \\ \dot{m}_{f,c} \end{bmatrix} = \begin{bmatrix} \text{discharge pressure of the oxidant pump} \\ \text{discharge pressure of the fuel pump} \\ \text{turbine mass flow rate} \\ \text{turbine bypass mass flow rate} \\ \text{oxidant mass flow rate in combustion chamber} \\ \text{fuel mass flow rate in combustion chamber} \end{bmatrix}$$

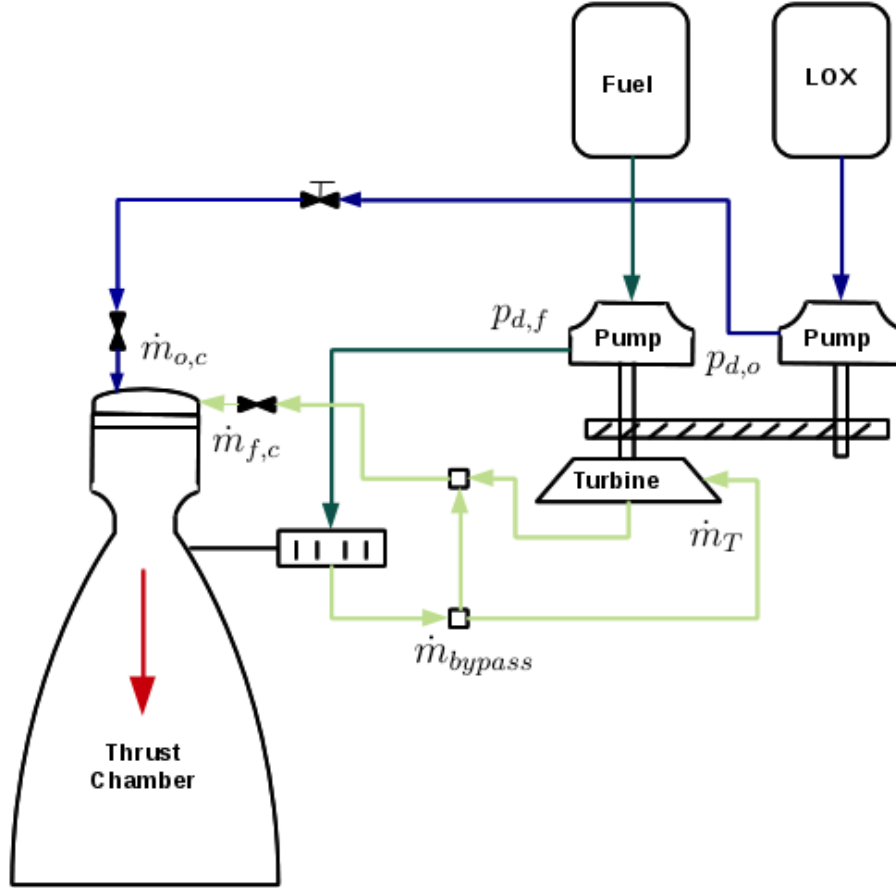


Figure 5.9 - Flow scheme of an expander cycle. The unknowns required to the simulation are shown.

The nonlinear system of equations are given by:

$$\eta_m P_T(\dot{m}_T) = P_{P,o}(p_{d,o}, \dot{m}_{o,c}) + P_{P,f}(p_{d,f}, \dot{m}_{f,c}) \quad (5.28)$$

$$r_{bypass} = \frac{\dot{m}_{bypass}}{\dot{m}_{f,c}} \quad (5.29)$$

$$r_c = \frac{\dot{m}_{o,c}}{\dot{m}_{f,c}} \quad (5.30)$$

$$p_{d,f} - p_c = \Delta p_{lines}^{fuel} + \Delta p_{valves}^{fuel} + \Delta p_{cool}^{fuel} + \Delta p_{turbine}^{gas} + \Delta P_{duct}^{gas} + \Delta p_{inj}^{fuel} \quad (5.31)$$

$$p_{d,o} - p_c = \Delta p_{lines}^{ox} + \Delta p_{valves}^{ox} + \Delta p_{inj}^{ox} \quad (5.32)$$

$$\dot{m}_{overall} = \dot{m}_{o,c} + \dot{m}_{f,c} \quad (5.33)$$

The numerical method applied to simulate the engine cycles was taken from the book of [Press et al. \(2007\)](#). The Newton's method or the multidimensional secant methods called Broyden's Method presented similar results, however both methods were implemented. The applicability of the simulation codes will be checked in Chapter 8.

6 TRAJECTORY MODELING AND OPTIMIZATION

Since the dawn of the space era launch vehicles are responsible to put satellites into orbit. This makes the cost of a satellite strongly related to the performance of the launch vehicle which in turn depends on the trajectory profile. This chapter begins describing mathematical models for the environment (i.e., atmospheric, gravitational), then two formulations of the state equations of the ascent trajectory of a launch vehicle are presented. Finally, the last part of this chapter is devoted on current methods to optimize the ascent trajectory.

6.1 Atmosphere Model

The atmosphere can be seen as a layer of gases attached to the surface of the Earth by gravitational attraction. The aerothermal loads on a launch vehicle depend on properties of the gases in the atmosphere, which in turn are functions of gravity, the planet rotation, chemical composition, solar radiation and Earth's magnetic field (TEWARI, 2007). As horizontal effect in the atmosphere, such as climate and the planet's rotation, has little impact on the thermodynamic properties that affect the vehicle, this model will address only variations of thermodynamic properties with altitude.

6.1.1 Standard Atmosphere

The standard atmosphere is modeled as adjacent layers of gases in which temperature depends on the altitude. In different layers, the temperature can be modeled as linear function of the altitude:

$$T = T_i + a(h - h_i) \quad (6.1)$$

where the subscript i refers to the base of the concerning layers, and a is a constant called *thermal lapse rate*. The pressure is given as:

$$p = \begin{cases} p_i \left[1 + \frac{a(h-h_i)}{RT_i} \right]^{-\frac{g_0}{aR} \left[1 + \frac{2}{r_0} \left(\frac{T_i}{a} - h_i \right) \right]} e^{\frac{2g_0}{aRr_0}(h-h_i)}, & \text{if } a \neq 0, \\ p_i e^{-\left[\frac{g_0(h-h_i)}{RT_i} \right] \left[1 - \frac{h-h_i}{r_0} \right]}, & \text{if } a = 0. \end{cases}$$

The density can be easily derived using the equation of state of the ideal gas:

$$\rho = \frac{p}{RT} \quad (6.2)$$

The parameters T_i , h_i , R and a are presented in Table 6.1 which is a hybrid table merging the references (COESA, 1976) and (COESA, 1962). A temperature profile of the atmospheric layers is presented in Figure 6.1.

Table 6.1 - Standard Atmosphere (TEWARI, 2007).

i	$h_i[km]$	$T_i[K]$	$R_i[J/kg.K]$	$a_i[K/km]$
1	0	288.15	287.0	-6.5
2	11.0191	216.65	287.0	0.0
3	20.0631	216.65	287.0	1.0
4	32.1619	228.65	287.0	2.8
5	47.3501	270.65	287.0	0.0
6	51.4125	270.65	287.0	-2.8
7	71.8020	214.65	287.02	-2.0
8	86	186.946	287.02	1.693
9	100	210.02	287.84	5.0
10	110	257.0	291.06	10.0
11	120	349.49	308.79	20.0
12	150	892.79	311.80	15.0
13	160	1022.2	313.69	10.0
14	170	1103.4	321.57	7.0
15	190	1205.4	336.68	5.0
16	230	1322.3	366.84	4.0
17	300	1432.1	416.88	3.3
18	400	1487.4	463.36	2.6
19	500	1506.1	493.63	1.7
20	600	1506.1	514.04	1.1
21	700	1507.6	514.04	0.0

6.2 Aerodynamics

During the flight a launch vehicle needs to cross the atmosphere in which reacts to the vehicle motion by means of aerodynamics forces, namely:

- Drag
- Lift

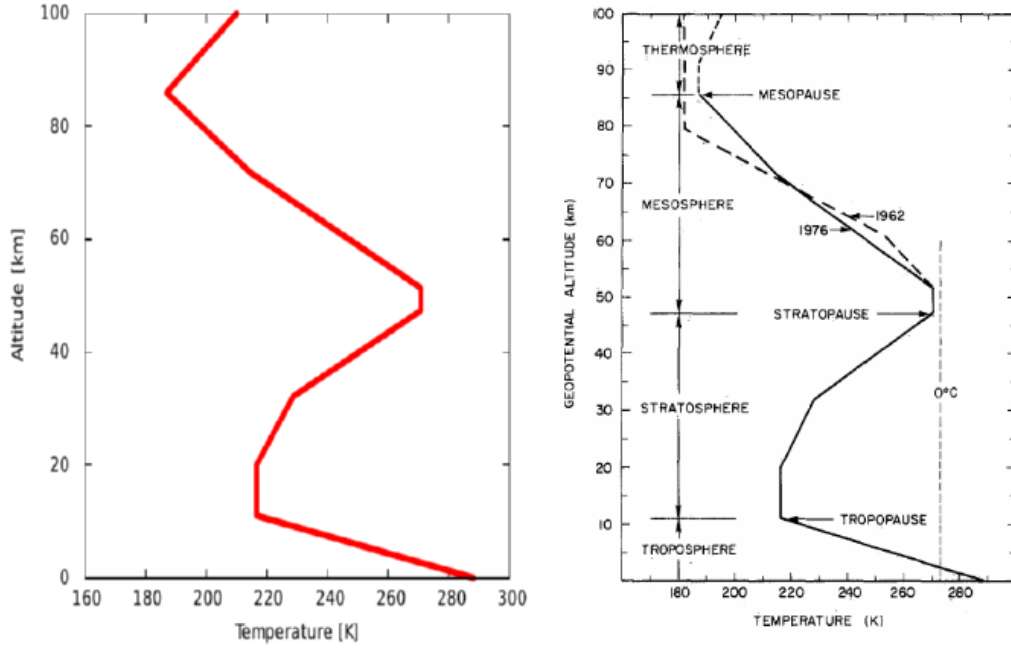


Figure 6.1 - Temperature in atmospheric layers.

SOURCE: (a) Plotted using values from Table 6.1 (b) Chapman et al. (1985)

The drag force arises due to friction between the body and the fluid. Defining S_{ref} = reference area of the body, C_D = drag coefficient, ρ = density of the air and V = absolute velocity, the drag equation can be written as:

$$D = \frac{1}{2}\rho(r)S_{ref}C_DV^2 \quad (6.3)$$

The lift is a reaction force to the angle of attack:

$$L = \frac{1}{2}\rho(r)S_{ref}C_LV^2 \quad (6.4)$$

where C_L is the lift coefficient.

6.2.1 Aerodynamics Coefficients

Aerodynamic coefficients are to calculate normal and axial forces on the launch vehicle. There are many methods to estimate these coefficients in the literature, among them it can be cited:

- **Software Missile DATCOM.** Missile DATCOM is a widely used tool for the preliminary design and analysis of missile aerodynamics, but is also used for rocket applications (BLAKE, 1997a; BLAKE, 1997b). This program is available as a supplement CD from the book of Hammond (2001).
- **Interpolation of available data from a given vehicle.** This method was used among other works in (TEWARI, 2007) and by Balesdent (2011) and Pagano (2010) in their Thesis (see Figure 6.2).
- **Formulas.** Considering contributions of shock wave in the rocket nose, body friction and base pressure, (FLEEMAN, 2008) developed formulas for many geometries. Although the formulas were developed for missile design, they can also be adapted to launch vehicle applications.
- **Constant value for certain phases of the flight.**

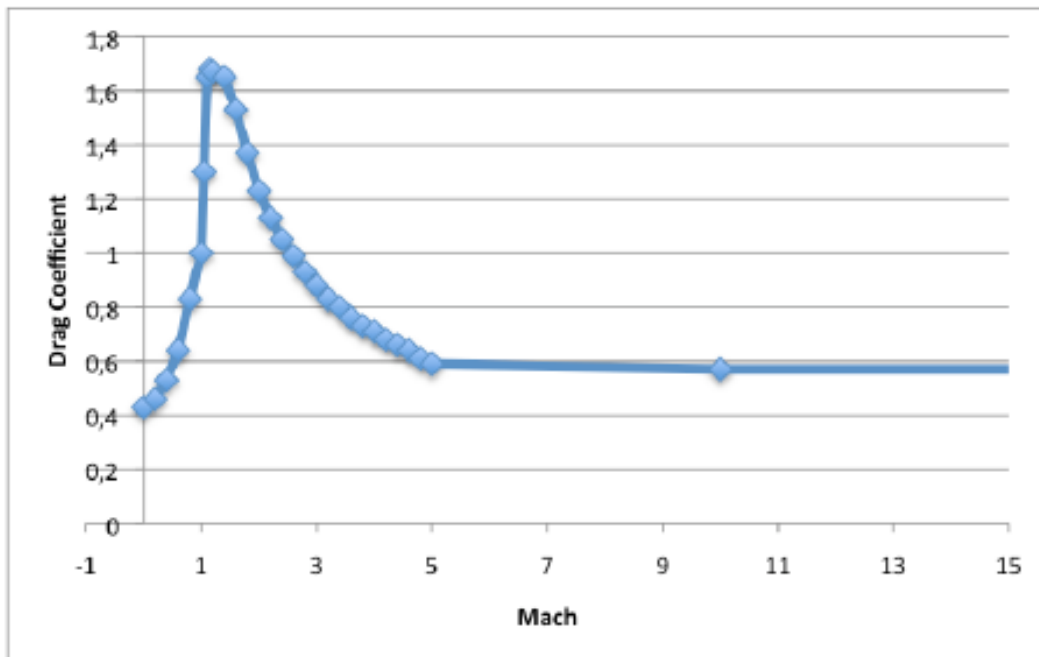


Figure 6.2 - Drag coefficients.

SOURCE: Pagano (2010) which in turn taken from ASTOS®

Except for interpolation from real flight data, the methods to estimate the drag coefficient is quite inaccurate. Fortunately, because the essential acceleration phase

begins in the exoatmospheric phase, usually the drag has little influence on launcher performance (SCHLINGLOFF, 2005).

6.3 Gravitational Model

The complexity of the equations representing the gravitational field depends on the accuracy desired for a given application. For preliminary studies, the planet can be modeled as spherical with homogeneous mass distribution. Thus, the gravity acceleration \mathbf{g} around a planet of mass M_{body} can be given as:

$$\mathbf{g} = -\frac{GM_{body}}{r^2}\hat{\mathbf{r}} \quad (6.5)$$

where G is the gravitational constant, r is the distance between the celestial body and the a given space vehicle, and $\hat{\mathbf{r}}$ is a unit vector directed from the celestial body to the vehicle. For a more accurate model, the oblateness of the body must be considered. So the spherical harmonics come into play and the following modeling can be adopted (TEWARI, 2007):

$$\mathbf{g} = g_r\mathbf{i}_r + g_\Phi\mathbf{i}_\Phi \quad (6.6)$$

The unit vectors \mathbf{i}_r and \mathbf{i}_Φ denote the radial and southward directions in the *local horizon frame* and:

$$g_\Phi = -\frac{GM}{r^2} \left[1 - 3J_2 \left(\frac{R_e}{r} \right)^2 P_2(\cos \Phi) - 4J_3 \left(\frac{R_e}{r} \right)^3 P_3(\cos \Phi) - 5J_4 \left(\frac{R_e}{r} \right)^4 P_4(\cos \Phi) \right] \quad (6.7)$$

$$g_r = -\frac{3GM}{r^2} \left(\frac{R_e}{r} \right)^2 \sin \Phi \cos \Phi \left[J_2 + \frac{1}{2}J_3 \left(\frac{R_e}{r} \right) \sec \Phi (5 \cos^2 \Phi - 1) + \frac{5}{6}J_4 \left(\frac{R_e}{r} \right)^2 (7 \cos^2 \Phi - 1) \right] \quad (6.8)$$

where $P_i(i = 1, 2, 3)$ are the Legendre polynomials, $J_i(i = 1, 2, 3)$ are called *Jeffery's* constants, $\Phi = \pi/2 -$ latitude and R_e is the equatorial radius of the celestial body:

$$P_2(\cos \Phi) = \frac{3}{2} \sin^2 \Phi - \frac{1}{2}$$

$$P_3(\cos \Phi) = \frac{5}{2} \sin^2 \Phi - \frac{3}{2} \sin \Phi$$

$$P_4(\cos \Phi) = \frac{35}{8} \sin^4 \Phi - \frac{30}{8} \sin^2 \Phi + \frac{3}{8}$$

For the Earth:

$$J_2 = 1.08263^{-3}$$

$$J_3 = 2.532153^{-7}$$

$$J_4 = 1.6109876^{-7}$$

$$R_e = \text{equatorial radius of the Earth [= 6378.135 km]}$$

For an oblate planet, the radius can be approximately expressed as function of the latitude:

$$R \approx R_e(1 - \epsilon \sin^2 \delta) \quad (6.9)$$

$$\epsilon = 1 - \frac{R_p}{R_e} \quad (6.10)$$

where R_p is the polar radius.

6.4 Equations of the Translational Motion

The modeling of the trajectory of a launch vehicle is usually performed by means of two reference frames (one with origin on the Earth center and the other one moving with the vehicle) and considerations or idealizations according to the requirements of the mission. To model the translational motion, the vehicle can be treated as a particle, ignoring the size and mass distribution. In modeling the rotational motion, the vehicle can be considered a rigid body, reducing the degrees of freedom from infinity (flexible body case) to just six (TEWARI, 2007). However, strictly speaking, a launch vehicle is far from being considered a rigid body. Mass is continuously expelled due to combustion of the propellants and for liquid rocket engines there is still the sloshing, which is the movement of fluid within the tanks and pipes and rotating equipment such as turbines and pumps. Especially for large launch vehicles, the deflection of the structure should be considered as well (CORNELISSE et al., 1979). However, this research is focused on the reference trajectory, thus treatment of the

translational motion is sufficient to fulfill this task. Two mathematical models for the trajectory are presented in the following section. The first one was taken from Schlingloff (2005) and the other one from Tewari (2007).

6.4.1 First Formulation

In this modeling the spherical celestial (inertial) coordinates and a moving coordinates in the orbit plane were considered. Both reference frames have the origin on the Earth center Figure 6.3. The vector of state variables is conveniently chosen as $\mathbf{y}(t) = [r(t) \ u(t) \ v(t) \ \Omega(t) \ \iota(t) \ \omega(t)]^T$. Thus the system of equation can be given as:

$$\dot{r} = u \quad (6.11)$$

$$\dot{u} = \frac{v^2}{r} - \frac{\mu}{r^2} + \frac{F}{m} \sin \beta \cos \delta + \frac{D_x}{m} + \frac{L_x}{m} \quad (6.12)$$

$$\dot{v} = -\frac{uv}{r} + \frac{F}{m} \cos \beta \cos \delta + \frac{D_y}{m} + \frac{L_y}{m} \quad (6.13)$$

$$\dot{\Omega} = \omega_x \frac{\sin \omega}{\sin \iota} \quad (6.14)$$

$$\dot{i} = \omega_x \cos \omega \quad (6.15)$$

$$\dot{\omega} = \frac{v}{r} - \omega_x \sin \omega \cot \iota \quad (6.16)$$

and

$$\omega_x = \frac{F \sin \delta + D_z + L_z}{v} \quad (6.17)$$

where

r : distance between origin of the reference frames [m]

u : vertical velocity [m/s]

v : horizontal velocity [m/s]

Ω, ω, ν : Euler angles [rad] (see Figure 6.3)

β : thrust angle in flight plane [rad]

δ : thrust angle out of flight plane [rad]

D_x, D_y, D_z : components of the drag force on vehicle axis [N]

L_x, L_y, L_z : components of the lift force on vehicle axis [N]

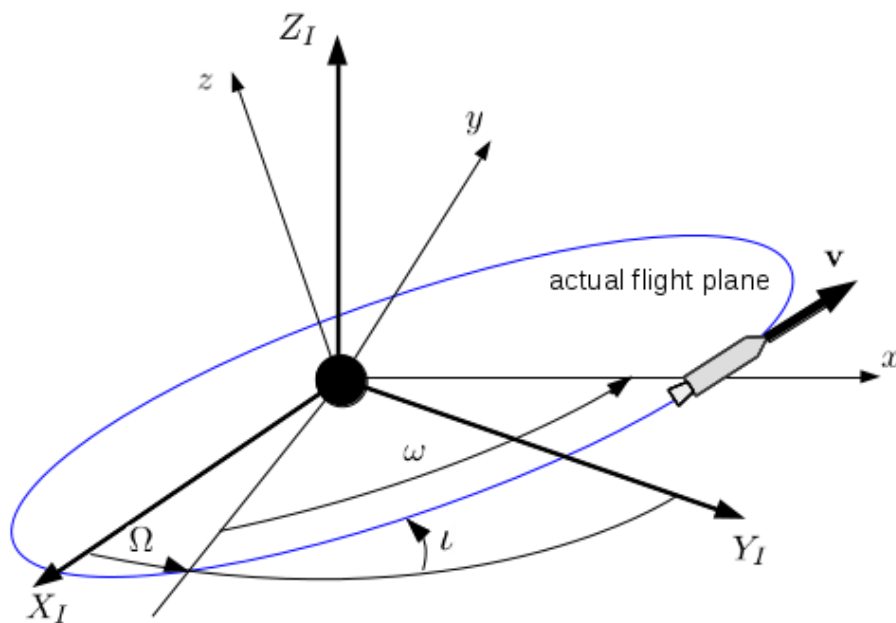


Figure 6.3 - Reference Frames

The first three equations of the system of differential equations are the dynamic equations of motion and the other ones are the cinematic equations. The dynamic equations are derived by application of the Newton's second law resolved into components of the moving system. The cinematic equations are deduced into two steps:

- a) Representation of the rotation velocity of the vehicle in a vector form
- b) Applying the Euler angles

Thus provided that the attitude of the moving system is determined by the position vector $\mathbf{r} = (r, 0, 0)$ and velocity vector $\mathbf{v} = (u, v, 0)$, we get:

$$\boldsymbol{\omega} = \begin{bmatrix} \omega_x \\ \omega_y \\ \omega_z \end{bmatrix} = \begin{bmatrix} \omega_x \\ 0 \\ v/r \end{bmatrix} \quad (6.18)$$

where

ω_x : inclination change

ω_y : disappearing (= 0)

ω_z : motion in flight plane

Finally, as the time derivative of the Euler angles are components of the angular velocity vector $\boldsymbol{\omega}$ of the moving system:

$$\boldsymbol{\omega} = \begin{bmatrix} \omega_x \\ 0 \\ v/r \end{bmatrix} = \begin{bmatrix} \dot{\Omega} \sin \iota \sin \omega + i \cos \omega \\ \dot{\Omega} \sin \iota \cos \omega - i \sin \omega \\ \dot{\omega} + \dot{\Omega} \cos \iota \end{bmatrix} \quad (6.19)$$

With an appropriate mathematical manipulation, the cinematic equations arise.

6.4.2 Second Formulation

The reference frames adopted in this modeling are the planet-fixed reference (SXYZ) frame and the local horizontal frame (oxyz), both are non-inertial (Figure 6.4). Here, some steps in the derivation of the modeling equation will be omitted, but as aforementioned a detailed derivation can be found in [Tewari \(2007\)](#). From Figure 6.4, the relative velocity \mathbf{v} and the local velocity of the local horizontal frame (oxyz) relative to the planet-centered rotating frame (SXYZ) can be expressed as:

$$\mathbf{v}(v, \gamma, \zeta) = v(\sin \gamma \mathbf{i} + \cos \gamma \sin \zeta \mathbf{j} + \cos \gamma \cos \zeta \mathbf{k}) \quad (6.20)$$

$$\boldsymbol{\Omega} = \dot{\xi} \mathbf{K} - \dot{\phi} \mathbf{j} \quad (6.21)$$

with a convenient rotation matrix, Eq. 6.21 can be written only in terms of axes of the body as:

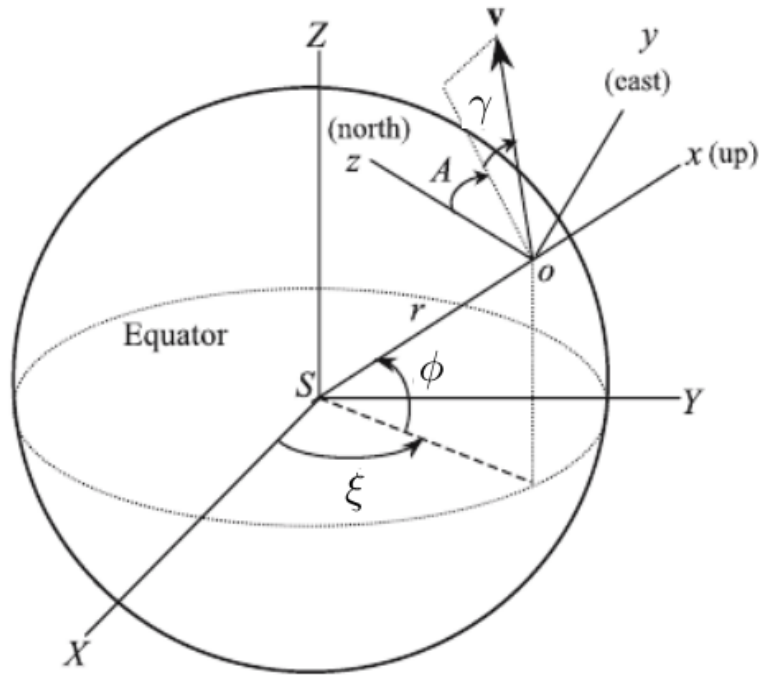


Figure 6.4 - Planet-fixed and local horizon frames for atmospheric flight.
SOURCE: (TEWARI, 2007)

$$\boldsymbol{\Omega} = \dot{\xi} \sin \phi \mathbf{i} - \dot{\phi} \mathbf{j} + \dot{\xi} \cos \phi \mathbf{k} \quad (6.22)$$

The relative velocity can also be expressed as:

$$\mathbf{v} = \dot{r} \mathbf{i} + \boldsymbol{\Omega} \times (r \mathbf{i}) \quad (6.23)$$

$$\mathbf{v} = \dot{r} \mathbf{i} + r \dot{\xi} \cos \phi \mathbf{j} + r \dot{\phi} \mathbf{k} \quad (6.24)$$

Comparing Eq. 6.20 and Eq. 6.24 the kinematic equations of motion are finally obtained:

$$\dot{r} = v \sin \gamma \quad (6.25)$$

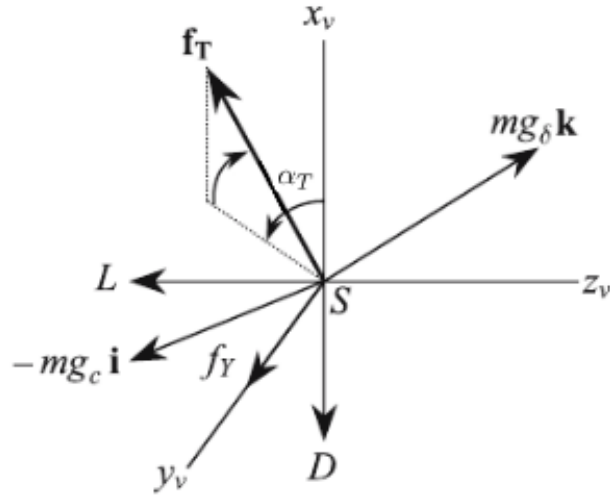


Figure 6.5 - External force resolved in the wind axes.
SOURCE: (TEWARI, 2007)

$$\dot{\xi} = \frac{v \cos \gamma \cos \zeta}{r \cos \phi} \quad (6.26)$$

$$\dot{\phi} = \frac{v \cos \gamma \sin \zeta}{r} \quad (6.27)$$

To derive the dynamic equations, the Newton's second law must be introduced:

$$\mathbf{f} = m\mathbf{a}_I = m \frac{d\mathbf{v}_I}{dt} \quad (6.28)$$

Choosing the wind axes to express the forces on the body Figure 6.5 and doing the appropriate transformation to perform \mathbf{a}_I in the wind axes, the remain equations to model the translational motion are obtained:

$$\dot{\gamma} = \frac{F \sin \alpha_T}{mv} + \left(\frac{v}{r} - \frac{\mu_E}{r^2 v} \right) \cos \gamma + \frac{L}{mv} + \cos \phi \left[2\omega_E \cos \zeta + \frac{\omega_E^2 r}{v} (\cos \phi \cos \gamma + \sin \phi \sin \gamma \sin \zeta) \right] \quad (6.29)$$

$$\dot{v} = \frac{F \cos \alpha_T}{mv} - \frac{\mu_E}{r^2} \sin \gamma - \frac{D}{m} + \omega_E^2 r \cos \phi (\cos \phi \sin \gamma - \sin \phi \cos \gamma \sin \zeta) \quad (6.30)$$

$$\dot{\zeta} = -\frac{v}{r} \tan \phi \cos \gamma \cos \zeta + 2\omega_E \cos \phi \tan \gamma \sin \zeta - \frac{\omega_E^2 r}{v \cos \gamma} \sin \phi \cos \phi \cos \zeta - 2\omega_E \sin \phi \quad (6.31)$$

where

α_T - angle of attack [rad]

ω_E - Earth's rotation [rad/s]

ϕ - latitude [rad]

ξ - longitude [rad]

A - Azimuth [rad]

γ - flight path angle [rad]

ζ - heading angle [= $\pi/2 - A$]

Eqs. (6.25-6.27) are the kinematical equations of motion and Eqs. (6.29-6.31) are the dynamical equations. With the integration of the system of differential equations, the position vector and the velocity vector of the vehicle can be determined by the following equations:

$$\mathbf{r}(r, \phi, \xi) = r(\cos \phi \cos \xi \mathbf{I} + \cos \phi \sin \xi \mathbf{J} + \sin \phi \mathbf{K}) \quad (6.32)$$

$$\mathbf{v}(v, \gamma, \zeta) = v(\sin \gamma \mathbf{i} + \cos \gamma \sin \zeta \mathbf{j} + \cos \gamma \cos \zeta \mathbf{k}) \quad (6.33)$$

It is known that having an inertial position vector and a velocity vector of a given body in orbit, the orbital elements (or Keplerian elements) can be readily determined. Thus, to get the orbital elements, it is necessary to perform an appropriate matrix rotation to obtain the desired inertial vectors.

6.5 Guidance Programme

From the launch pad into the desired orbit in its ascent trajectory, the launch vehicle goes through four distinct phases:

- Vertical lift-off
- Pitch over
- Gravity turn
- Orbital coast phase and circularization

The first phase is necessary for safety issues, i.e., the launch vehicle must follow a vertical ascent for a few seconds until the vehicle is safely away from the launch pad. After that, a pitch over maneuver prepares to “kick” the vehicle for the gravity turn. Through the gravity turn maneuver the aerodynamic stress is minimized due to the naturally curving trajectory, maintaining low or even zero angle of attack. There are numerous control laws in the literature to model the flight trajectory. In [Markl \(2001\)](#), [Castellini \(2012\)](#) and [Pagano \(2010\)](#) a guidance programme is used which is divided into 5 phases, one more phase (bi-linear tangent law) is added between gravity turn and the last phase in the aforementioned flight phases. The bi-linear tangent law was derived in [Bryson and Ho \(1975\)](#) (see Eq. 6.34) for a very simple problem but can be used with good results in the exoatmospheric phase or vacuum.

$$\tan \beta = \frac{c_2 t + c_4}{c_1 t + c_3} \quad (6.34)$$

where c_1 , c_2 , c_3 and c_4 are constants to be determined. Another way to represent the control law, often used in literature and also used in this work, is performed simply by adjusting a polynomial function ([SILVA, 1995](#); [VANDAMME, 2012](#); [PAGANO, 2010](#)). This method can reduce significantly the number of control variables.

6.6 Path Constraints

To avoid unrealistic flight simulation and to preserve the payload integrity or crew safety in case of manned missions some path constraints should be included:

- Dynamic pressure
- Bending load
- Axial acceleration
- Heat flux

- Angle of attack

The dynamic pressure q is one of the most important parameters in flight trajectory. This parameter is function of the air density and air speed:

$$q = \frac{1}{2}\rho(r)V^2 \leq q_{max} \quad (6.35)$$

During the ascent trajectory the fairing is jettisoned when the aerothermal flux achieves a certain value. The aerothermal heat is function of the dynamic pressure q and air speed V :

$$Q = qV = \frac{1}{2}\rho(r)V^3 \leq Q_{max} \quad (6.36)$$

For the axial acceleration the following equation can be used:

$$a_{axial} = \frac{F(t) - D(t)}{mg_0} \leq a_{max} \quad (6.37)$$

6.7 Optimization

6.7.1 Background

In order to obtain the maximal payload capacity of a given launch vehicle, and consequently, make the access to space less expensive, trajectory optimization techniques have been for decades a subject of intense research. The trajectory optimization can be categorized basically into direct and indirect methods. In the referred papers of [Betts \(1999\)](#) and [Rao \(2009a\)](#) a comprehensive survey about both methods was made. To take advantage of both methods, a combination of both techniques can also be done, i.e., a hybrid method can also be considered ([STRYK; BULIRSCH, 1992](#); [PONTANI; TEOFILATTO, 2014](#); [GATH; CALISE, 2001](#); [GATH, 2002](#)).

6.7.1.1 Optimal Control Problem

The optimal control problem is detailed in a large number of publications as in the works of [Bryson and Ho \(1975\)](#), [Schlingloff \(2005\)](#) and [Tewari \(2011\)](#). The calculus of variations can be considered the foundations of this subject. The start point of the calculus of variations can be considered in 1696 when Bernoulli proposed the famous *brachistochrone curve* problem as a challenge for European mathematicians. Since

then, the theory was continuously developed during the centuries until becoming a subject of wide interest after the second war (Space Race) due to many applications in the aerospace field.

Indirect Method

The reason for this method be called “indirect” comes from the strategy to convert the original optimal control problem into a boundary-value problem. The most common indirect methods found in the literature are the shooting method (see Figure 6.6), the multiple-shooting method, and collocation methods as one can see in former reports of Brown et al. (1969) and Teren and Spurlock (1966), recent works as in the paper of Miele (2003) and in the Master thesis of Zerlotti (1990) which uses the algorithm BNDSCO (OBERLE; GRIMM, 1990). A manner to visualize the shooting method is considering an analogy with a cannon. Suppose it is intended to hit a given target and one have to determine the initial angle of the cannon. So a first shot is done (initial guess) and then, the angle is constantly adjusted until the target is hit. The main drawbacks of indirect shooting are; (a) the need of derivation of the first-order optimality conditions and, (b) to get a reasonable accurate estimate of the initial guesses for the adjoint equations, or costate variables. The sensitivity of the indirect shooting method for suffering from numerical problems for a wide range of problems are summarized elegantly in the following quote from Bryson and Ho (1975):

“The main difficulty with these methods is getting started; i.e., finding a first estimate of the unspecified conditions at one end that produces a solution reasonably close to the specified conditions at the other end. The reason for this peculiar difficulty is the extremal solutions are often very sensitive to small changes in the unspecified boundary conditions. . . . Since the system equations and the Euler-Lagrange equations are coupled together, it is not unusual for the numerical integration, with poorly guessed initial conditions, to produce “wild” trajectories in the state space. These trajectories may be so wild that values of $x(t)$ and/or $\lambda(t)$ exceed the numerical range of the computer!”

To enlarge the convergence radius of the shooting method, a multiple-shooting technique can be considered. However, even the multiple-shooting method can present sensitivity propagated by the initial guesses as well.

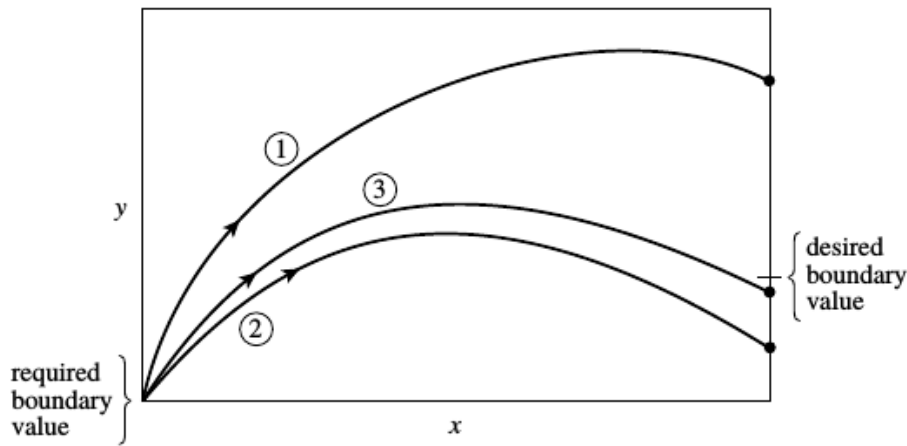


Figure 6.6 - Schematic of Indirect Shooting Method.
SOURCE: Rao (2009b)

Direct Method

Presumably because of the possibility of solving very complex problems with a minimum effort of mathematical analysis, this method is preferred for most of the researches (HARGRAVES; PARIS, 1987; HERMAN; CONWAY, 1996; SEYWALD, 1994; SILVA, 1995; BALESIDENT, 2011). The problem is characterized by a set of parameters which define the control law. Perhaps the most popular software representing this category is the POST (Program to Optimize Simulated Trajectories) (BRAUER et al., 1977). This problem is a typical Non Linear Programming Problem (NLP) and can be solved using classical Gradient-based methods (deterministic methods) such as Sequential Quadratic Program (SQP) or by heuristic methods. According to Betts (1999), heuristic optimization algorithms is not computationally competitive with gradient methods. Even though presumably because of ease of implementation without a detailed understanding of the problem, in the last two decades a lot of papers using Particle Swarm Optimization (PSO), genetic algorithms (GA) among others were applied to solve trajectory optimization problems. As for indirect methods, the direct methods can be categorized in direct (multiple) shooting or collocation. In the case where only the control variables are adjusted by a function, the method is called a shooting method. When both the state and control are parameterized, the method is called a collocation method (Figure 6.7.2.1). A well-known software developed by the University of Stuttgart which addresses the direct collocation method is *the AeroSpace Trajectory Optimization Software* (ASTOS). For either direct or indirect approaches, perhaps the most important benefit gained from a multiple shooting

formulation compared to its precursor (single shooting) is enhanced robustness.

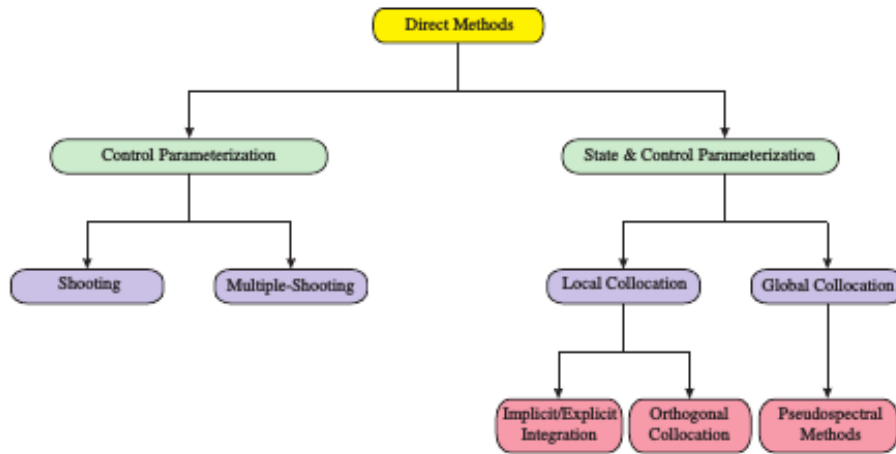


Figure 6.7 - Different Types of Direct Methods.
SOURCE: Rao (2009a)

6.7.2 Methodology

In this section the techniques used to solve the trajectory optimization problem are presented. The first approach was based on the Master thesis of Silva (1995). The second one describes a hybrid algorithm at which merges the direct and indirect methods.

6.7.2.1 First Approach - Direct Method

The method applied within the framework of this approach is based on the work of Silva (1995). Here a polynomial control function is used to model the flight profile. Four parameters are optimized in order to get the maximum payload mass which are the coast time duration t_{coast} (when it is applied) and three parameters of the polynomial control function. A code from Jacob (1972)'s report written in FORTRAN is transcript to C++ language and adapted to solve the problem.

$$\beta = \begin{cases} \pi/180, & \text{if } t \leq t_v, \\ b_0 - b_1(t - t_v) + b_2(t - t_v)^2, & \text{if } t_v < t \leq t_{b1}. \\ b_3 - b_4(t - t_{tf1}) + b_5(t - t_{b1})^2, & \text{if } t_{b1} < t \leq t_{bf}. \end{cases}$$

where

$$b_0 = \frac{\pi}{2}$$

$$b_1 = \frac{\beta_1 \pi}{180(t_{b1} - t_v)}$$

$$b_2 = -\frac{b_0 - \beta_2 \pi / 180 - b_1(t_{b1} - t_v)}{(t_{b1} - t_v)^2}$$

$$b_3 = \frac{\beta_2 \pi}{180}$$

$$b_4 = \frac{\beta_3 \pi}{180(t_{bf} - t_{b1})}$$

$$b_5 = \frac{b_3 - b_4(t_{bf} - t_{b1})}{(t_{bf} - t_{b1})^2}$$

t_v - vertical flight time [s]

t_{b1} - first stage burn time [s]

t_{bf} - overall flight time [s]

β_1, β_2 and β_3 - set of optimization control parameters

Thus, the trajectory optimization problem can be formulated as:

$$\text{Find } \mathbf{X} = \begin{bmatrix} t_{coast} \\ \beta_1 \\ \beta_2 \\ \beta_3 \end{bmatrix} \text{ which maximize the payload mass } F(\mathbf{X}) = m_{pl}$$

subject to the constraints at orbit injection. Thus, for the first formulation of equations of motion:

$$r = R_e + h_f \tag{6.38}$$

$$u = 0 \tag{6.39}$$

$$v = \sqrt{\frac{\mu}{r}} \tag{6.40}$$

and for the second one:

$$r = R_e + h_f \quad (6.41)$$

$$\gamma = 0 \quad (6.42)$$

$$v_I = \sqrt{v^2 + (\omega_{Er} \cos \phi)^2 + 2v\omega_{Er} \cos \phi \cos \gamma \cos \zeta} = \sqrt{\frac{\mu}{r}} \quad (6.43)$$

6.7.2.2 Second Approach - Hybrid Method

The idea behind the strategy is to divide the flight trajectory into two distinct phases, one while the vehicle ascends the dense atmosphere and the other one when the vehicle is virtually in vacuum space, i.e., where aerodynamic effects can be ignored. In the aforementioned sections it was stated that the sensibility of the indirect shooting or even multiple shooting method depends on the initial guess, however, it is possible to compute the initial co-states variable for optimal thrust arcs in vacuum fairly easy using almost arbitrary initial guess when direct and indirect methods are merged.

Stages before coasting - Direct method

To fulfill this task, the method used in the first method is applied here. In other words, the same control variables will be obtained until the beginning of the coast arc. Furthermore, this step gives the gross lift-off mass (GLOW) of the vehicle.

Upper Stage Trajectory - Indirect method

In this phase the vehicle is assumed to be out of the denser layers of the atmosphere, so that the aerodynamics forces can be neglected. Thus the trajectory of the upper stage is accomplished in the orbit plane. The upper stage flight is divided into two phases: a coast arc and a thrust arc. The equations of motion were taken from Schlingoff (1986) and presented below.

$$\dot{r} = u \quad (6.44)$$

$$\dot{u} = \frac{v^2}{r} - \frac{\mu}{r^2} + \frac{F}{m} \sin \beta \quad (6.45)$$

$$\dot{v} = -\frac{uv}{r} + \frac{F}{m} \cos \beta \quad (6.46)$$

Applying the Lagrange method, the Hamiltonian H is constructed as:

$$H = \lambda_u \left(\frac{v^2}{r} - \frac{\mu}{r^2} + \frac{F}{m} \sin \beta \right) + \lambda_v \left(-\frac{uv}{r} + \frac{F}{m} \cos \beta \right) + \lambda_r \quad (6.47)$$

The adjoint equations for the co-state (Euler-Lagrange equations) are:

$$\dot{\lambda}_u = -\frac{\partial H}{\partial u} = \frac{v}{r} \lambda_v - \lambda_r \quad (6.48)$$

$$\dot{\lambda}_v = -\frac{\partial H}{\partial v} = -2\frac{v}{r} \lambda_u + \frac{u}{r} \lambda_v \quad (6.49)$$

$$\dot{\lambda}_r = -\frac{\partial H}{\partial r} = \left(\frac{v^2}{r^2} - 2\frac{\mu}{r^3} \right) \lambda_u - \frac{uv}{r^2} \lambda_v \quad (6.50)$$

Using the Pontryagin minimum principle, the optimal thrust angle control can be expressed as a function of the co-states:

$$\frac{\partial H}{\partial \beta} = \frac{F}{m} (\lambda_u \cos \beta - \lambda_v \sin \beta) = 0 \quad (6.51)$$

and finally:

$$\tan \beta = \frac{\lambda_u}{\lambda_v} \quad (6.52)$$

Thus, to get the optimal trajectory, Eqs. 6.44-6.46 along with Eqs. 6.48-6.50 should be integrated. However, as the Lagrange multipliers have no physical meaning and the flight path depends very sensitively on the initial guesses, it is difficult to solve these equation. To deal with this problem [Schlingloff \(1986\)](#) developed an analytical

method to eliminate the Lagrange multipliers getting formulas that can be represented by a smaller number of variables. Thus, defining z :

$$z = \frac{r^2 \dot{\beta} - rv}{\cos^2 \beta} \quad (6.53)$$

Schlingloff (1986) got alternative differential equations to represent the control law:

$$\tan \dot{\beta} = \frac{z}{r^2} + \frac{v}{r}(\tan \beta^2 + 1) \quad (6.54)$$

$$\dot{z} = \frac{\tan \beta}{r}(4vz + 3\mu) \quad (6.55)$$

Thus, to get the new system of first-order differential equations, the control equations 6.54 and 6.55 must be joined to the equations of motion 6.44-6.46. To integrate this system, since the initial condition for the state equations are fixed, just the initial guesses to the control equations must be set. To take into account the coast, the optimization problem can be stated as:

Find $\mathbf{X} = \begin{bmatrix} \beta_0 \\ z_0 \\ t_{coast} \end{bmatrix}$ which minimize the propellant mass of the upper stage $F(\mathbf{X}) = m_{prop}$. It implies maximizing the payload mass that can be injected into the desired orbit. The constraints at orbit injection are:

$$r = R_e + h_f \quad (6.56)$$

$$u = 0 \quad (6.57)$$

$$v = \sqrt{\frac{\mu}{r}} \quad (6.58)$$

To solve this problem we can use the same algorithm used in the first phase or heuristic methods such as particle swarm optimization (PSO).

7 PROGRAMME SETUP

In this chapter the general architecture of the application program is described. As previously mentioned a modular approach using object-oriented programming (OOP) is chosen and to allow a better visualization of the codes, UML diagrams will be used. The mathematical models developed in the previous chapters will be part of the functionality of each code module.

In order to clarify the subject, in the following sections a brief discussion about OOP and the UML software is presented.

7.1 Object-oriented Programming (OOP)

The fundamental idea behind object-oriented languages consists in dealing data and functions that operate on that data like a single “object”. Besides the aforementioned term “object”, another key concept of OOP are the “classes”. We can understand a class as a “factory” of objects, in other words, an object is an instantiation of a class. A class can be seen as a type defined by the user, i.e., a class can be used similarly as the built-in data types (e.g., *int*, *double*, *char*, *bool*, ...). The four pillars of the development of OOP are:

- Encapsulation
- Hiding data
- Heritage
- Polymorphism

By means of encapsulation and hiding data, a well defined class acts as an entity completely encapsulated, the users do not need to understand how the class works, they just need to know how to use it instead. Heritage means reusability, i.e., from a base class other subclass can be derived which “inherits” all the characteristics (functions and attributes) from the mother class.

The basic characteristics between object-oriented and the traditional procedural programming language is listed in Table 7.1.

Usually OOP is not the first option for engineers or researchers, this is in part because they are already relatively acquainted with procedural programming and also

Table 7.1 - Comparison between object-oriented and function-oriented (procedural) programming.

Items	Procedural Programming	Object-oriented Programming
1. Relationship data/functions	Separate data from functions	They are combined in a single unit (the object)
2. Abstraction	Low	High
3. Reusable	Not easy (Programmers must often “recreate the wheel)	Easy
4. Data security	Low	High
5. Idea behind Real-World modeling	Different	Similar
6. Speed	Quickly	Lower
7. Write a code	Relatively simple	Harder

SOURCE: Lafore (2002) and Farrell (2013)

because of the inherent complexity to deal with objects. In fact, the task of creating a well-designed class hierarchy describing a launch vehicle, the subsystems and the environment is quite challenging. Besides the class interface and its functionality does not proceed in a straightforward manner, instead requires many trial and error, and rearrangement (HINCKEL, 1995). In this work we have classes from components of a rocket engine such as pumps or turbines, a whole engine, a launch vehicle to classes representing the environment like atmosphere and gravitational field.

7.2 Unified Modeling Language (UML)

UML is a tool for modeling object-oriented codes. It is used to visualize the code and the communication between objects enabling a high degree of abstraction. The UML interface for a class can be represented by the Figure 7.1.

To represent the different types of communication between two objects, different types of “arrows” are used, i.e.; depending on the relationship between them, a different arrow is assigned. The dashed arrow shown in Figure 7.2 represents the dependency relationship of the classes *Orbit* on the class *Aster* (e.g., the functions *Period()* and *InertialVelocity()* from *Orbit* require the standard gravitational parameter μ from *Aster*). This type of dependency will be also observed with the rocket

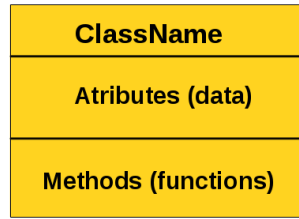


Figure 7.1 - UML Interface.

engine and launch vehicle.

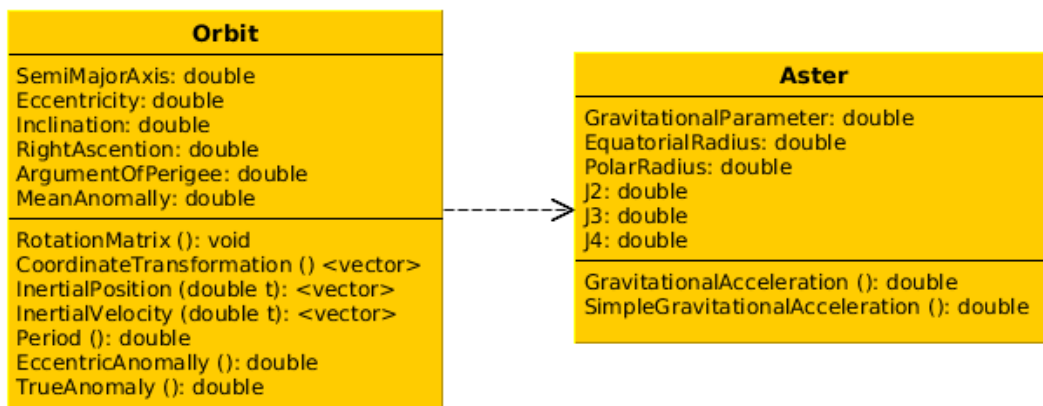


Figure 7.2 - Dependency relationship between orbit class and aster class.

In the following section the way that components of a LRE can be grouped in order to create a subsystem or system and the way a launch vehicle interacts with the environment will be outlined. Thus, the communication among components of a LRE and between the launch vehicle and the environment will be facilitate by making use of UML diagrams.

7.3 Overview of the Main Components Functionality

In the previous chapters many modeling equations were presented. Although some of them are used to model the same event, all of them were implemented. It means that each component or (sub)system can store many functions. Thus, in order to avoid an exhaustive discussion only the functions required to balance the powerhead and calculate the engine dry mass will be described (see Table 7.2).

Table 7.2 - Overview of the main components functionality of a liquid rocket engine required in order to perform the simulation of the engine cycle.

Components	Main functions	Source	Description
Pump	$Power()$	Eq. 3.1	Output pressure and mass flow rate are the unknowns.
Turbine	$Power()$	Eq. 3.7 or Eq. 3.9	Mass flow rate is the unknown. These functions depends on the gas generator component which in turn stores data from the CEA program. However the first equation can also be used when Δh is given by the user (i.e. in booster turbopump or expander cycle application)
Turbopump	$Mass()$	Eq. 4.6	Depends on power turbine and average density of propellants. Two others relations are presented in Chapter 4.
Combustion Chamber	$Mass()$, HeatCapacityRatio(), SpecificHeat(), MolarMass(), CharacteristicVelocity()	Chap. 4 (first function)	The gas generator/pre-burner dry mass is embedded within the $Mass()$ function. Data from CEA program are stored in the other functions.
Nozzle extension	$Mass()$	Chap. 4	Simple relation function of the thrust force and chamber pressure, and nozzle extension ratio.
Injector head	$Mass()$	Chap. 4	Simple relation function of the thrust force and chamber pressure.
Thrust chamber	$Thrust()$, $Isp()$	Eqs. 3.21, 3.22	Mass flow rate is the unknown of the thrust function. Data from CEA program are stored in $Isp()$.
Gas generator/Pre-burner	Same as used in combustion chamber	-	Store data taken from CEA program.
Valves	$Mass()$	Chap. 4	Simple relation function of the thrust force and chamber pressure.

7.4 Engine Components Assembly Modeling

The idea behind this section is to present the first ideas about the degree of relationship between different objects, i.e., the dependency between them will be shown.

7.4.1 Turbopump Assembly Modeling

A turbopump is basically a set of turbine(s) and pump(s) working together to transport or to provide energy to a given working fluid. So we can readily see two kinds of relationships with respect to the turbopump, namely:

- Strong aggregation. The pump(s) and turbine(s) are part of the TPA.
- Weak aggregation. The working fluid flows through the TPA unit but it is not integral part of the equipment.

In Figures 7.3 and 7.4 are presented, respectively, a single-shaft and dual-shaft turbopump. From the figures, the communication between objects (components and fluid) are represented by an arrow with filled diamond at the end (strong aggregation) and an arrow with unfilled diamond at the end (weak aggregation).

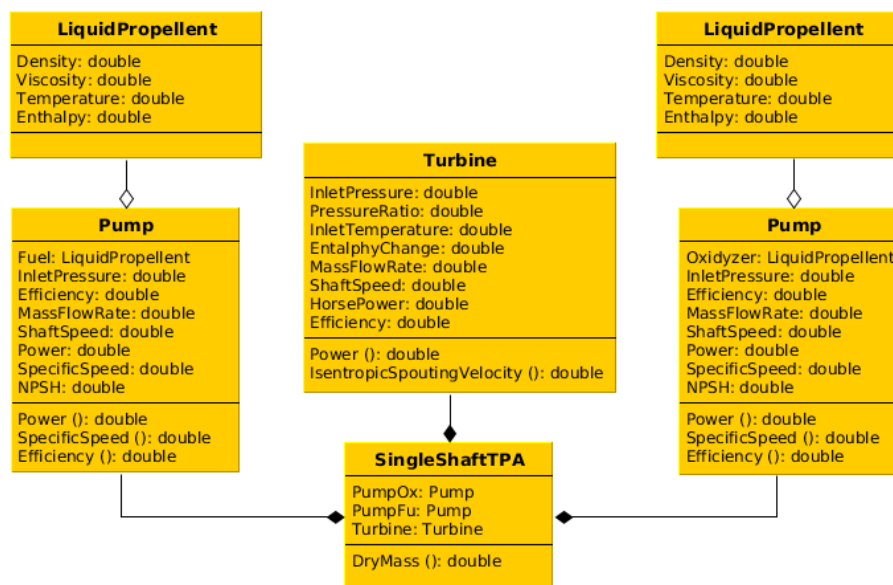


Figure 7.3 - UML - Single Shaft TPA.

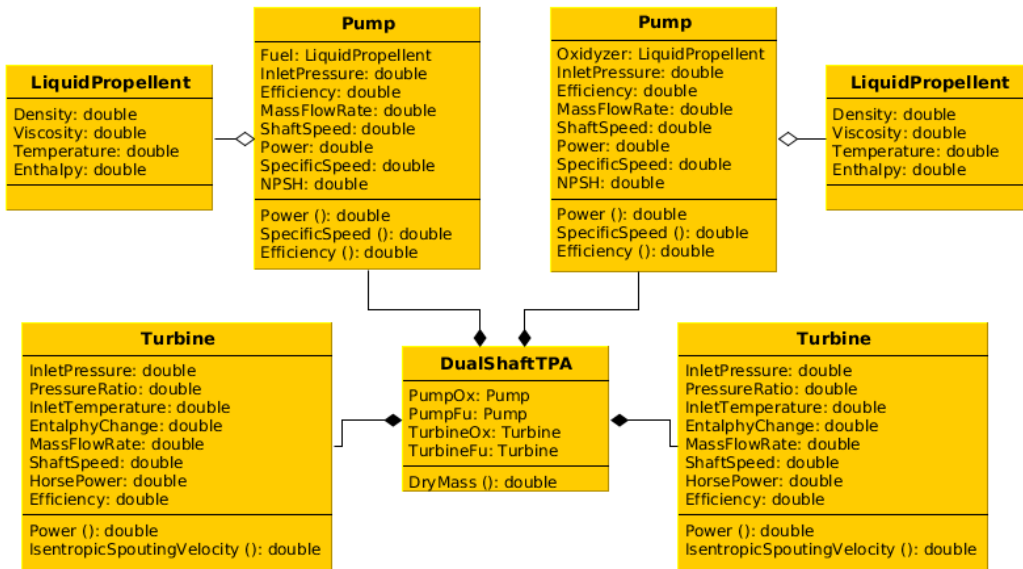


Figure 7.4 - UML - Dual Shaft TPA.

7.4.2 Thrust Chamber Assembly Modeling

The thrust chamber is assembled of combustion chamber, nozzle and injector head. As in the above case for a turbopump, we can see arrows showing the two types of aggregation in the thrust chamber (Figure 7.5).

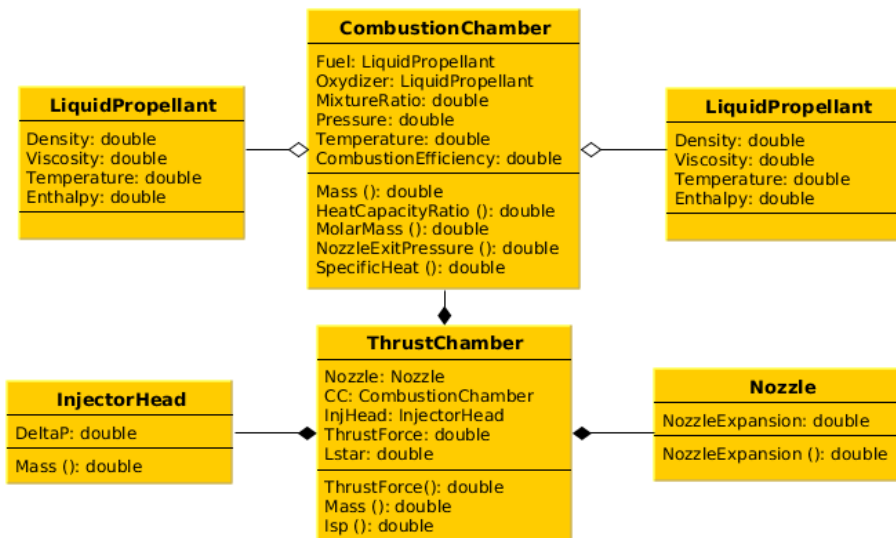


Figure 7.5 - UML - Thrust Chamber Assembly.

7.5 Engine Cycle Modeling

In Figure 7.6 is presented a possible UML diagram for a liquid rocket engine with gas generator cycle and single shaft turbopump. The configuration of the diagram was conveniently chosen to represent the L75 rocket engine. From the diagram we can see some parameters and functions of each component and the relationship between them. In order to make the diagrams clear, some parameters and functions are omitted. The rocket engine is compound of objects of the following components (classes): *Turbopump*, *ThrustChamber*, *Valves*, *GasGenerator* and *LiquidPropellant*. These objects along with with specific impulse, thrust force, mixture ratio and feed lines pressure drops form the parameters of the rocket engine (class *LiquidRocketEngine*). The functionality of each model was developed in Chapters 3-5. From *LiquidRocketEngine* class, important functions to be highlighted are *RocketSimulator()* where the modeling equations were developed in Chapter 5 and *DryMass()* where the modeling equations were presented in Chapter 4.

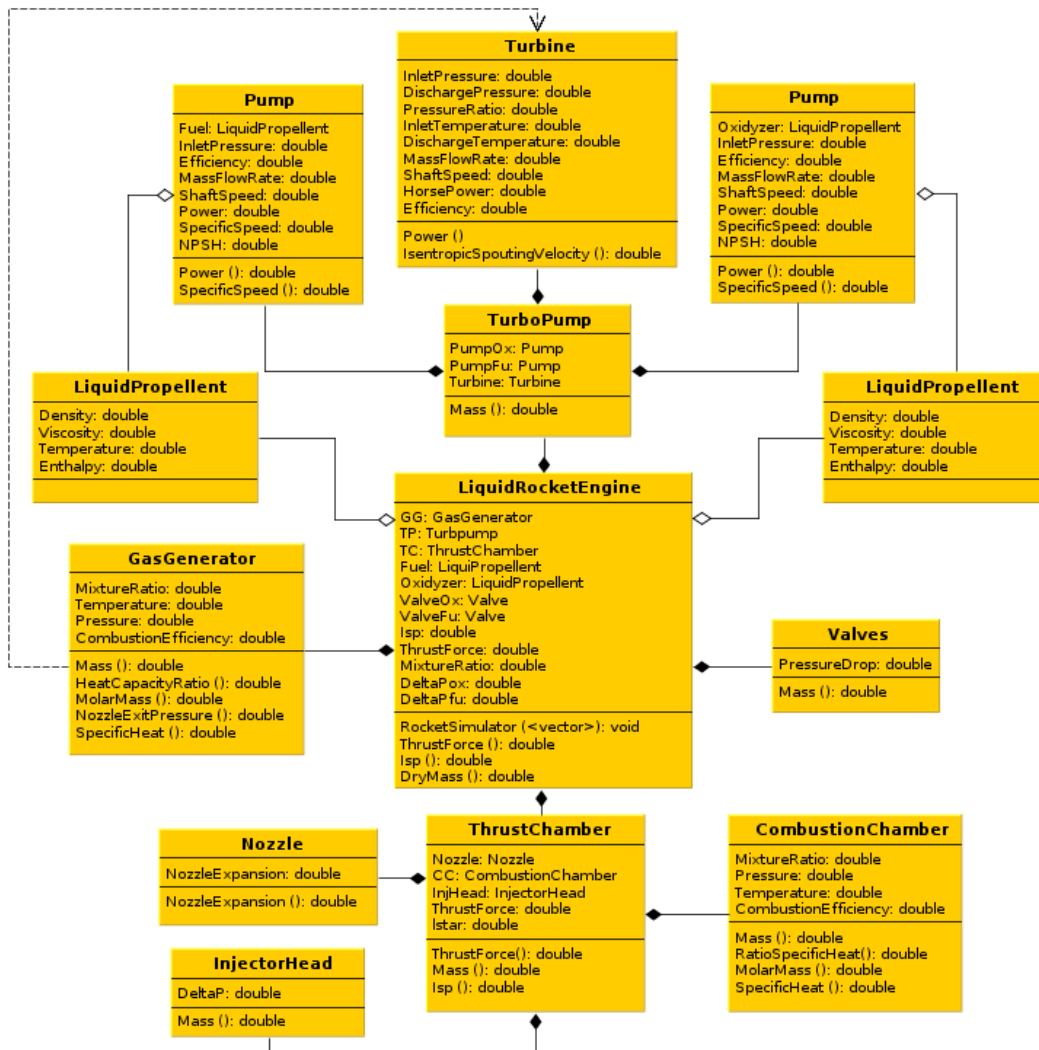


Figure 7.6 - UML diagram of a gas generator cycle.

The dashed arrow between gas generator and turbine represents the dependency of turbine functionality on gas generator functions, i.e., the function $Power()$ depends on combustion gas parameters which are functions of gas generator class. In order to represent a LRE with booster-pump, the Space Shuttle Main Engine (SSME) was chosen. From the Figure 7.7 we can see that the referred staged combustion engine receives four turbopumps, namely the main turbopumps (HPOTP and HPFTP) and the auxiliary turbopumps (LPOTP and LPFTP).

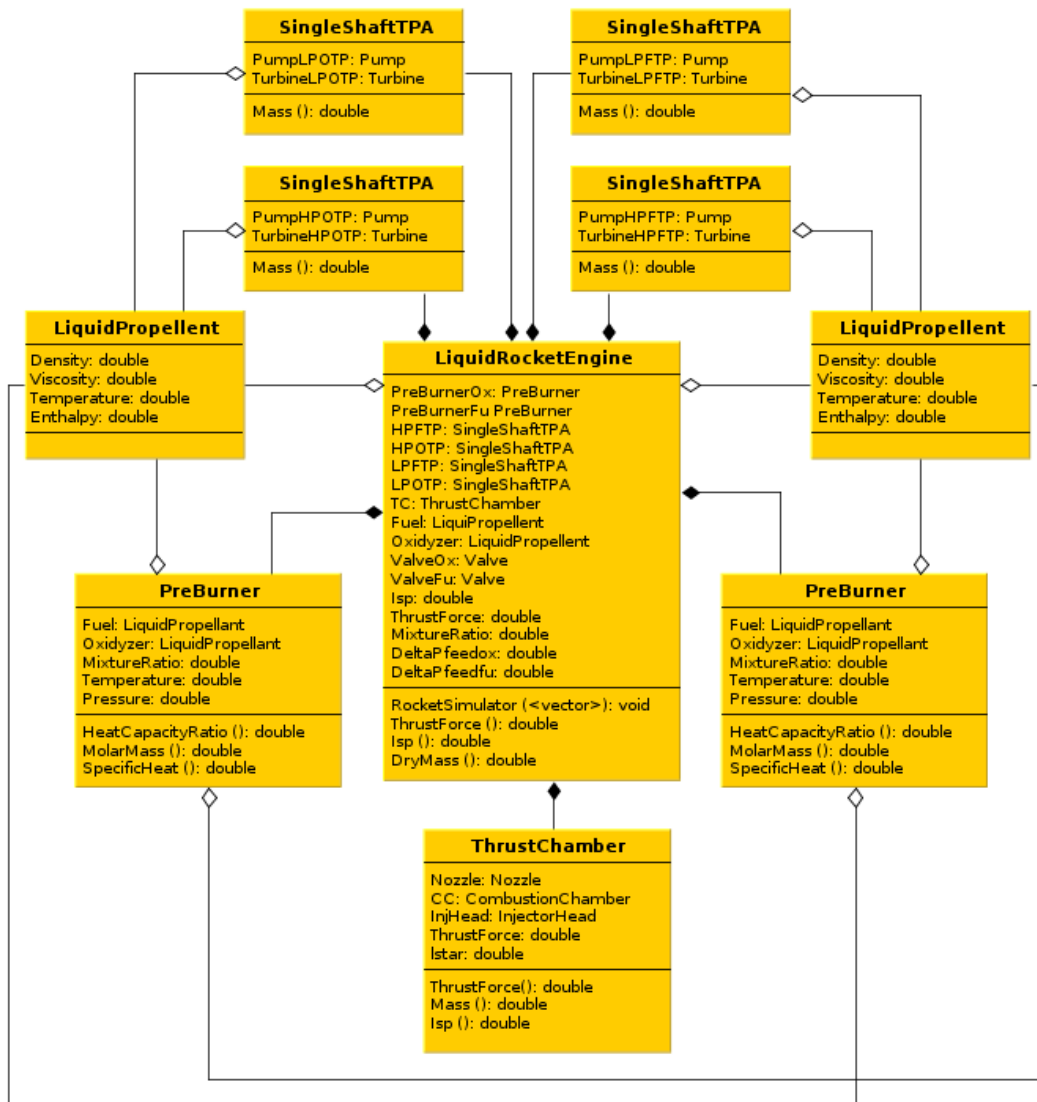


Figure 7.7 - UML diagram of a staged-combustion liquid rocket engine.

7.6 Launch Vehicle Modeling

A possible UML diagram for a launch vehicle is given in Figure 7.8. The configuration of these diagram was conveniently chosen to represent the Brazilian VLS-alfa. From the diagram we can see some parameters and functions of each component and the relationship between them. In order to make the diagram clear, some parameters and functions are omitted. In Figure 7.8 is shown which parameters define the launch vehicle and the interactions with the environment.

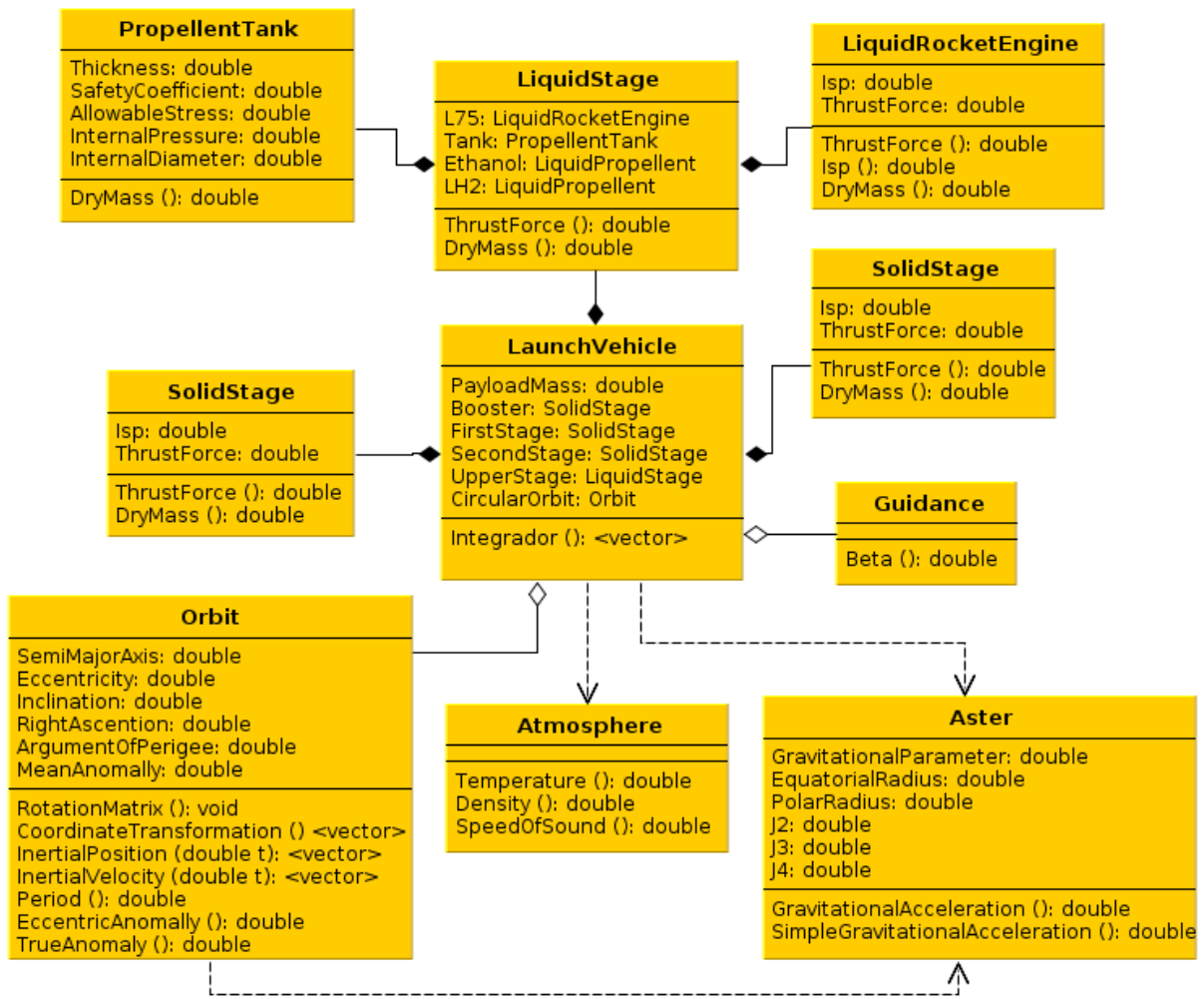


Figure 7.8 - UML - Launch Vehicle Model.

The seventh chapter of this work was designated to join in a modular way all mathematical models developed in previous chapters. To explicit the dependency of elements and how to group single classes in order to create composed classes, UML diagrams were used. Thus, the communication between components of liquid rocket engines, propulsion system and launch vehicle, and launch vehicle and environment was considerably facilitated which is intended to allow a better reusability and extensibility of the codes. The following chapters are responsible to show the applicability of the developed tool.

8 RESULTS 1: SIMULATION OF LIQUID ROCKET ENGINES

Based on mass and energy conservation laws, in Chapter 5 was presented a modeling of different power cycles of liquid rocket engines. This chapter is devoted to verify the efficiency and applicability of the developed codes for engine cycles performance. In other words, liquid rocket engines with open cycle and closed cycle arrangement will be simulated. The following section shows the results for LREs operating at the design point and the last one presents a simplified analysis of engines cycles operating at different operating points.

8.1 Performance of a Liquid Rocket Engine

Here, only the traditional cycles will be considered. The following types of liquid rocket engines were chosen to represent each type of cycle:

- Gas generator cycle: L75, Vulcain and HM7B
- Staged combustion cycle: SSME

Detailed flow schemes of these rocket engines are shown in Annex .

L75

To begin with, a LRE which uses an unusual propellant combination (LOX/Ethanol) is considered. The Brazilian L75 rocket engine (in development - see Figure A.1) will operate in open cycle with a single shaft turbopump. Since the gases expelled by the turbine will be used for thrust vector control (TVC), its contribution to the thrust force is neglected. A simplified UML diagram of the L75 with only the function responsible to perform the simulation *RocketSimulator()* is shown in Figure 8.1.

The vector of unknowns which will be determined by the simulation of the set of nonlinear algebraic equations (embedded in the function *RocketSimulator()*) as already described in Chapter 5 is presented here again just for convenience as follows:

$$\mathbf{X} = \begin{bmatrix} p_{d,o} \\ p_{d,f} \\ \dot{m}_{o,g} \\ \dot{m}_{f,g} \\ \dot{m}_T \\ \dot{m}_{o,c} \\ \dot{m}_{f,c} \end{bmatrix} = \begin{bmatrix} \text{discharge pressure of the oxidizer pump} \\ \text{discharge pressure of the fuel pump} \\ \text{oxidizer mass flow rate in the gas generator} \\ \text{fuel mass flow rate in the gas generator} \\ \text{turbine mass flow rate} \\ \text{oxidizer mass flow rate in the combustion chamber} \\ \text{fuel mass flow rate in the combustion chamber} \end{bmatrix}$$

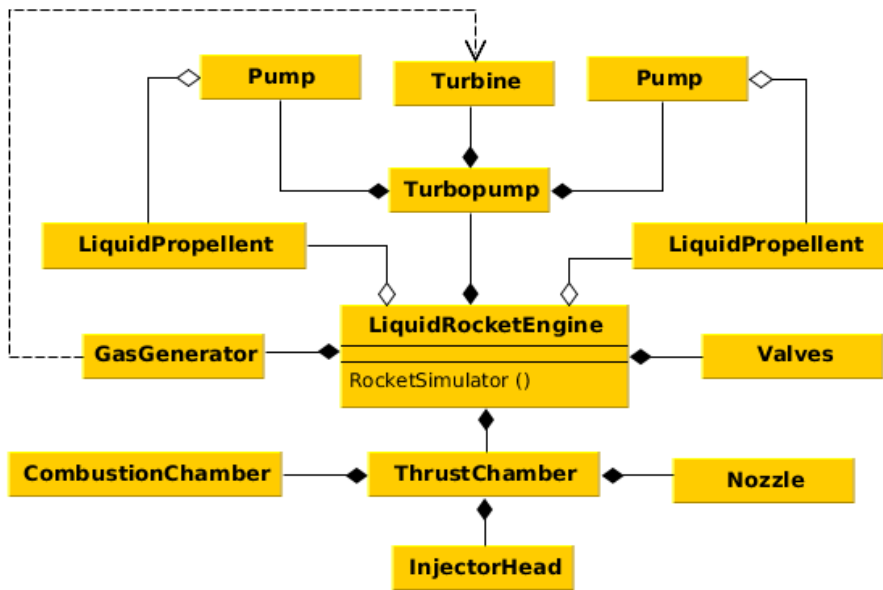


Figure 8.1 - Simplified UML diagram representing the L75 rocket engine.

Figure 8.2 presents the inputs and outputs used in the simulation of the engine. A comparison with actual values is given in Table 8.1.

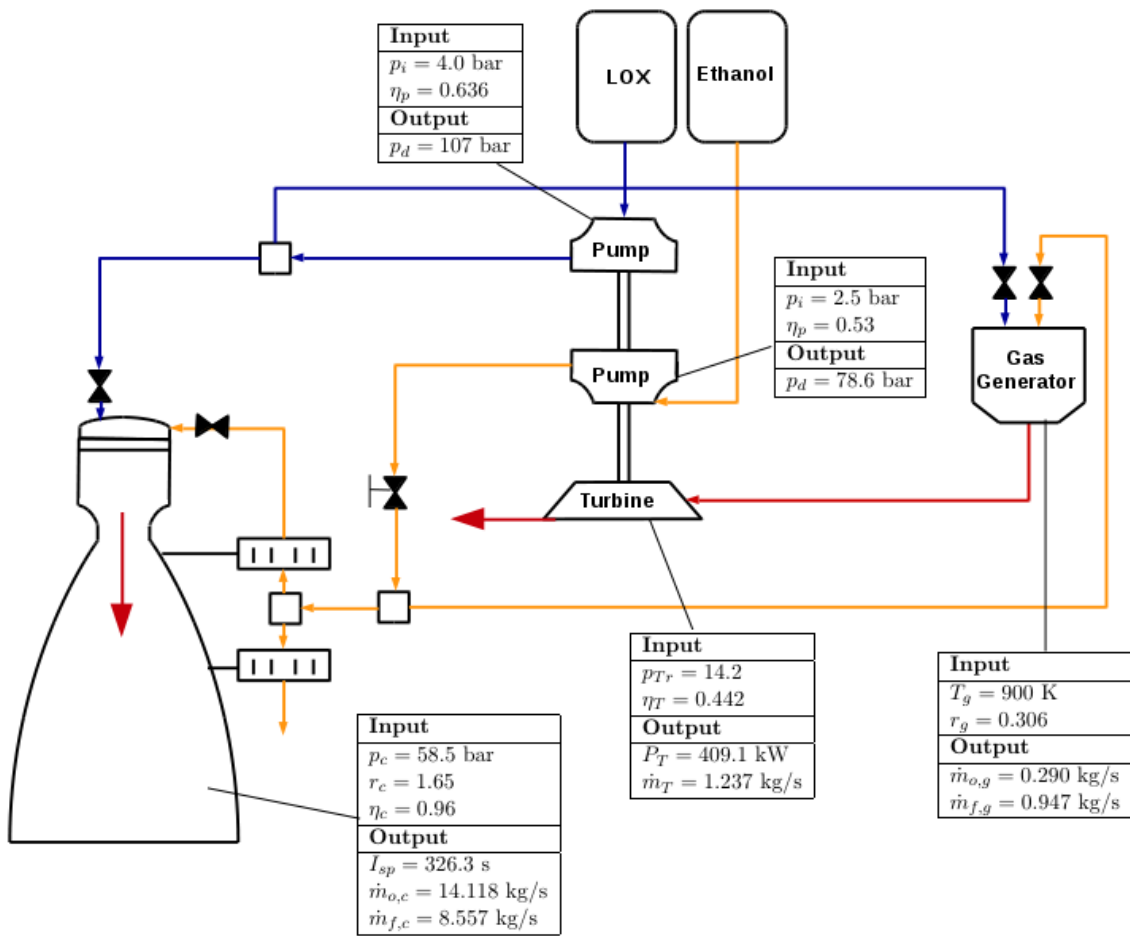


Figure 8.2 - L75 input/output.

SOURCE: The input data are courtesy of IAE.

Table 8.1 - Verification of the simulated parameters of the L75: Comparison with the literature.

L75	actual (courtesy of IAE)	calculated	error [%]
Key input			
F [kN]	75		
p_c [bar]	58.5		
r_c	1.65		
A_e/A_t	147		
Output			
I_{sp} [s]	326.5	326.268	0.07
$p_{d,o}$ [bar]	78	78.6	0.77
$p_{d,f}$ [bar]	106	107	0.94
$\dot{m}_{o,g}$ [kg/s]	0.30	0.290	3.33
$\dot{m}_{f,g}$ [kg/s]	0.99	0.947	4.34
$\dot{m}_{o,c}$ [kg/s]	14.35	14.118	1.62
$\dot{m}_{f,c}$ [kg/s]	8.55	8.557	0.08
P_T [kW]	403	409.1	1.51

From the results we can see values in excellent agreement with the literature.

Vulcain

The European Vulcain which is used as main engine by Ariane 5 is another type of gas generator cycle (see flow scheme in Figure A.2). Differently from the L75 the Vulcain has one turbine for each of the propellants. This is due to the relatively large difference of densities between its propellant combination LOX/LH2. It implies in one more unknown (mass flow rate through the second turbine) in the system of equations which in turn has one more equation in order to make the system possible. The inputs necessary to solve the problem and outputs are shown in Figure 8.3. A comparison with actual values is given in Table 8.2.

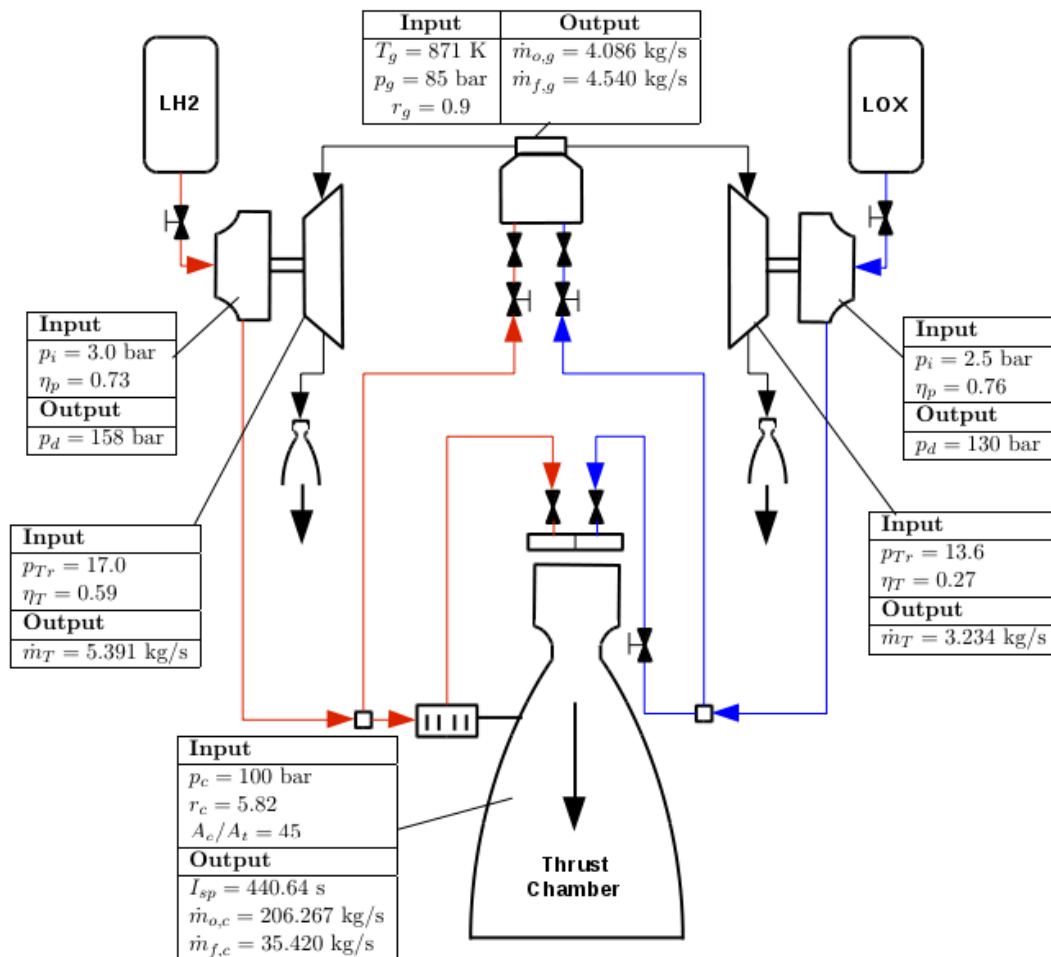


Figure 8.3 - Vulcain input/output.

SOURCE: The input data were taken from Pouliquen (1983) and Hugh (1995).

Table 8.2 - Verification of the simulated parameters of the Vulcain: Comparison with the literature.

Vulcain	actual (POULIQUEN, 1983; HUGH, 1995)	calculated	error [%]
Key input			
F [kN]	1025		
p_c [bar]	100		
r_c	5.9		
A_e/A_t	45		
Output			
I_{sp} [s]	433.5	433.291	0.05
$p_{d,o}$ [bar]	158	158	0.0
$p_{d,f}$ [bar]	130	130	0.0
\dot{m}_g [kg/s]	8.4	8.625	2.68
$\dot{m}_{T,o}$ [kg/s]	-	3.234	-
$\dot{m}_{T,f}$ [kg/s]	-	5.391	-
$\dot{m}_{o,c}$ [kg/s]	198.0	206.267	4.17
$\dot{m}_{f,c}$ [kg/s]	34.0	35.420	4.18
$P_{T,o}$ [MW]	3.0	3.13	4.33
$P_{T,f}$ [MW]	11.2	12.054	7.63

The major discrepancy was observed for the power of the fuel turbine (7.63%). The reason for that was already stated in Chapter 3 saying that Eq. (3.3) can substantially deviate from the expected values when used for a low density fluid under extremely high pressure. However the values can be considered in good agreement with the literature.

HM7B

The European HM7B which is another example of a gas generator cycle is used to power the upper stage of Ariane rocket family (see Figure A.3). A geared turbopump is responsible to provide the necessary energy to the cryogenic propellants LOX/LH2. As in the case of the L75, the HM7B has only one turbine, hence to simulate the performance of the engine the same set of unknowns are required. The input and outputs are shown in Figure 8.4 and Table 8.3.

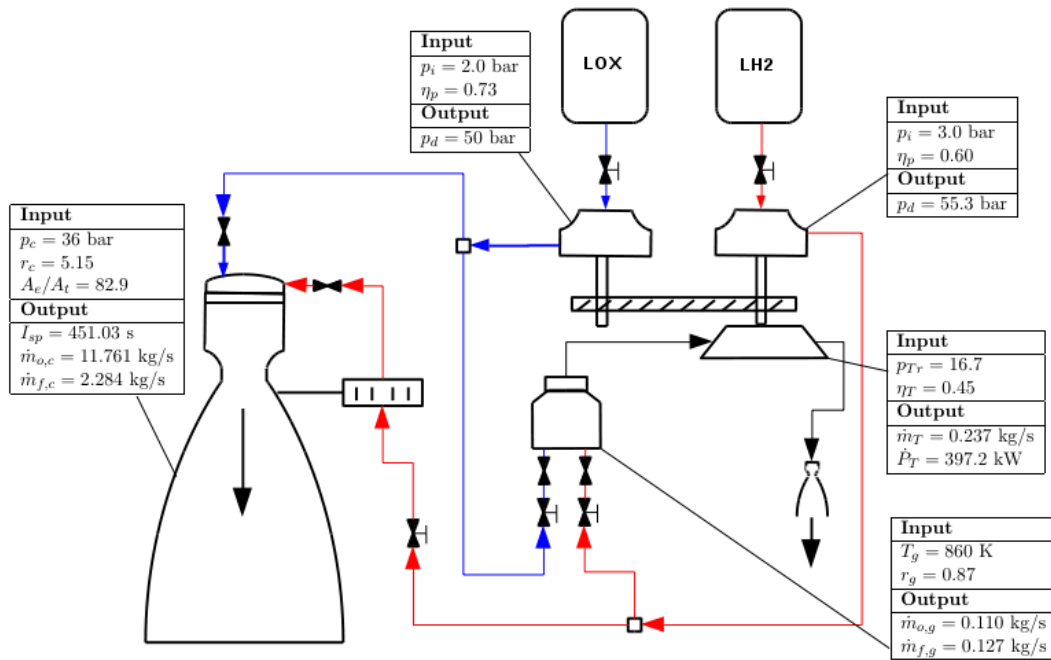


Figure 8.4 - HM7B input/output.

SOURCE: The input data were taken from Hugh (1995).

Table 8.3 - Verification of the simulated parameters of the HM7B: Comparison with the literature.

HM7B	actual (HUGH, 1995)	calculated	error [%]
Key input			
F [kN]	62.2		
p_c [bar]	36		
r_c	5.15		
A_e/A_t	82.9		
Output			
I_{sp} [s]	445.5	451.03	1.24
$p_{d,o}$ [bar]	50.2	50	0.40
$p_{d,f}$ [bar]	55.5	55.3	0.36
\dot{m}_g [kg/s]	0.25	0.237	5.2
\dot{m}_T [kg/s]	0.25	0.237	5.2
\dot{m}_c [kg/s]	13.9	14.045	1.04
P_T [kW]	404	397.2	1.68

The results of the last gas generator engine cycle shows also an excellent agreement with the actual values.

SSME

The Space Shuttle Main Engine (SSME) was the core engine responsible to power the Space Shuttle. Each of the two main turbopumps (HPOTP and HPFTP) are driven by a fuel-rich pre-burner (see flow scheme in Figure A.5). To increase the inlet pressure of the both main pumps, booster turbopumps are used. The set of unknowns along with the set of nonlinear algebraic equations were previously defined in Chapter 5. Figure 8.5 presents the inputs the main results obtained from the simulation. Table 8.4 compares the results with the literature.

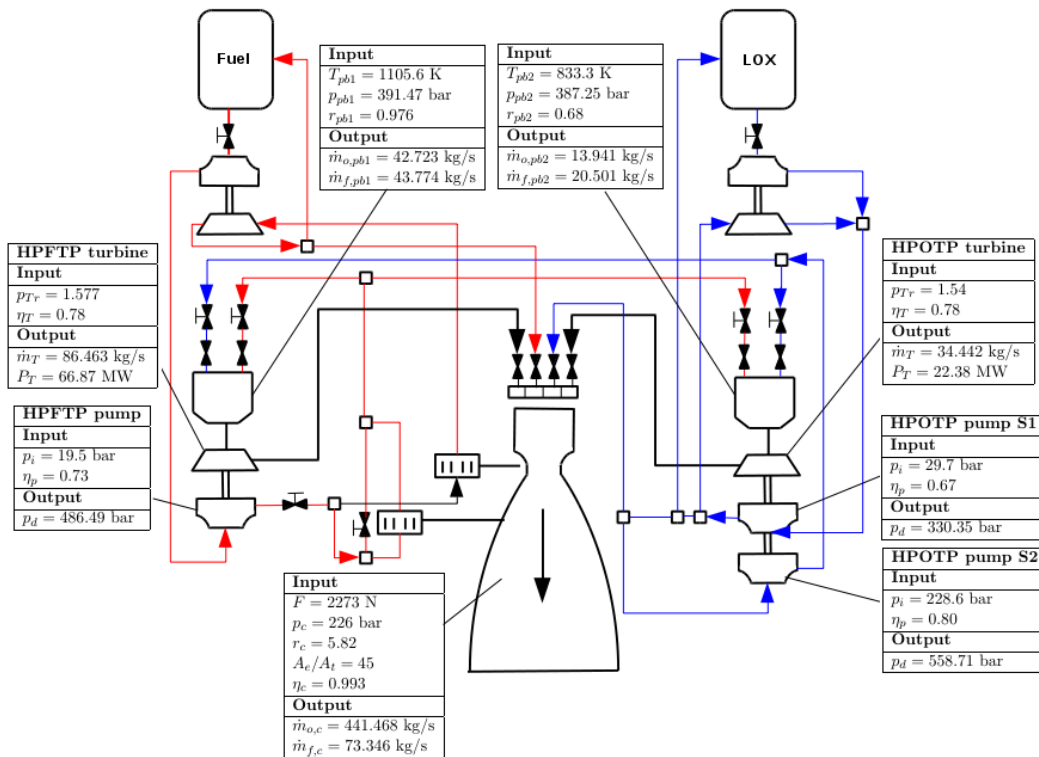


Figure 8.5 - SSME input/output.

SOURCE: The input data were taken from Manski et al. (1998).

Table 8.4 - Verification of the simulated parameters of the SSME: Comparison with the literature.

SSME	actual (MANSKI et al., 1998)	calculated	error [%]
Key input			
F [kN]	2273		
p_c [bar]	219.70		
r_c	6.019		
A_e/A_t	77.5		
Output			
I_{sp} [s]	444.0	451.267	1.63
$p_{d,o}$ [bar]	558.71	558.71	0.0
$p_{d,f}$ [bar]	486.49	486.49	0.0
$\dot{m}_{o,pb1}$ [kg/s]	36.90	42.723	15.8
$\dot{m}_{f,pb1}$ [kg/s]	37.81	43.774	15.8
$\dot{m}_{o,pb2}$ [kg/s]	13.56	13.941	2.81
$\dot{m}_{f,pb2}$ [kg/s]	19.94	20.501	2.81
$\dot{m}_{T,LPOTP}$ [kg/s]	83.06	82.89	0.20
\dot{m}_c [kg/s]	511.46	514.814	0.66
$P_{T,HPFTP}$ [MW]	57.79	66.87	15.7
$P_{T,HPOTP}$ [MW]	21.77	22.38	2.8

Apart from the mass flow rate through the fuel pre-burner and the power of the HPFTP turbine ($P_{T,HPFTP}$), all the calculated parameters are very reasonable. The deviations here are due to the same reason presented for the Vulcain engine. Manski et al. (1998) uses a relation function of the enthalpy change to estimate the pump power, therefore this large deviation is assured attributed to it.

8.2 Sensitivity Analysis

This section is devoted in changes in design parameters in order to control a desirable variable. However, to accomplish this task some considerations must be taken into account since the engine will operate at different operating points (off-design). To this end, the turbine and pump efficiency are assumed constant as well as the pressure drop in the feed system.

Gas Generator Cycle

To study the influence of the chamber pressure on overall specific impulse of a gas generator rocket engine, the L75 is used. To accomplish this analysis, the thrust is kept constant and the nozzle expansion ratio ϵ varies in order to extract the maximum kinetic energy. Thus, for a pressure vector $p_c = [30 \ 40 \ 50 \ 58.5 \ 80 \ 100]^T$,

the values of specific impulse at thrust chamber and nozzle expansion are given in Table 8.5.

Table 8.5 - Values of specific impulse and nozzle expansion for different chamber pressures.

L75	p_c [bar]					
	30	40	50	58.5	80	100
$I_{sp(vac)}$ [m/s]	3485.4	3516.6	3539.4	3554.9	3584.1	3603.8
A_e/A_t [-]	87.828	109.56	130.16	147	187.51	223.22

To calculate to global specific impulse of the engine we must consider the contribution of the gas generator. The following equation is used:

$$I_{sp,oa} = \frac{\dot{m}_g I_{sp,g} + \dot{m}_c I_{sp,c}}{\dot{m}_{ox,oa} + \dot{m}_{fu,oa}} \quad (8.1)$$

where the subscripts g , c , and oa stands for gas generator, combustion chamber and overall, respectively. After the simulation of the engine for each chamber pressure, we finally get the results as presented in Figure 8.6.

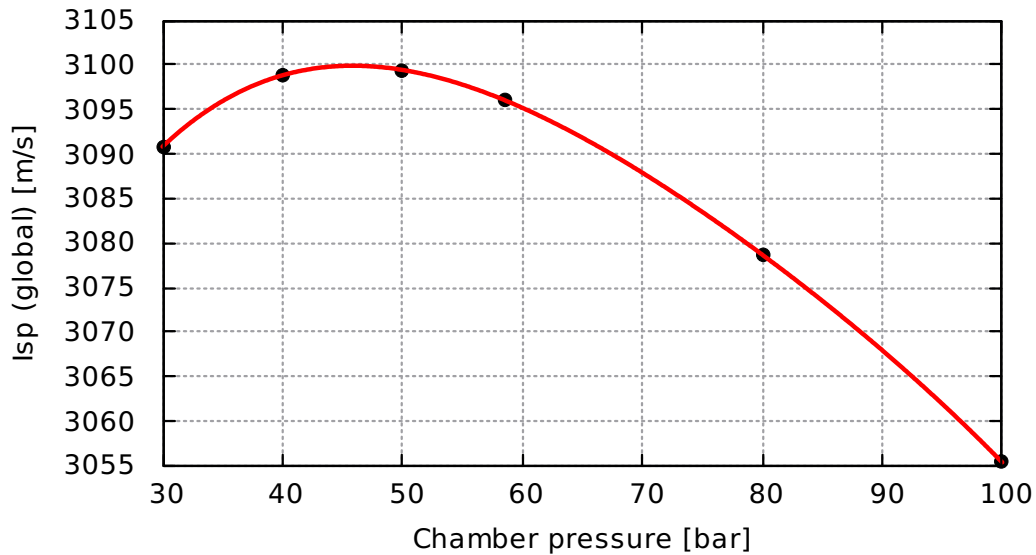


Figure 8.6 - Performance of the L75 rocket engine as function of the chamber pressure.

The curve profile was as expected for a gas generator cycle. As the chamber pressure increases, the specific impulse at combustion chamber increases but this is offset with

the increased power of the turbine by means of turbine mass flow rate.

9 RESULTS 2: TRAJECTORY SIMULATION

To validate the trajectory program two launch vehicles will be considered, namely; the Brazilian VLS and the European Ariane 5. Both mathematical modeling of the ascent trajectory presented in Chapter 6 will be used in order to verify the concordance between them. The trajectory optimization will be performed using direct and hybrid method.

9.1 Direct Method

As previously mentioned the idea behind this method is to make use of a simple (e.g., polynomial) function to model the control law in order to get the optimum trajectory (Section 6.7.2.1). This section presents the simulation of the VLS-1 using both modeling of state equations presented in Section 6.4 and the simulation of the Ariane 5 launch vehicle.

9.1.1 VLS launch Vehicle

The under development VLS-1 is the future Brazilian satellite launch vehicle. Its development started in 1984, however due to technical problems the vehicle could not be qualified up to now. VLS-1 is composed of four solid stages. The first stage is equipped with four solid boosters S43 (see Figure 9.1). The vehicle is designed to perform a non-powered coast arc between third and upper stages. Key parameters of the vehicle used in the simulation are given in Figure 9.1. The mission is to launch a satellite into a reference circular orbit of 500 km of altitude from the Alcântara Launch Center ($2^{\circ}22'39.52'' S$, $44^{\circ}23'57.71'' W$).

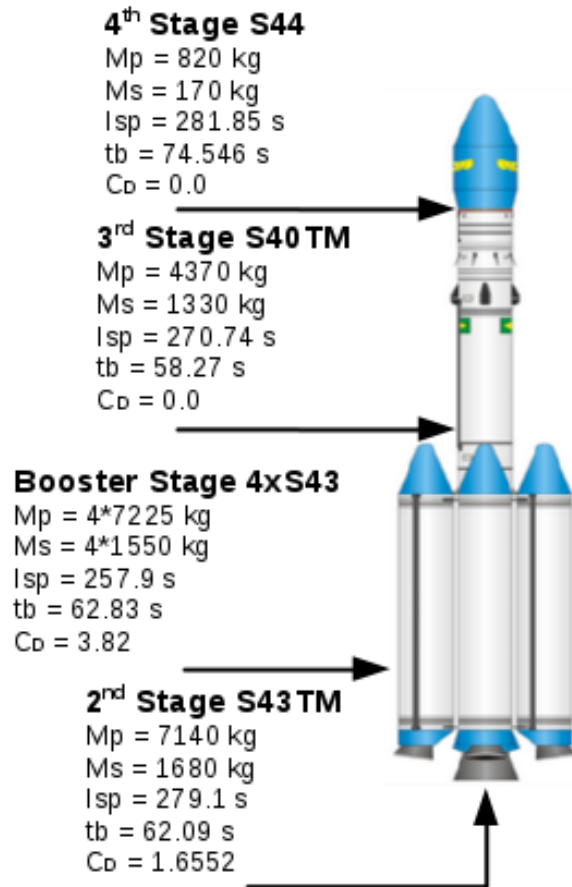


Figure 9.1 - VLS-1 design parameters.

Simulation Using First Formulation of State Equations

This section presents the simulation of the VLS-1 using the equations of the translational motion as described in Section 6.4.1. Table 9.1 summarizes the corner instants between flight phases and Table 9.2 presents the control parameters obtained by optimization subroutine. The cost-arc between third and upper stages presented a time duration of 347.71 seconds and the payload mass injected into orbit was 270.5 kg.

Table 9.1 - Values for state variables at start, inter-stage and end instants.

t (s)	h (km)	u (m/s)	v (m/s)	Ω (deg)	i (deg)	ω (deg)
0.0	0.0	0.0	421.5	90.0	-2.4	-44.4
62.8	23.5	763.5	1390.0	90.4	-2.4	-63.3
124.9	75.4	1023.9	2729.1	91.5	-2.4	-64.1
183.2	154.5	1927.9	4947.7	93.4	-2.4	-64.1
530.9	498.1	69.8	4700.4	107.5	-2.4	-64.1
605.4	499.8	1.2	7612.6	111.2	-2.4	-64.1

Table 9.2 - Optimized control parameters.

m_p (kg)	t_{coast} (s)	β_1	β_2	β_3
270.5	347.71	72.57	31.47	-0.08

The altitude and velocity profiles are presented in Figures 9.2 and 9.3 with the powered phase described by red curves and in blue the non-powered phase. In Figure 9.4 a path constraint (dynamic pressure) of the flight is shown.

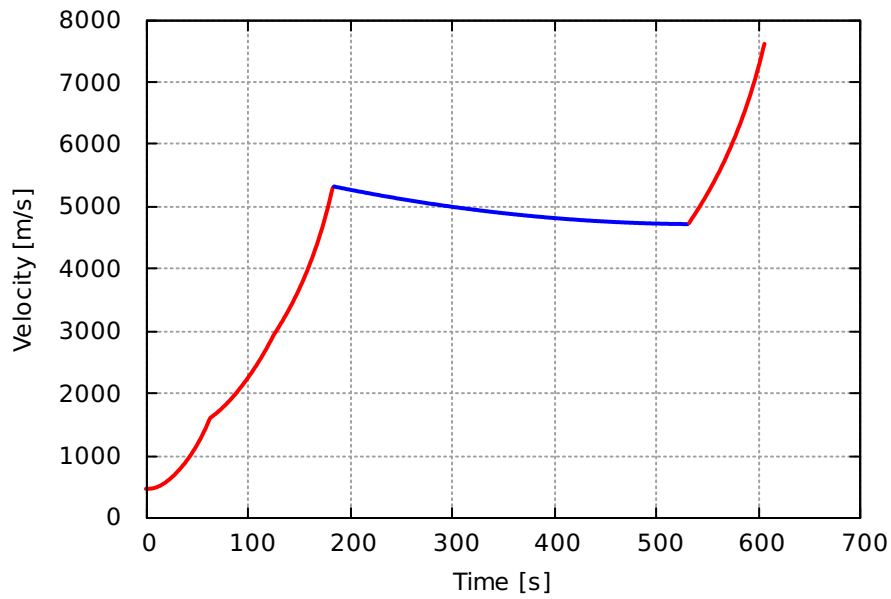


Figure 9.2 - Velocity profile of the VLS launch vehicle using first formulation of state equations.

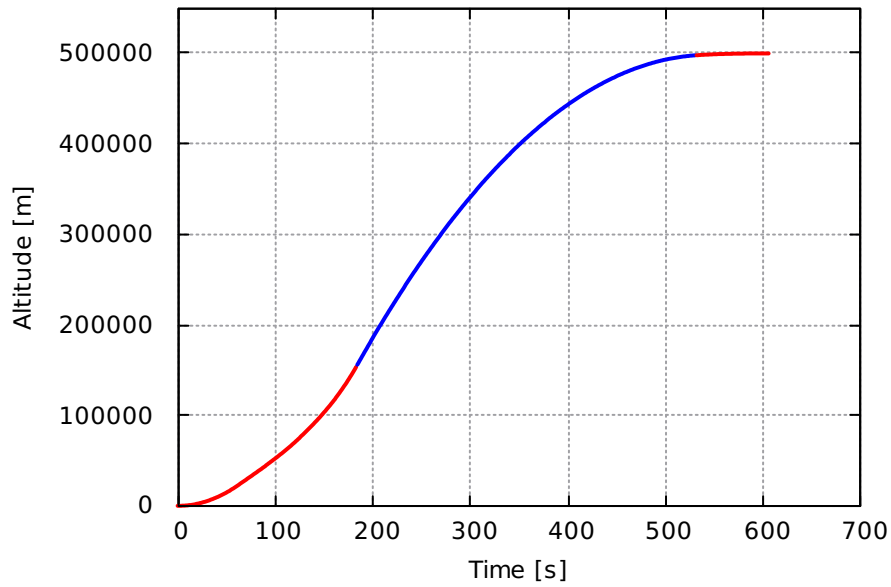


Figure 9.3 - Altitude profile of the VLS launch vehicle using first formulation of state equations.

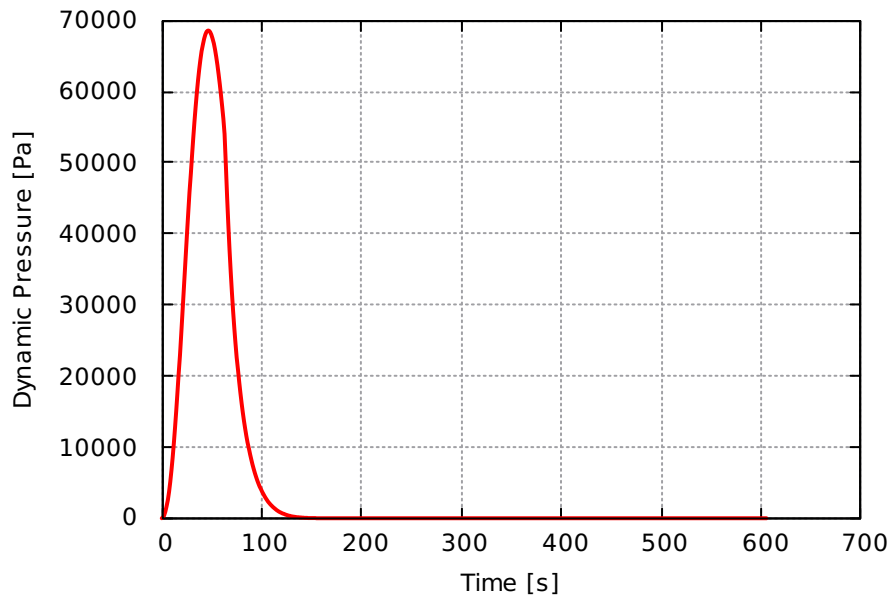


Figure 9.4 - Dynamic pressure profile of the VLS launch vehicle using first formulation of state equations.

Simulation Using Second Formulation of State Equations

The simulation of the VLS-1 using the equations of the translational motion described in Section 6.4.2 is presented here. Table 9.1 summarizes the corner instants between flight phases and Table 9.2 presents the control parameters obtained by optimization subroutine. The maximum payload mass (269.40 kg) presented a value very close to the one obtained using the first formulation of state equations.

Table 9.3 - Values for state variables at start, inter-stage and end instants.

t (s)	h (km)	v (m/s)	ξ (deg)	ϕ (deg)	γ (deg)	ζ (deg)
0.0	0.0	0.0	-44.4	-2.4	90	0
62.8	23.4	1211.0	-44.2	-2.4	38.9	0.4
124.9	75.2	2493.5	-43.4	-2.4	24.2	0.4
183.2	154.4	4881.4	-41.8	-2.4	23.3	0.5
530.9	498.0	4213.5	-29.1	-2.2	1.0	1.1
605.5	499.9	7116.8	-25.7	-2.1	0.0	1.3

Table 9.4 - Optimized control parameters.

m_p (kg)	t_{coast} (s)	β_1	β_2	β_3
269.40	347.48	72.86	31.61	-0.07

In Figures 9.5 and 9.6 the altitude and relative velocity profiles are presented and in Figure 9.7 we can see a path constraints of the flight. The ground track is presented in Figure 9.8.

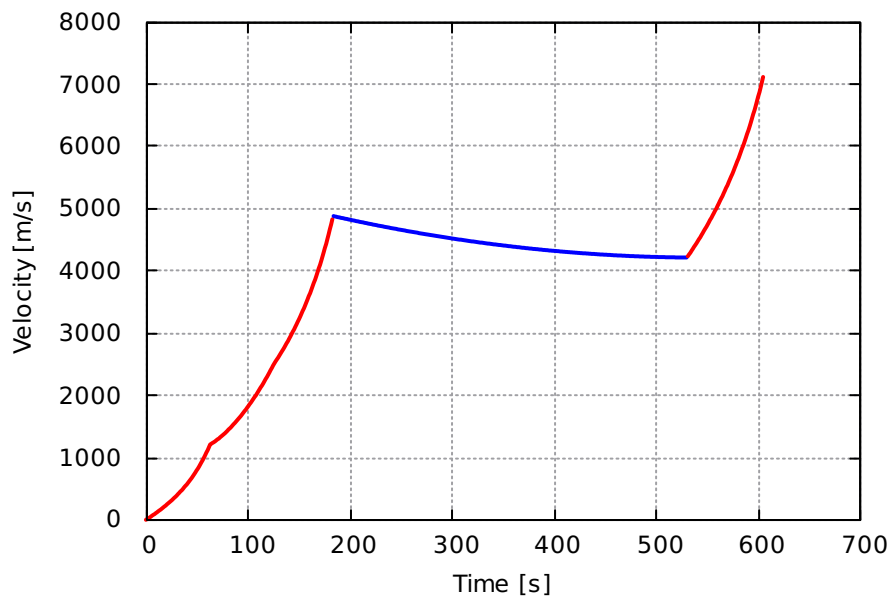


Figure 9.5 - Velocity profile of the VLS launch vehicle using second formulation of state equations.

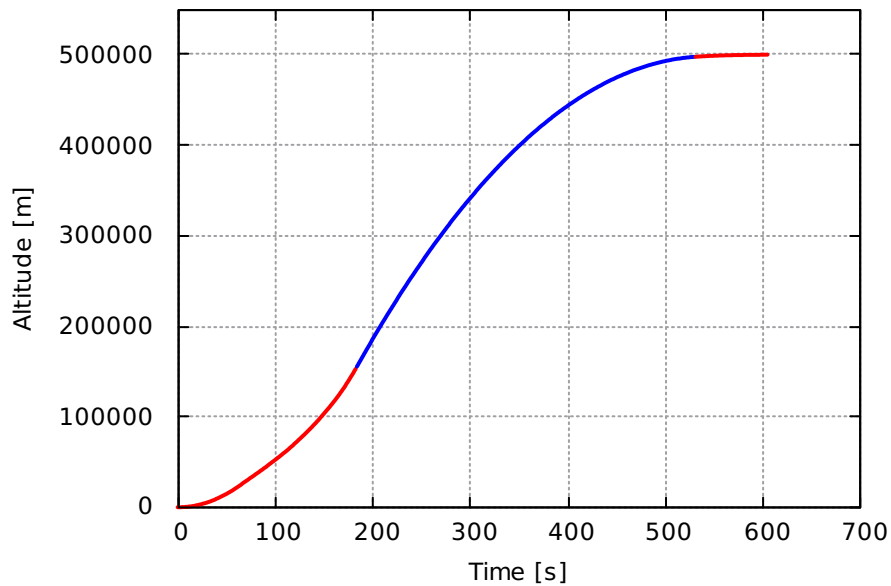


Figure 9.6 - Altitude profile of the VLS launch vehicle using second formulation of state equations.

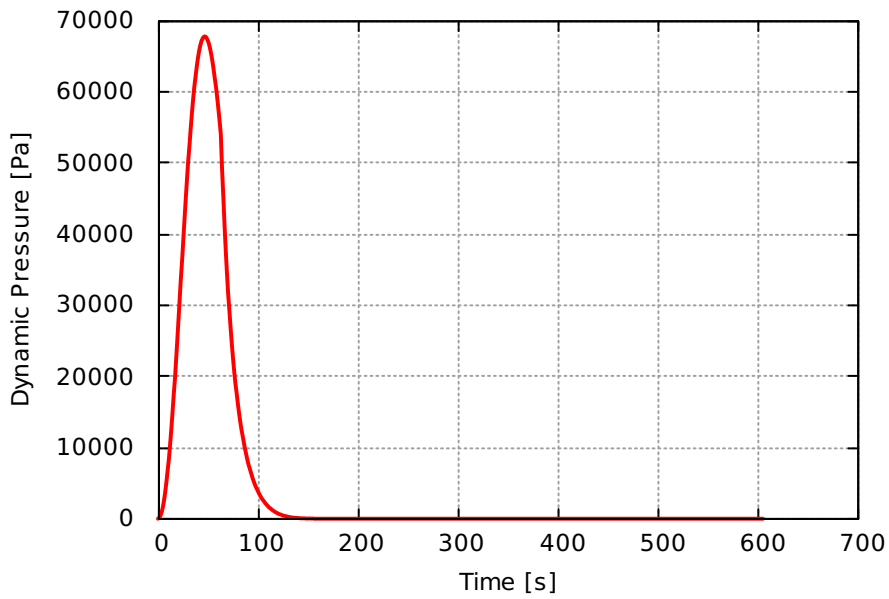


Figure 9.7 - Dynamic pressure profile of the VLS launch vehicle using second formulation of state equations.

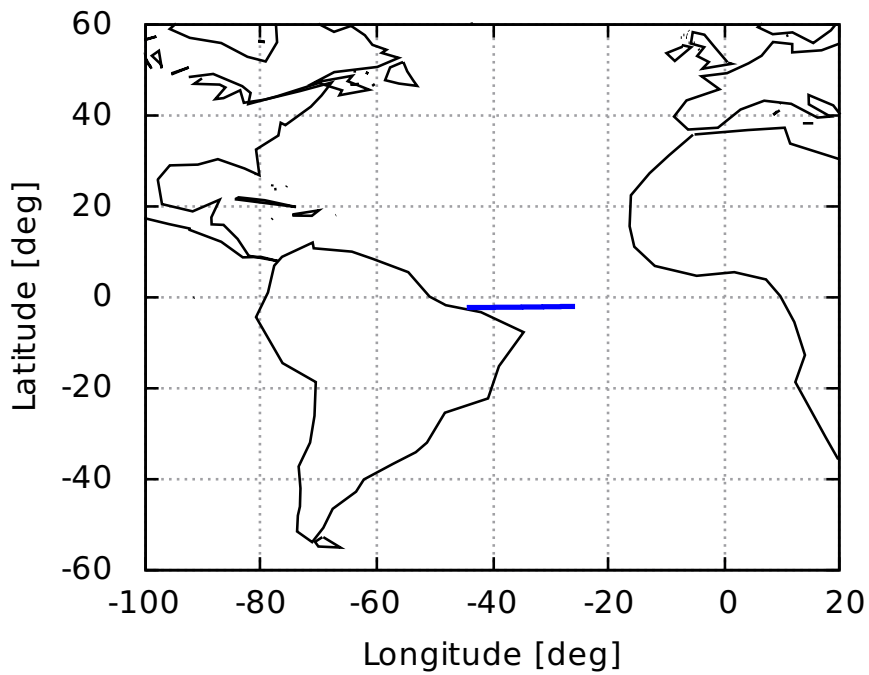


Figure 9.8 - Ground track.

Comparing the results from the Tables 9.2-9.3, we can verify that indeed both mathematical modelings are equivalent. Although the method treated in this work is sub-optimal trajectory, for the purpose of a preliminary analysis of liquid rocket engine this method is sufficiently accurate.

9.1.2 Ariane 5 Launch Vehicle

Built under supervision of European Space Agency (ESA), Ariane 5 is a European launch vehicle that is part of the Ariane rocket family. The vehicle is used to deliver payload into low earth orbit (LEO) and geostationary transfer orbit (GTO) orbits. Within the framework of this work, the mission is to launch a satellite from Kourou to a low earth orbit (LEO) of 200 km of altitude. The key parameters of the vehicle are given in Table 9.9.

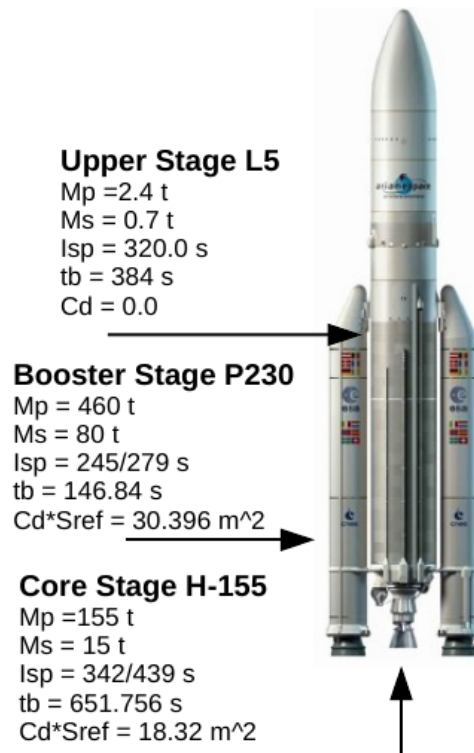


Figure 9.9 - Data: European Launch vehicle.
SOURCE: Schlingloff (1991)

The trajectory can be divided into two main phase. To take the vehicle from the ground and minimize the gravitational losses, the first phase is powered by two solid booster and the core stage using the propellants combination LOX/LH2. After

146.84 seconds takes place the booster stage are decoupled from the vehicle and the motion is powered only by the core stage. Differently from the VLS-1 this launch vehicle does not perform a non-powered coast-arc. In Figures 9.5 and 9.6 the altitude and relative velocity profiles are presented.

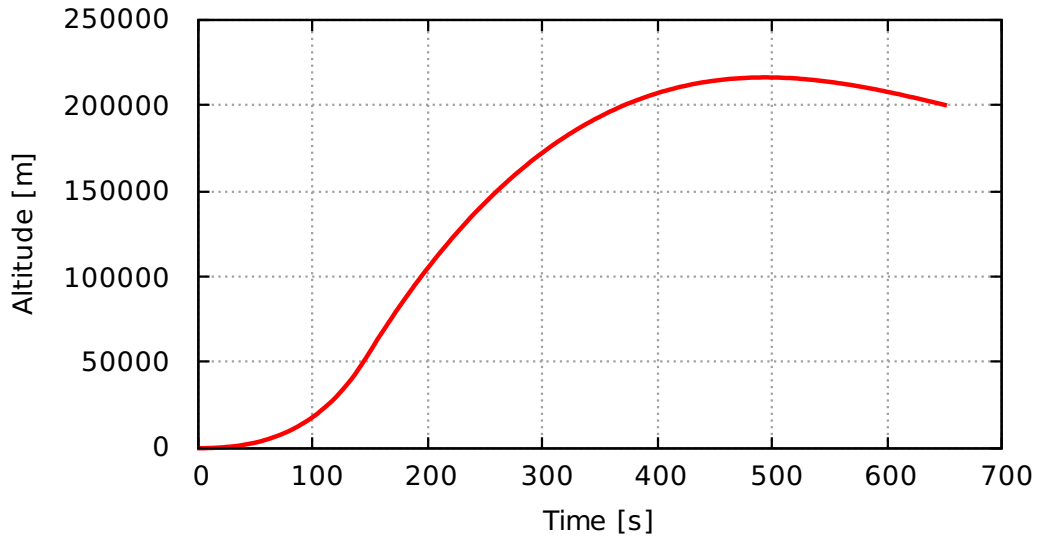


Figure 9.10 - Altitude profile of the European Ariane 5.

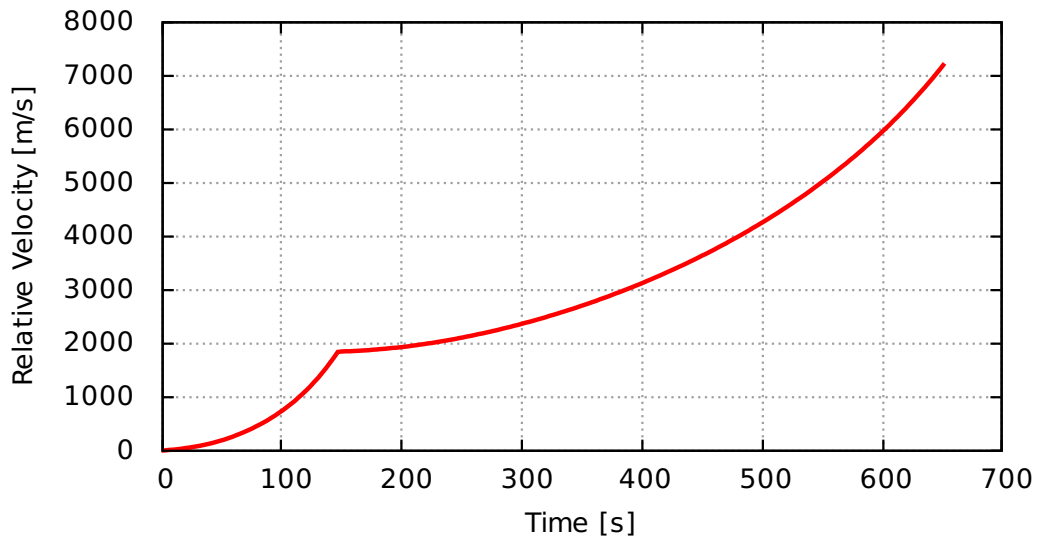


Figure 9.11 - Velocity profile of the European Ariane 5.

From the figures we can notice that the behavior of the altitude profile firstly exceed

the desired altitude (LEO with 200 km) reaching a maximum altitude and then the desired altitude is obtained. The reason for that is presumably because the flight does not perform a non-powered phase, so the vehicle takes longer to get the right inclination in order to be injected into orbit.

9.2 Hybrid Method

This section presents the simulation of the VLS-1 using a theoretically better method of optimization, the so-called hybrid method. In the atmospheric phase the control function is parameterized by a polynomial function and in the remaining flight phase (exo-atmospheric) where the vehicle is virtually in vacuum space the differential equations derived from theory of Hamilton-Lagrange dictates the control function law.

The velocity profile of this method in comparison with the method presented in the previous section is shown in Figure 9.12 .

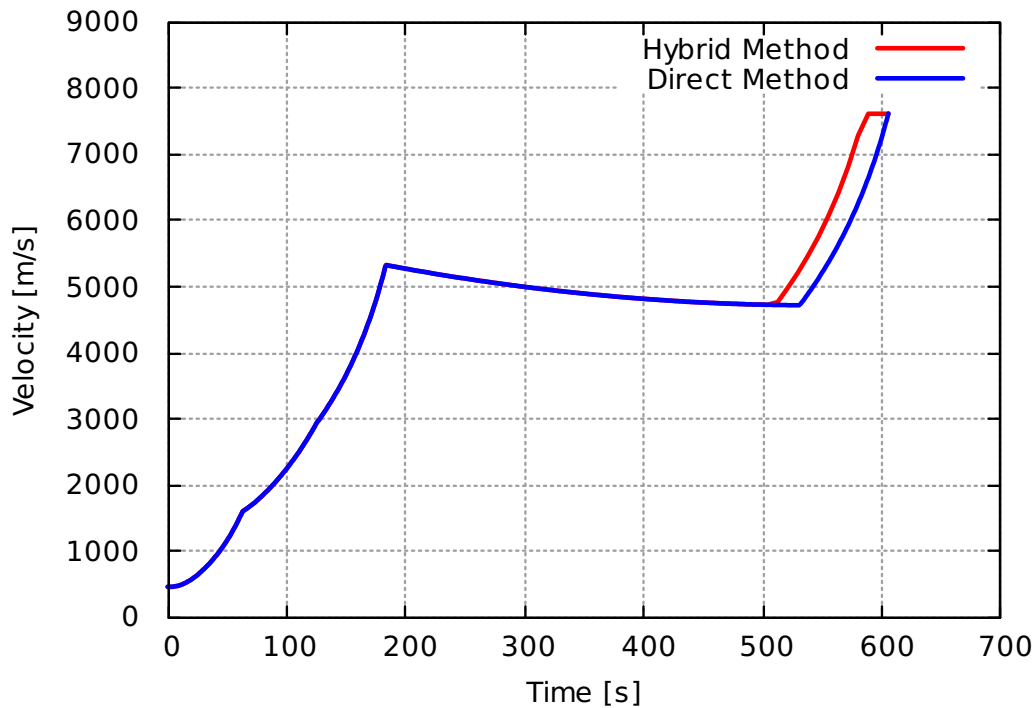


Figure 9.12 - Comparison.

The optimized control parameters are summarized in Table 9.5. Comparing Tables 9.4 and 9.5 we can see that indeed, a payload mass gain was obtained by the hybrid

method. However, it is important to mention the drawbacks embedded by the hybrid method. The initial guesses for the second phase is not straightforward and requires many trial and errors.

Table 9.5 - Optimized control parameters.

m_p (kg)	t_{coast} (s)
272.5	341.9 9

10 MISSION ANALYSIS

In the last two chapters the codes to simulate liquid rocket engine cycles and the trajectory were tested . By means of a mission analysis the communication between the disciplines will be studied in the present chapter. The simulation of the future Brazilian launch vehicle VLS-Alfa will be performed and the influence of changes in LRE design parameters on launcher performance will be investigated.

10.1 Flight Simulation

It is known that the VLS-Alfa will replace the last two solid stages of the former VLS-1 by a single liquid upper stage. Then since the VLS-Alfa is an improvement of the former VLS-1, the VLS-1 will be used as a reference vehicle to perform the simulations. The upper stage of the VLS-Alfa presumably will perform a coast phase, so the L75 is supposed to support restart capability. The mission is to launch a satellite into a reference circular orbit of 500 km of altitude from the Alcântara Launch Center ($2^{\circ}22'39.52'' S$, $44^{\circ}23'57.71'' W$). The parameters of the vehicles are given in Tables 10.1 and 10.2.

Table 10.1 - Data: Brazilian launch vehicle VLS

VLS	m_{pl} (kg)	m_s (kg)	I_{sp} (m/s)	t_b (s)	C_d
1st Stage	28900	6200	257.9	62.826	3.82
2nd Stage	7140	1680	279.1	62.087	1.6552
3rd Stage	4370	1330	270.74	58.267	0.0
4th Stage	820	170	281.85	74.546	0.0

Table 10.2 - Data: Brazilian launch vehicle VLS-Alfa

VLS-Alfa	m_{pl} (kg)	m_s (kg)	I_{sp} (m/s)	t_b (s)	C_d
1st Stage	28900	6200	257.9	62.826	3.82
2nd Stage	7140	1680	279.1	62.087	1.6552
3rd Stage (before coasting)	5800	987.422	315.0	243.657	0.0
3rd Stage (after coasting)	1100	987.422	315.0	46.219	0.0

As the mission of the VLS-Alfa is still not totally defined, the propellant mass of the upper stage had to be estimated. Thus, an amount of 6900 kg was conveniently defined. From this value an amount of 1100 kg was taken for the phase after coasting, i.e., for orbit injection. In Figure 10.2 the altitude and relative velocity profiles for

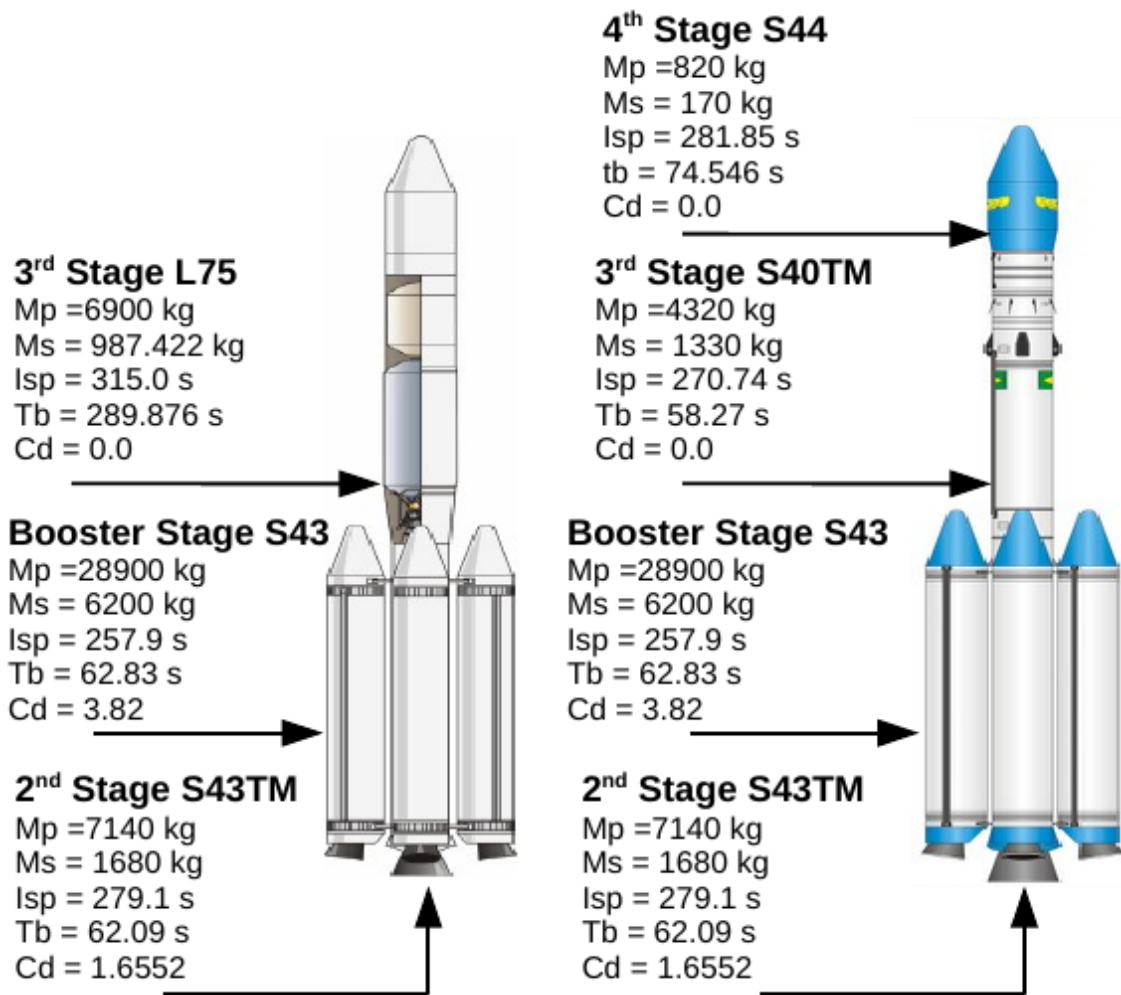


Figure 10.1 - Design parameters of the Brazilian launch vehicles (a) VLS-Alfa and (b) VLS-1.

both vehicles are presented and in Figure 10.4 we can see the ground track of the launch vehicle VLS-Alfa.

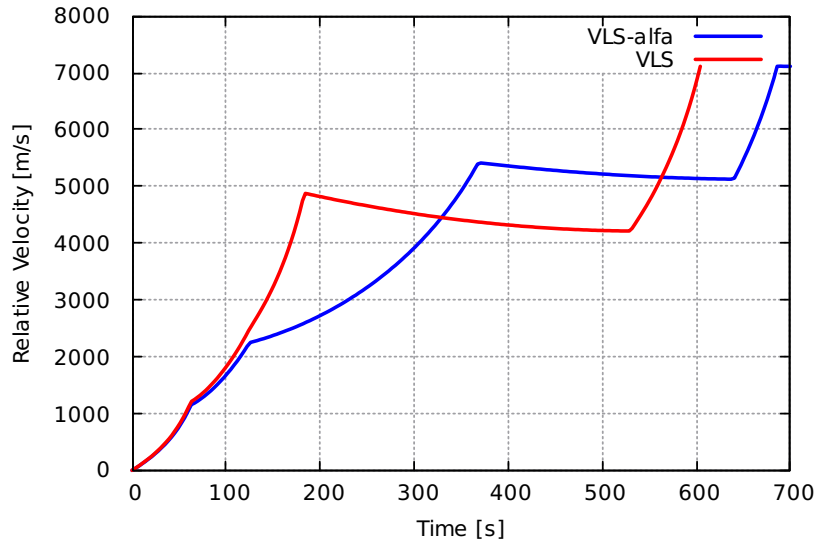


Figure 10.2 - Relative velocity profile of the former and future Brazilian launch vehicle.

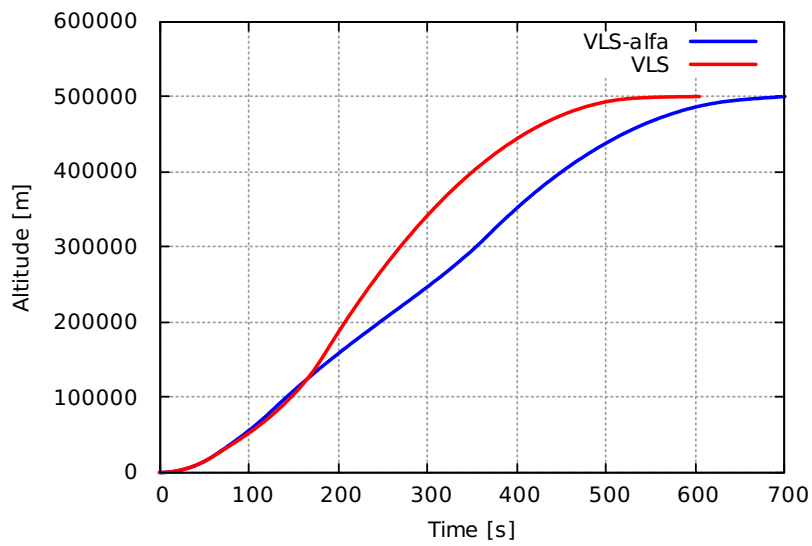


Figure 10.3 - Altitude profile of the former and future Brazilian launch vehicle.

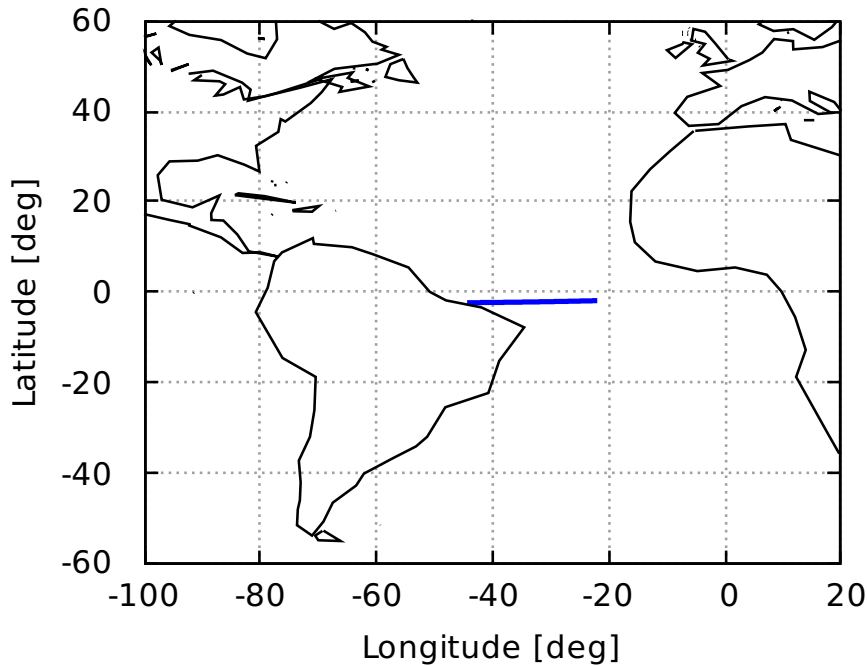


Figure 10.4 - Ground track for VLS-Alfa.

10.2 Influence of Engine Parameters on the Launcher Performance

The assessment of the performance of a liquid rocket engine at different operating points was already performed in the last section of Chapter 8. Here, the assumptions considered will be the same, i.e., the pump and turbine efficiency remains constant as well as the pressure drop in the feed system. Thus, the power of the turbine will be only function of the mass flow rate.

To study the influence of mixture ratio and chamber pressure on the payload mass the overall propellant mass is maintained constant. Fixing the thrust force, the burn time of the propellants will vary and the simulation of the set of equations from Section 5.2 will be performed with Equation 5.9. The analysis will be carried out by the following steps:

- Performance simulation. With the simulation of the engine at different operating points, the mass flow distribution through the engine cycle is determined. Hence, the power of the turbomachinery and engine performance is obtained.
- Dry mass calculation. Making use of the results from previous item, the engine and stage dry mass can be calculated.

- Trajectory optimization. Since the dry mass of the upper stage and the burn time was calculated, the performance of the launch vehicle can be evaluated.

The nominal parameters of the L75 are given in Figure 10.5.

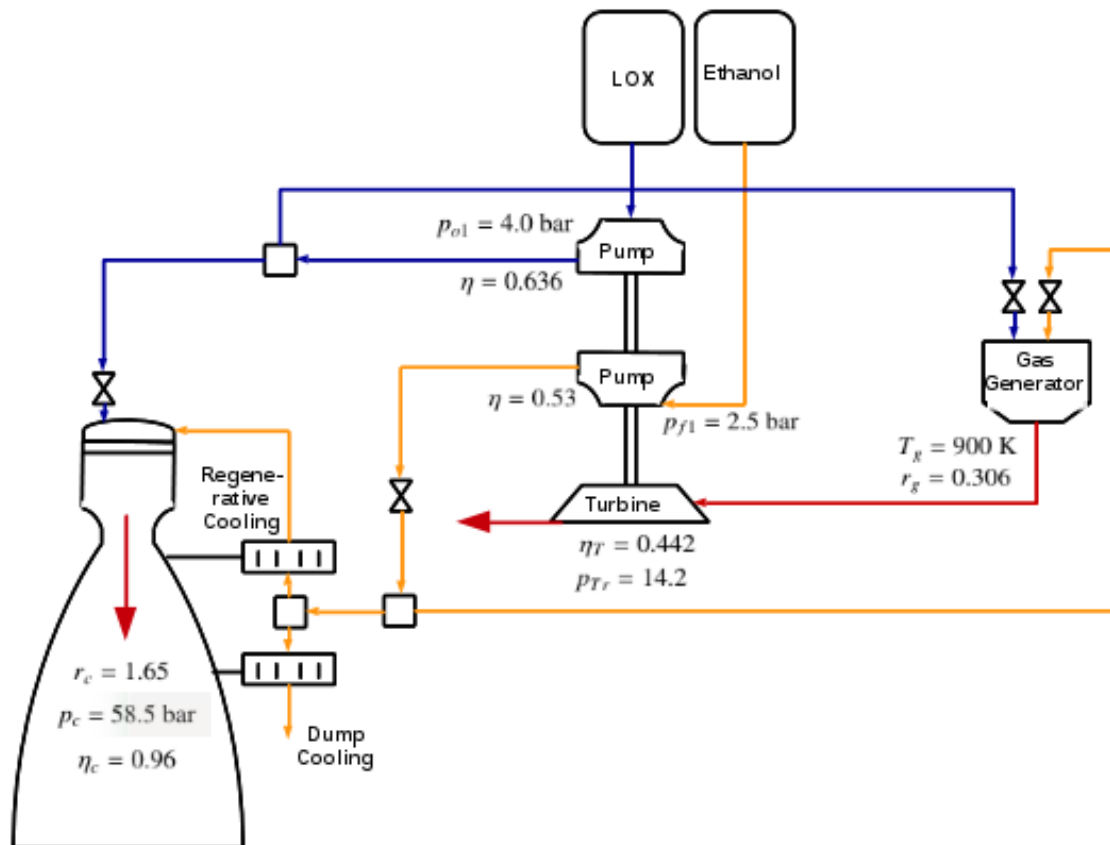


Figure 10.5 - Key parameters of the L75 rocket engine.

Influence of Chamber Pressure Change

Differently from the analysis performed in the last section of Chapter 8 where the nozzle expansion was variable, here this parameter remains constant. Thus, if we choose pressure values of $p_c = [20 \ 30 \ 40 \ 50 \ 58.5 \ 80 \ 100 \ 150 \ 200]^T$, the engine and stage dry mass profile present a minimum as shown in Figure 10.6. This minimum value corresponds exactly to the design point of the L75.

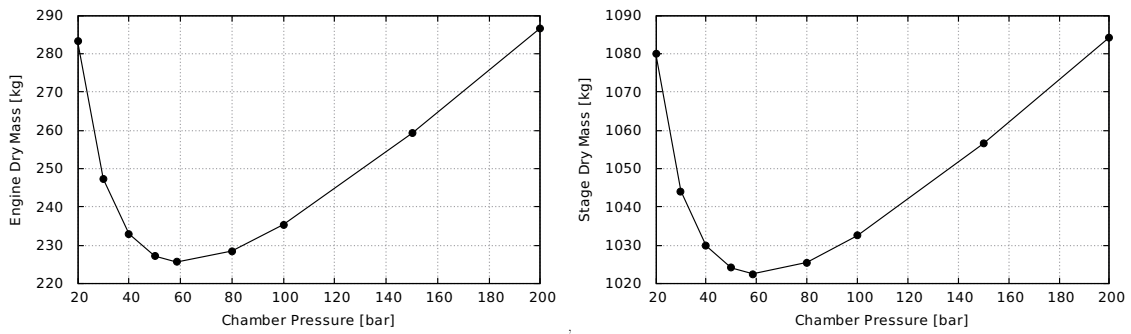


Figure 10.6 - Influence of the chamber pressure p_c on (a) engine dry mass and (b) stage dry mass.

Finally, the payload mass profile is shown in Figure 10.7. It is interesting to see that although the minimum stage dry mass is obtained in the design point (58.5 bar) the maximum payload mass was found at different design point (40 bar).

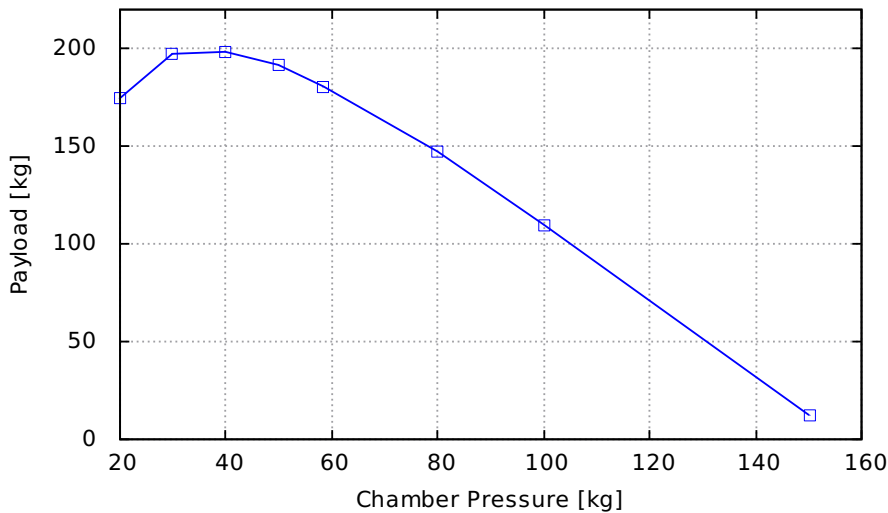


Figure 10.7 - Influence of the chamber pressure p_c on the payload mass.

Influence of Mixture Ratio Change

Usually we are interested in set a mixture ratio which maximizes the specific impulse or engine performance. However conflicting design parameters must also be taken into account. For example, the optimum specific impulse will not necessarily give the minimum stage dry mass or maximum payload mass. Besides, technical issues as the limiting combustion chamber temperature must be pointed out. Making clear these issues, the aim of this study is to assess the payload performance. Thus, if the mixture

ratio vector $r_c = [1.0 \ 1.5 \ 1.65 \ 1.8 \ 2.0 \ 2.5 \ 3 \ 4.0 \ 5.0]^T$ is considered, the engine and stage dry mass profile present a minimum as shown in Figure 10.8.

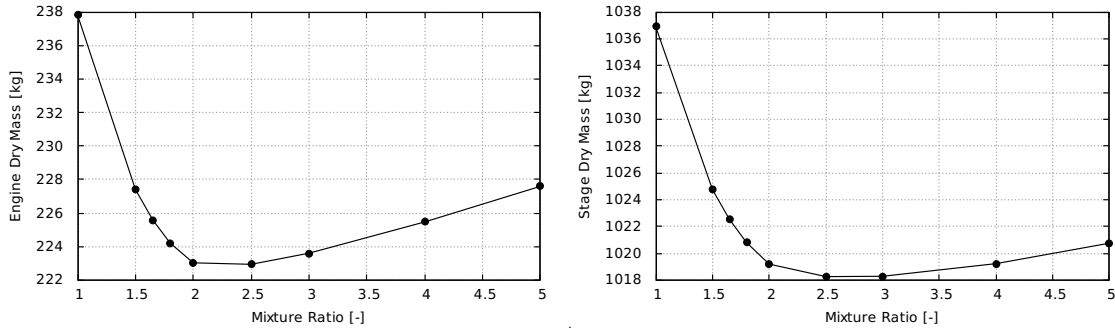


Figure 10.8 - Influence of the mixture ratio r_c on (a) engine dry mass and (b) stage dry mass.

At last, the payload mass behavior is presented in Figure 10.9. We can see that the maximum payload can be approximately 40 kg higher ($r_c = 2.0$) than the one obtained from mixture ratio at design point ($r_c = 1.65$). This is a very relevant increase which shows the high degree of coupling that exists between these two disciplines.

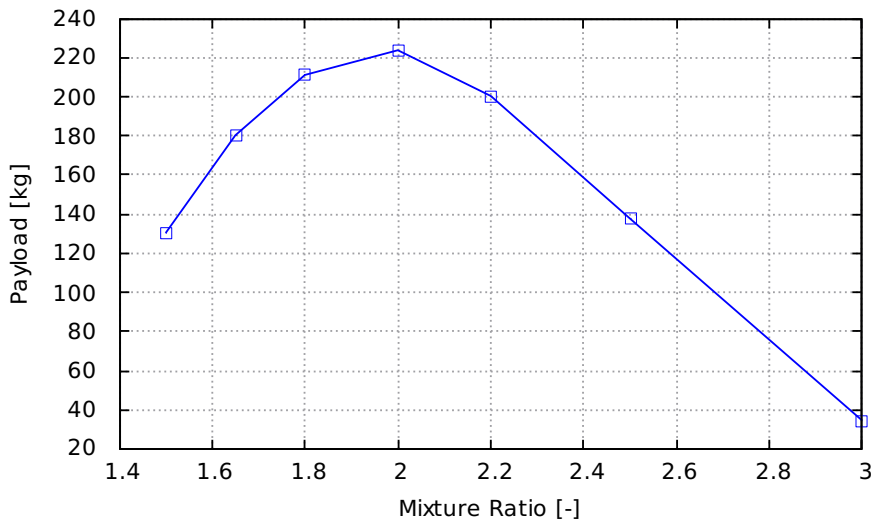


Figure 10.9 - Influence of the mixture ratio r_c on the payload mass.

11 CONCLUSION AND SUGGESTIONS

In the last chapter of this doctoral thesis, the conclusions and suggestions that were drawn during this work are summarized.

11.1 Conclusion

An objected-oriented tool comprising propulsion system and launch vehicle performance was created and verified. A comprehensive mathematical modeling comprising the main components of a liquid rocket engine and its performance were presented as well as equations of the translational motion of a launch vehicle. Expander (bleed and closed), staged combustion and gas generator cycle were modeled. To improve the performance of a launch vehicle, i.e., to maximize the payload mass capability two optimization methods (namely direct and hybrid) were described. In the first one a simple polynomial function models the control law while the second one split the trajectory into atmospheric and exo-atmospheric phase in order to make use of direct method in the first phase and the indirect method in the remaining flight phase in which the atmospheric effect can be neglected.

The UML (Unified Modeling Language) tool was chosen to model the architecture of the codes. UML diagrams help to visualize the structure of the codes and communication between objects. Furthermore these diagrams provide a high degree of abstraction, i.e., only the relevant functionality of the codes are explicit to the user. Thus, anyone that has some acquaintance with object-oriented can easily understand the main functions and parameters of each single class as well as the relationship between objects.

The trajectory optimization codes were verified by the Brazilian launch vehicle VLS-1 and the European Ariane 5 using the direct method of optimization. The VLS-1 was simulated for two mathematical modeling of state equation in order to check the agreement between them which was readily verified. The hybrid method of optimization was applied in the VLS-1. Concerning the methods we can conclude that the hybrid one can provide a better performance to the vehicle. However the hybrid method increases the number of control variables which in turn increases the number of initial guesses.

To verify the applicability and efficiency of the engine performance codes the liquid rocket engines L75, Vulcain, HM7B, and SSME were simulated. All the cases considered presented good agreement with the literature.

In order to study the influence of engine parameters on the performance of a launch vehicle under development the VLS-Alfa was chosen. The analysis was performed on the upper stage which is driven by the L75 rocket engine, since the lower stages are powered by solid propulsion. The L75 engine was simulated for different values of mixture ratio and chamber pressure. The results showed that the design parameters could be changed to achieve a better performance, i.e. a considerable payload gain could be obtained. It shows the advantages of integrating more than one discipline into a single tool, i.e. the communication between disciplines can be readily assessed.

11.1.1 Contribution of This Work

The main contributions of this work was the development of a tool capable of:

- Investigating the influence of rocket engine design parameters on launch vehicle performance
- Being reusable and extensible
- Making easier the communication between objects

An important application of this tool was performed on the future Brazilian VLS-Alfa launch vehicle. Thus, another relevant contributions were:

- Simulation of the VLS-Alfa launch vehicle.
- Analysis of influence of the L75 rocket engine parameters on performance of VLS-Alfa launch vehicle.

Among other contributions brought by this work, we can mention:

- Wide range of mathematical modeling approaches. For instance, for the mass model it was presented many possible models from simple to detailed ones, and for the trajectory modeling was presented two different set of equations of motion and many ways on how to proceed an optimization.
- Hybrid method for trajectory optimization. In order to take the main advantages of direct and indirect methods, a hybrid method was formulated.

11.2 Suggestions

Since the idea behind this study was to develop a tool that could be easily expanded and reusable, and given the generality of the problem, suggestions for future works are many as possible. Among specific improvements we can suggest:

- Improve the modeling of each component. More functions can be added and some functions can be replaced in order to increase the efficiency of the codes.
- Integration of more disciplines, e.g. models for cost, reliability, and aerodynamics could be conveniently implemented in some classes interface.
- Methods of optimization (heuristic/deterministic) could be applied to single disciplines.
- Implementation of Multidisciplinary Design Optimization (MDO).
- Mathematical model for transient state. This is important for start-up, ignition and re-ignition.
- Development of an own code to perform gas properties from propellants combustion. Although CEA is a recognized standard program for chemical equilibrium calculation used world wide, the dependency of this program is an inherent limitation.
- Modeling of the cooling jacket. Due to strength limitation of the material it is really important to determine the temperature along the combustion chamber and nozzle. A model for the cooling system is also particularly important for expander cycles, since the cooling jacket has an extra function of changing phase the fuel to feed the turbomachinery.

Since this topic was designed to future developments, the tool could also be used to study new concepts of engines and launch vehicles. Reusable Launch Vehicle (RLV), Single-Stage-To-Orbit (SSTO), Airbreathing or even new configurations for the Brazilian launch vehicle VLS-Alfa would be a possible and interesting field of study.

REFERENCES

- ALMEIDA, D. S.; PAGLIUCO, C. M. M. Development status of I75: A Brazilian liquid propellant rocket engine. **J. Aerosp. Technol. Manag.**, v. 6, n. 4, p. 475–484, 2014. DOI: 10.5028/jatm.v6i4.386. 3, 145
- ARIANESPACE. **Ariane 5 user's issue 5 manual revision 1**. Evry Courcouronnes Cedex France, July 2011. 7
- BALESDENT, M. **Multidisciplinary design optimization of launch vehicles**. 239 p. PhD Thesis — ONERA, France, 2011. 15, 16, 72, 84
- BETTS, J. T. Survey of numerical methods for trajectory optimization. **Journal of Guidance, Control, and Dynamics**, v. 21, n. 2, p. 193–207, 1999. 15, 16, 82, 84
- BINDER, M.; TOMSIK, T.; VERES, J. P. **RL10A-3-3A rocket engine modeling project**. Brook Park, Ohio, 1997. NYMA, Inc. 149
- BISSEL, W. R. **Rocket engine turbopump tutorial**. Rockwell International, Rocketdyne Division, 1985. Rocketdyne-RI/RD 85-245, USAF Contract F33657-82-C-0346 for Analysis of Foreign Chemical Propulsion Systems. 57
- BLAKE, W. B. **Missile DATCOM: users manual: 1997 fortran 90 revision**. Wright-Patterson Air Force Base, Ohio, 1997. AFRL-VA-WP-TR-1998-3009. 72
- _____. **Missile DATCOM: 1997 status and future plans**. Wright Patterson AFB, Ohio, 1997. 538-548 p. AIAA, Inc. 72
- BOEING ENGINEERING. **Thrust chamber**. 2015.
www.k – makris.gr/RocketTechnology/ThrustChamber/Thrust_Chamber.htm.
Accessed: 24 August 2015. 32
- BRADFORD, J. E. SCORES-II design engine analysis tool for liquid rocket. In: JOINT PROPULSION CONFERENCE AND EXHIBIT, 2002, Indianapolis, Indiana. **Proceedings...** Indianapolis: AIAA, 2002. 12
- BRADFORD, J. E.; CHARANIA, A.; GERMAIN, B. S. REDTOP-2: Rocket engine design tool featuring engine performance, weight, cost and reliability. In: 40TH AIAA/ASME/SAE/ASEE JOINT PROPULSION CONFERENCE AND EXHIBIT, 2004, Fort Lauderdale, Florida. **Proceedings...** Fort Lauderdale: AIAA, 2004. 12, 53

BRAUER, G. L.; CORNICK, D. E.; STEVENSON, R. **Capabilities and applications of the program to optimize simulated trajectories (POST)**. Denver, CO., 1977. 127 p. 16, 84

BROWN, K. R.; HARROLD, E. F.; JOHNSON, G. W. **Rapid Optimization of Multiple-Burn Rocket Flights**. Marschall Space Flight Center, Alabama, 1969. 15, 83

BRYSON, A. E.; HO, Y. C. **Applied Optimal Control**. New York: Hemisphere, 1975. 81, 82, 83

BUENO NETO, C. O. **Proposta de abordagem para a otimização de um veículo lançador de satélites a combustível sólido e de sua trajetória**. (INPE-3968-TD/232). Master Thesis — Instituto Nacional de Pesquisas Espaciais (INPE), São José dos Campos, Brazil, 1986. 15, 16

BURKHARDT, H.; SIPPEL, M.; HERBERTZ, A.; J., K. Comparative study of kerosene and methane propellant engines for reusable liquid booster stages. In: 4TH INTERNATIONAL CONFERENCE ON LAUNCHER TECHNOLOGY "SPACE LAUNCHER LIQUID PROPULSION", 2002, Liège, Belgium. **Proceedings...** Liège, 2002. 12

_____. Kerosene vs methane: a propellant tradeoff for reusable liquid booster stages. **Journal of Spacecraft and Rockets**, v. 41, n. 5, p. 762–769, 2004. 12

CASTELLINI, F. **Multidisciplinary design optimization for expendable launch vehicles**. 148 p. PhD Thesis — Politecnico Di Milano, Milano, 2012. 15, 28, 40, 41, 81

CHAPMAN, K. S. W.; COLE, A. E.; KASTOR, A. **Standard and reference handbook of geophysics and the space environment**,. 1985. Retrieved from http://www.cnofs.org/Handbook_of_Geophysics_1985/Chptr14.pdf. Accessed: 24 August 2015. 71

COESA. **U.S. standard atmosphere 1962**. Washington, D.C., 1962. 70

_____. **U.S. standard atmosphere 1976**. Washington, D.C., 1976. 227 p. 70

CORNELISSE, J. W.; SCHÖYER, H. F. R.; WAKKER, K. F. **Rocket propulsion and spaceflights dynamics**. London: Pitman, 1979. 5, 46, 74

ECOSIMPRO. **Ecosimpro**: system modeling and simulation software. 2015. [Www.ecosimpro.com/products/ecosimpro/](http://www.ecosimpro.com/products/ecosimpro/). Accessed: 31 August 2015. 13, 14

ENCYCLOPAEDIA BRITANNICA. **Launch vehicle**: rocket system. 2015.
Http://www.http://global.britannica.com/topic/launch-vehicle. Accessed: 31
August 2015. 4

ERNST, R. **Liquid rocket analysis (LiRA)**: development of a liquid
bi-propellant rocket engine design, analysis and optimization tool. 170 p. Master
Thesis — Delft University of Technology, Holand, 2014. 13, 40

FARRELL, J. **An object-oriented approach to programming logic and
design**. Boston: Course Technology. Cengage Learning, 2013. 92

FELBER, R. **Einige Beiträge Zur Optimierung von Chemischen
Raketentriebwerken**. Munich, 1979. 14, 42, 43

FLEEMAN, E. L. Professional development short course on tactical missile design.
2008. 72

GATH, P. **CAMTOS - a software suite combining direct and indirect
trajectory optimization methods**. 172 p. PhD Thesis — Universität Stuttgart,
Stuttgart, 2002. 16, 82

GATH, P. F.; CALISE, A. J. Optimization of launch vehicle ascent trajectories
with path constraints and coast arcs. **Journal of Guidance, Control and
Dynamics**, v. 24, n. 2, p. 296–304, 2001. 16, 82

GERMAIN, B. D. S. **Technique for the optimization of the powerhead
configuration and performance of liquid rocket engines**. 192 p. PhD Thesis
— Georgia Institute of Technology, Atlanta, 2003. 53

GOERTZ, C. A modular method for the analysis of liquid rocket engine cycles. In:
31ST AIAA/ASME/SAE/ASEE JOINT PROPULSION CONFERENCE AND
EXHIBIT, 1995, San Diego, CA. **Proceedings...** San Diego: AIAA, 1995. 12, 53

GORDON, S.; MCBRIDE, B. J. **Computer Program for Calculation of
Complex Chemical Equilibrium Compositions and Applications: Volume
I: Analysis**. Cleveland, Ohio, 1994. 11

_____. **Computer Program for Calculation of Complex Chemical
Equilibrium Compositions and Applications: Volume II: Users Manual
and Program Description**. Cleveland, Ohio, 1996. 11

Haidn, O. J. **Advanced rocket engines**: In advances on propulsion technology for high speed aircraft. Lampoldshausen, Germany, 2008. Educational Notes RTO-EN-AVT-150. 30

HAMMOND, W. E. **Design methodology for space transportation systems**. Huntsville, Alabama: *AIAA Educational Series*, 2001. 2, 72

HARGRAVES, C. R.; PARIS, S. W. Direct trajectory optimization using nonlinear programming and collocation. **Journal of Guidance**, v. 10, n. 4, p. 338–342, 1987. 15, 16, 84

HERMAN, A. L.; CONWAY, B. A. Direct optimization using collocation based on high-order gauss-lobatto quadrature rules. **Journal of Guidance, Control and Dynamics**, v. 19, n. 3, p. 592–599, 1996. 15, 16, 84

HILL, P.; PETERSON, C. **Mechanics and thermodynamics of propulsion**. Massachusetts: Addison-Wesley, 1992. 6

HINCKEL, J. N. An object oriented approach to launch vehicle performance analysis. In: 31ST AIAA/ASME/SAE/ASEE JOINT PROPULSION CONFERENCE AND EXHIBIT, 1995, San Diego, CA. **Proceedings...** San Diego: AIAA, 1995. 1, 92

HUGH, B. M. Numerical analysis of existing liquid rocket engines as a design process starter. In: 31ST AIAA/ASME/SAE/ASEE JOINT PROPULSION CONFERENCE AND EXHIBIT, 1995, San Diego, CA. **Proceedings...** San Diego: AIAA, 1995. 44, 104, 105, 106

HUMBLE, R. W.; HENRY, G. N.; LARSON, W. J. **Space propulsion analysis and design**. New York: McGrawHill, 1995. 6, 18, 19, 21, 22, 28, 31, 32, 34, 39, 45, 47, 48, 50, 53, 55, 57

HUZEL, D. K.; HUANG, D. H. **Modern engineering for design of liquid-propellant rocket engines**. Washington DC, USA: AIAA, 1992. 6, 22, 26, 47, 50, 53

JACOB, H. G. **An engineering optimization method with application to stol-aircraft approach and landing trajectories**. Moffett Field, Calif., 1972. 85

KAUFFMANN, J.; HERBERTZ, A.; SIPPEL, M. Systems analysis of a high thrust, low-cost rocket engine. In: 4TH INTERNATIONAL CONFERENCE ON

- GREEN PROPELLANTS FOR SPACE PROPULSION, 2001, Noordwijk, Netherlands. **Proceedings...** Noordwijk, 2001. 30
- KESAEV, K. V.; ALMEIDA, D. S. **Teoria e cálculo de motores foguete a propelente líquido (Internal Report)**. São José dos Campos, Brazil, 2005. 31, 32, 34, 53
- KITSCHKE, W. **Operation of a cryogenic rocket engine**: an outline with down-to-Earth and up-to-space remarks. Hardthausen, Germany: Springer, 2011. 146
- LAFORE, R. **Object-oriented programming in C++**. Indianapolis, Indiana: Sams Publishing, 2002. 92
- MANSKI, D.; GOERTZ, C.; H., S. Cycles for earth-to-orbit propulsion. **Journal of Propulsion and Power**, v. 14, n. 5, p. 588–604, 1998. 12, 107, 108
- MANSKI, D.; MARTIN, J. A. Optimization of the propulsion cycles for advanced shuttles part 2: Performance model methodology. In: AIAA/SAE/ASME/ASEE 26TH JOINT PROPULSION CONFERENCE. Orlando, FL, 1990. 12
- _____. Evaluation of innovative rocket engines for single-stage earth-to-orbit vehicles. **Journal of Propulsion**, v. 7, n. 6, p. 929–937, 1991. 12
- MARKL, A. W. **An initial guess generator for launch and reentry vehicle trajectory optimizations**. 182 p. PhD Thesis — Institut für Flugmechanik und Flugregelung der Universität Stuttgart, Stuttgart - Germany, 2001. 81
- MATTEO, F. **Modeling and simulation of liquid rocket engine ignition transients**. 200 p. PhD Thesis — La Sapienza, Roma - Italy, 2011. 53
- MIELE, A. Multiple-subarc gradient-restoration algorithm, part 1: Application to a multistage launch vehicle design. **Journal of Optimization Theory and Applications**, v. 116, n. 1, p. 19–39, 2003. 15, 83
- MORAES JUNIOR, P.; TEIXEIRA, A. J.; SANTANA JUNIOR, A.; BÔAS, D. J. F. V.; CARRIJO, D. S.; YAMAMOTO, M. K. Mission analysis and performance improvement of the Brazilian launch vehicle VLS Alfa. In: 4TH EUROPEAN CONFERENCE FOR AEROSPACE SCIENCES (EUCASS), 2011, Saint Petersburg, Russia. **Proceedings...** Saint Petersburg, 2011. 3

- MUNSON, B. R.; YOUNG, D. F.; OKIISCHI, T. H.; HUEBSCH, W. W. **Fundamentals of fluid mechanics**. USA: John Wiley and Sons, Inc., 2009. 35, 36
- MUSIELAK, D. SABRE: A high speed for the SSTO SKYLON air breathing spaceplane rocket engine. In: AIAA - HIGH SPEED AIR BREATHING PROPULSION TECHNICAL COMMITTEE, 2012. **Proceedings...** [S.l.]: AIAA, 2012. 5
- NASA. **Liquid rocket engines (J-2X, RS-25, general)**. 2015. [Http://blogs.nasa.gov/J2X/tag/space-shuttle-main-engine/](http://blogs.nasa.gov/J2X/tag/space-shuttle-main-engine/). Accessed: 29 September 2015. 54, 55
- _____. _____. 2015. [Https://blogs.nasa.gov/J2X/tag/oxidizer-turbine-bypass-valve/](https://blogs.nasa.gov/J2X/tag/oxidizer-turbine-bypass-valve/). Accessed: 29 September 2015. 54
- NASA GLENN RESEARCH CENTER. **Chemical equilibrium with applications (CEA)**. 2010. [Http://www.grc.nasa.gov/WWW/CEAWeb/](http://www.grc.nasa.gov/WWW/CEAWeb/). Accessed: 31 August 2015. 11
- OBERLE, H. J.; GRIMM, W. **BNDSCO**: a program for the numerical solution of optimal control problems. Oberpfaffenhofen, Germany, 1990. 15, 83
- O'LEARY, R.; J.E., B. Nozzle design. **Pratt and Whitney Rocketdyne's Engineering Journal of Power Technology**, 1992. 28
- PAGANO, A. **Global launcher trajectory optimization for lunar base settlement**. 161 p. Master Thesis — Delft University of Technology, Delft - Netherlands, 2010. 72, 81
- PAVLI, A. J.; CURLEY, J. K. **Design and cooling performance of a dump-cooled rocket engine**. Washington, D.C., 1966. 48 p. 32, 33
- PONTANI, M.; TEOFILATTO, P. Simple method for performance evaluation of multistage rockets. **ACTA Astronautica**, v. 94, p. 434–445, 2014. 16, 82
- POULIQUEN, M. F. HM60 cryogenic rocket engine for future European launchers. **Journal of Spacecraft**, v. 21, n. 4, p. 346–353, 1983. 104, 105
- PRESS, W. H.; TEULOLSKY, S. A.; VETTERLING, W. T.; FLANNERY, B. P. **Numerical recipes: the art of scientific computing**. Cambridge: Cambridge University Press, 2007. 68

- PUGH, S. **Total design**: integrated methods for successful product engineering. [S.l.]: Addison Wesley Longman, 1991. 2
- RAO, A. V. A survey of numerical methods for optimal control. **Journal of Guidance, Control, and Dynamics**, 2009. 15, 82, 85
- RAO, S. S. **Engineering optimization**: theory and practice. Hoboken, New Jersey: John Wiley and Sons, Inc., 2009. 84
- SCHLINGLOFF, H. Control laws for optimal spacecraft navigation. **Journal of Spacecraft**, v. 24, n. 1, p. 48–51, 1986. 87, 88, 89
- _____. **SKYNAV**: a design tool for space launcher analysis and flight performance optimization. Munich, Germany, 1991. 118
- _____. **Astronautical engineering**: an introduction to the technology of spaceflight. Bad Abach, Germany: Ingenieurbüro Dr. Schlingloff Publications, 2005. 29, 43, 45, 73, 75, 82
- SCHMUCKER, R. H. **A simple performance calculation method for LH2/LOX engines with different power cycles**. Alabama, 1973. 22, 23, 29
- SEGAL, C. Propulsion systems for hypersonic flight. **RTO-EN-AVT-116**, 2004. 5
- SEYWALD, H. Trajectory optimization based on differential inclusion. **Journal of Guidance, Control, and Dynamics**, v. 17, n. 3, p. 480–487, 1994. 15, 16, 84
- SILVA, C. S. C. **Simulação de sistemas de motores foguetes a propelentes líquidos**. 117 p. Master Thesis — Instituto Tecnológico de Aeronáutica, São José dos Campos, Brazil, 1995. 15, 16, 53, 81, 84, 85
- SIPPEL, M.; HERBERTZ, A.; MANFLETTI, C.; BURKHARDT, H.; IMOTO, T.; HAESELER, D.; GÖTZ, A. Studies on expander bleed cycle engines for launchers. In: 39TH AIAA/ASME/SAE/ASEE JOINT PROPULSION CONFERENCE AND EXHIBIT, 2003, Fort Lauderdale, Florida. **Proceedings...** Huntsville: AIAA, 2003. 12
- SIPPEL, M.; YAMASHIRO, R.; CREMASCHI, F. Staged combustion cycle rocket engine design trade-offs for future advanced passenger transport. In: SPACE PROPULSION, Bourdeaux, France. **Proceedings...** Bourdeaux, 2012. 12
- SP-8097, N. **Liquid rocket valves assemblies**. Washington D.C., 1973. 36

SP-8107, N. **Turbopump system for liquid rocket engine**. Washington D.C., 1974. 18, 56

SP-8110, N. **Liquid rocket engine turbines**. Washington D.C., 1974. 21

SP-8123, N. **Liquid rocket lines, bellows, flexible hoses, and filters**. Washington D.C., 1977. 36

SPACEWORKS SOFTWARE. **Redtop pro product comparison**. 2015.
[Http://www.spaceworkssoftware.com/products/desktop/redtop-pro.shtml](http://www.spaceworkssoftware.com/products/desktop/redtop-pro.shtml).
Accessed: 31 August 2015. 12, 13

STRYK, v. O.; BULIRSCH, R. Direct and indirect methods for trajectory optimization. **Annals of Operations Research**, v. 37, p. 357–373, 1992. 16, 82

SUTTON, G. P.; BIBLARZ, O. **Rocket propulsion elements**. New Jersey: John Wiley, 2010. 6, 8, 24, 25, 27, 28, 33, 53

TEREN, F.; SPURLOCK, O. F. **Payload optimization of multistage launch vehicles**. Cleveland, Ohio, 1966. 15, 83

TEWARI, A. **Atmospheric and spaceflight dynamics**. Boston: Birkhäuser, 2007. xvii, 5, 6, 69, 70, 72, 73, 74, 75, 77, 78, 79

_____. **Advanced control of Aircraft and Spacecraft**. UK: John Wiley and Sons, Ltd, 2011. 82

TURNER, M. J. L. **Rocket and spacecraft propulsion: principles, practice and new developments**. Chichester, UK: Springer, 2005. 147

VANDAMME, J. **Assisted-launch performance analysis using trajectory and vehicle optimization**. 156 p. Master Thesis — Delft University of Technology, Delft - Netherlands, 2012. 81

VERDERAIME, V. **Booster parametric design method for performance and trajectory analysis: Part ii: propulsion**. Huntsville, Alabama, 1964. 14

WALSH, P.; FLETCHER, P. **Gas turbine performance**. Oxford: Blackwell Science, 2008. 2nd edition. 21

WAY, D. W.; OLDS, J. R. SCORES: developing an object-oriented rocket propulsion analysis tool. In: 34TH AIAA/ASME/SAE/ASEE JOINT PROPULSION CONFERENCE AND EXHIBIT, Cleveland, Ohio. **Proceedings...** Cleveland: AIAA, 1998. 12

_____. SCORES: web-based rocket propulsion analysis for space transportation system design. In: 35TH AIAA/ASME/SAE/ASEE JOINT PROPULSION CONFERENCE AND EXHIBIT, Los Angeles, CA. **Proceedings...** Los Angeles: AIAA, 1999. 12

WHITE, F. M. **Fluid mechanics**. [S.l.]: McGraw-Hill, 1998. 17

WIEGAND, A. W.; MÖLLMANN, C.; BARRIO, A. M. New concurrent design optimisation models of ASTOS. In: 4TH INTERNATIONAL WORKSHOP ON SYSTEM & CONCURRENT ENGINEERING FOR SPACE APPLICATIONS, Lausanne, Switzerland. **Proceedings...** Lausanne, 2010. 1

WIKIPEDIA. **Space shuttle main engine**). 2015.

https://en.wikipedia.org/wiki/Space_Shuttle_main_engine. Accessed: 29 September 2015. 148

ZANDBERGEN, B. **Simple mass and size estimation relationships of pump fed rocket engines**. Delft, Netherlands, 2013. 40

_____. Simple mass and size estimation relationships of pump fed rocket engines for launch vehicle conceptual design. In: EUROPEAN CONFERENCE FOR AERONAUTICS AND SPACE SCIENCES (EUCASS), Krakow, Poland. **Proceedings...** Krakow, 2015. 15

ZERLOTTI, R. F. **Otimização da trajetória ascendente de veículos lançadores de satélites utilizando o algoritmo de múltiplos tiros**. 128 p. Master Thesis — Instituto Tecnológico de Aeronáutica, São José dos Campos, Brazil, 1990. 15, 83

ANEXO A - Flow Schemes of Liquid Rocket Engines

This annex brings flow diagrams of the liquid rocket engines simulated in Chapter 8.

A.1 L75

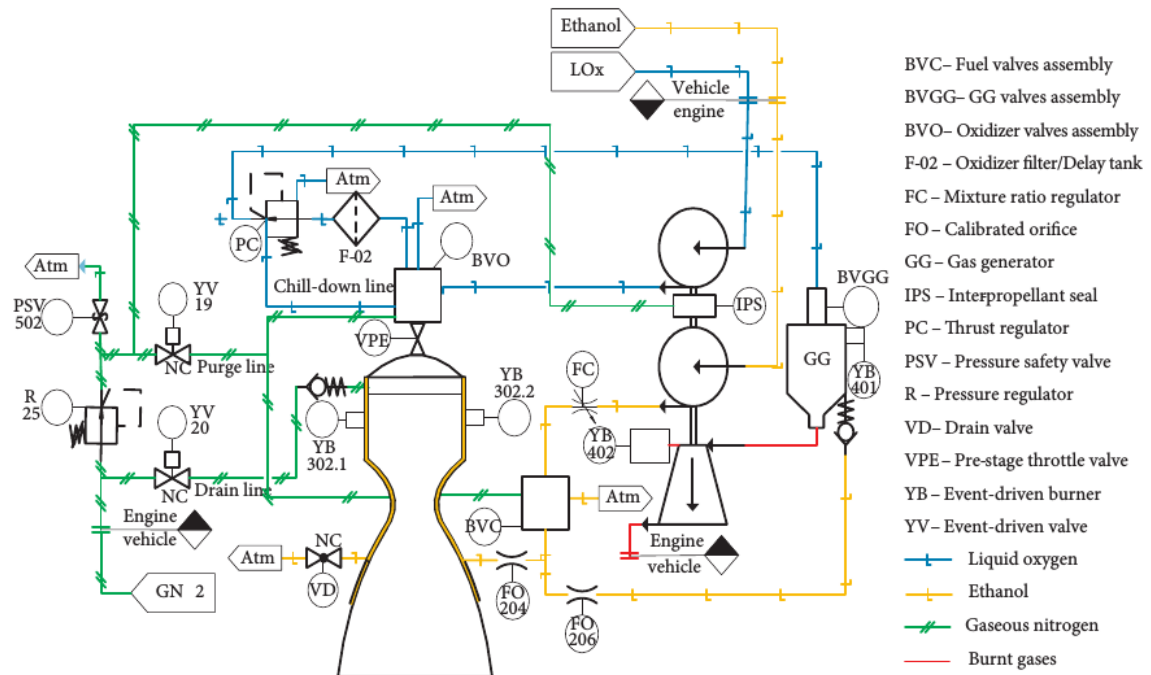


Figure A.1 - L75 scheme.

SOURCE: Almeida and Pagliuco (2014)

A.2 Vulcain

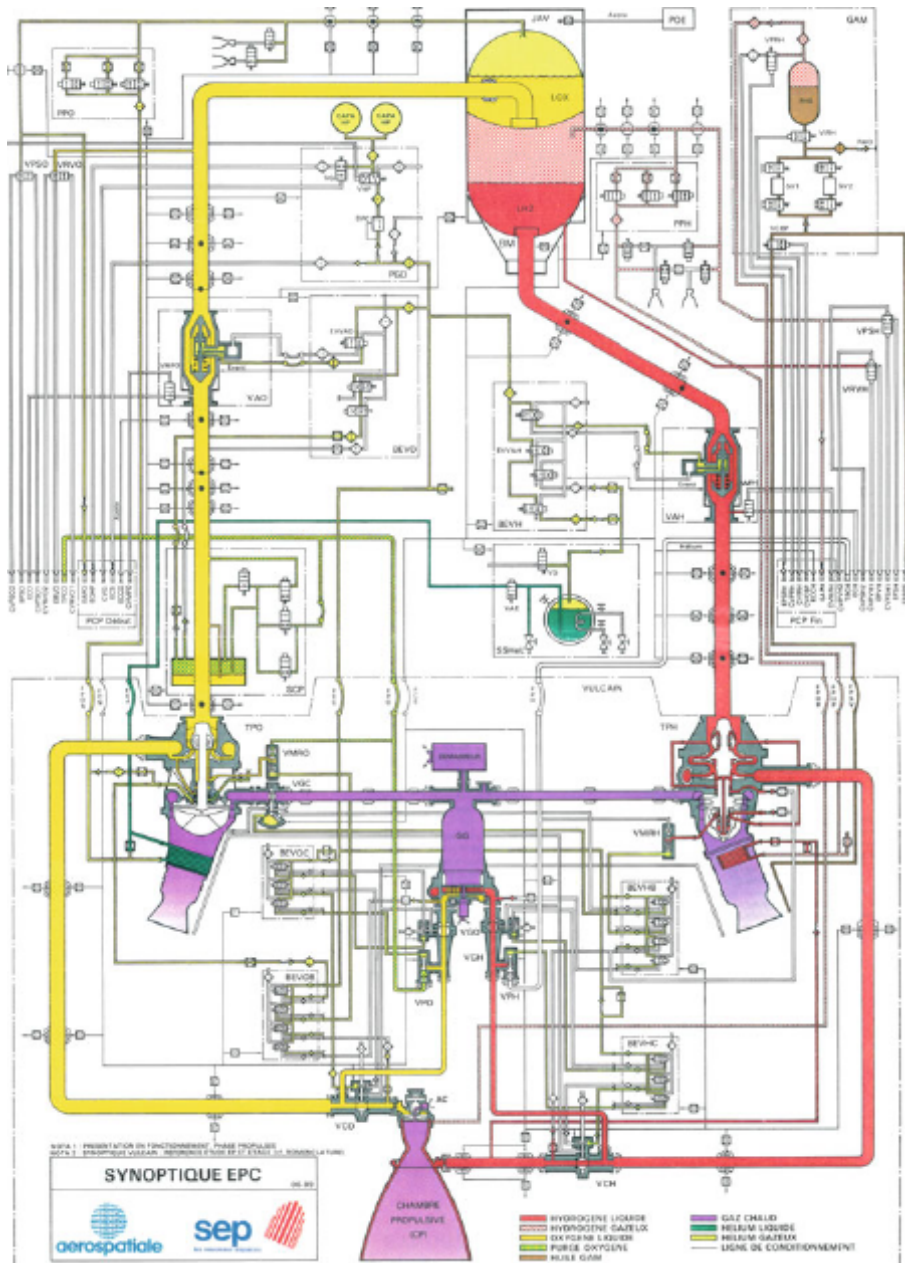


Figure A.2 - Flow schemes Vulcain.
 SOURCE: Kitsche (2011)

A.3 HM7B

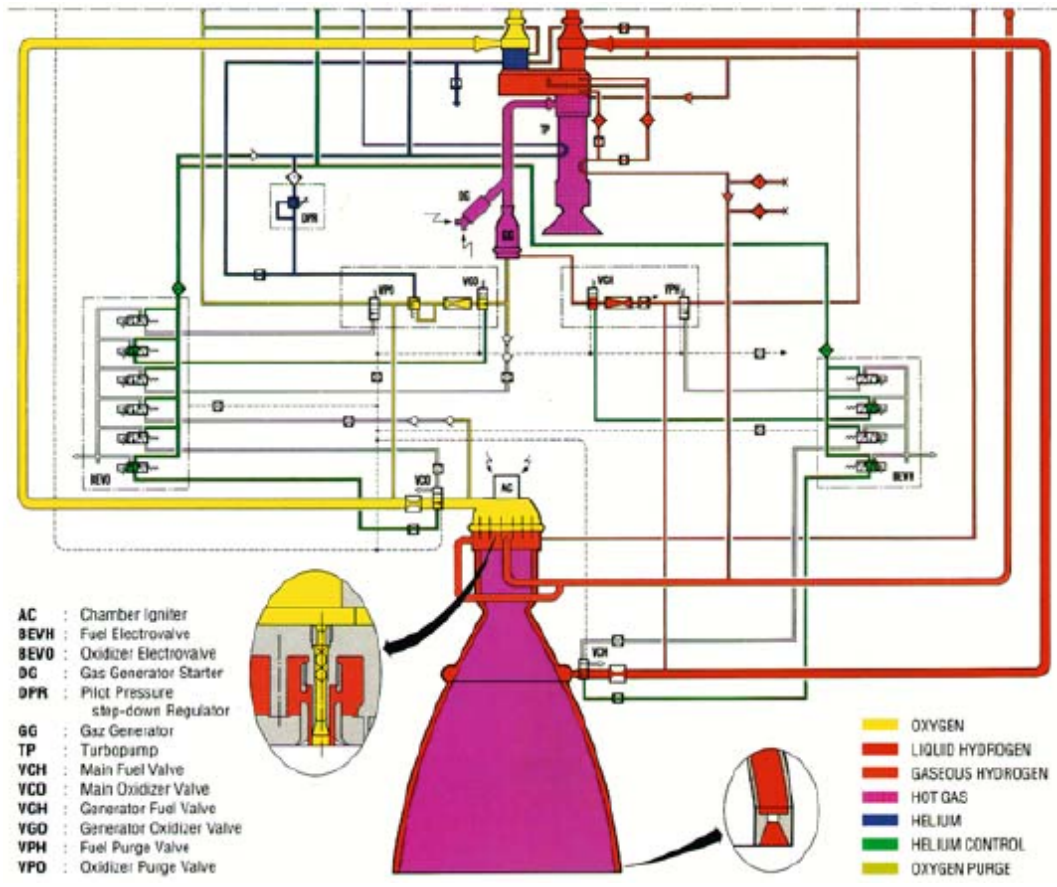


Figure A.3 - Flow scheme HM7B.
SOURCE: Turner (2005)

A.4 SSME

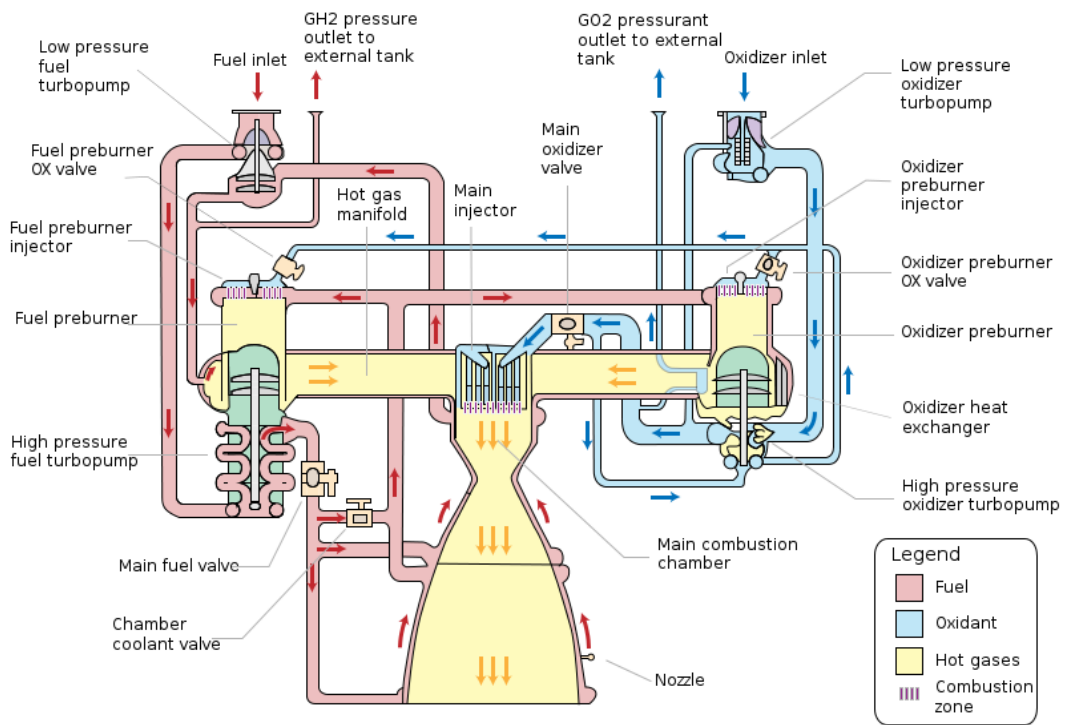


Figure A.4 - Flow scheme SSME.
SOURCE: Wikipedia (2015)

A.5 RL10-A-3A

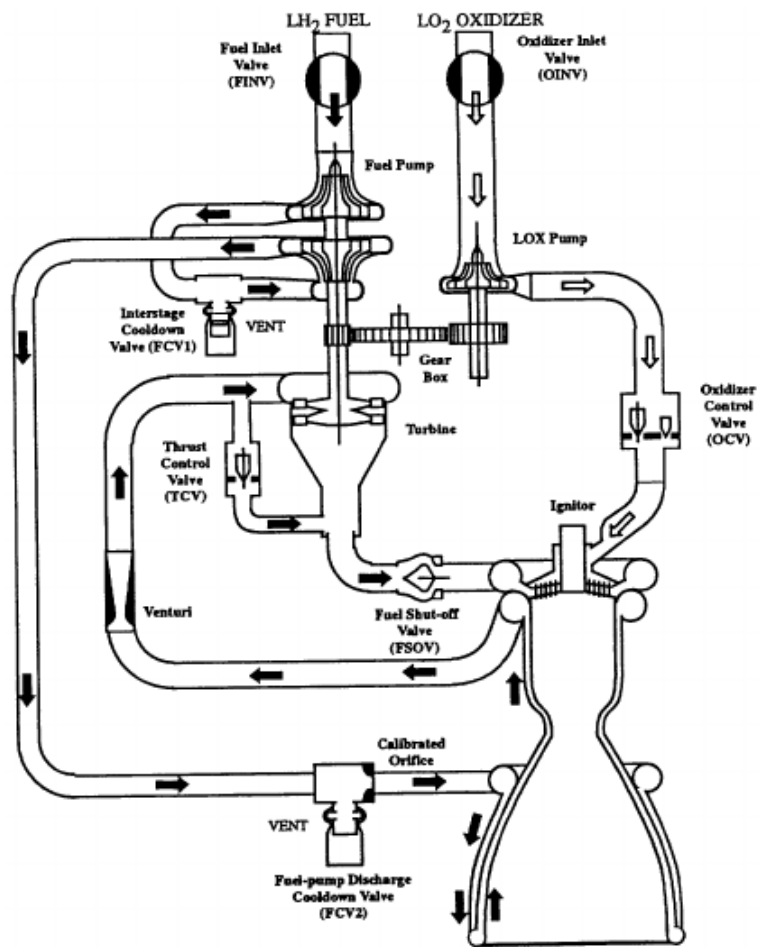


Figure A.5 - RL10-A-3A scheme.
 SOURCE: Binder et al. (1997)